

THE CYCLIC UNITS OF THE UPPER CRITICAL  
ZONE ON MAANDAGSHOEK 254 KT  
EASTERN BUSHVELD COMPLEX

by

STEPHEN BRYANT GAIN

Submitted in partial fulfilment of the  
requirements for the degree of  
MASTER OF SCIENCE  
in the Faculty of Science,  
University of Pretoria

November, 1981

## ABSTRACT

The farm Maandagshoek 254 KT is situated in the eastern lobe of the Bushveld Complex. The investigated sequence forms part of the Winterveld Norite-Anorthosite of the critical zone and consists of the UG1, UG2, UG3 and UG3A cyclic units. These cyclic units consist of a basal chromitite with or without olivine, overlain successively by melanorite, norite, and leuconorite to an anorthosite layer above. The cyclic units are punctuated by sharp contacts and a remarkable persistence along strike and dip.

The En content of orthopyroxene and the An content of plagioclase decrease and increase respectively upwards through the UG1 and UG2 cyclic units. Breaks in this trend occur below the chromitite layers where the En content of bronzite increases and in the anorthosite layers at the top of the cyclic units where the An content of plagioclase increases. A trace element study showed Rb and Zr to increase upward in the UG1 and UG2 cyclic units. Rb and Sr display a reasonable antipathetic relationship. The Cr and Ni content of the orthopyroxenes increases upwards irregularly in the cyclic layers, but the Ni content decreases where visible sulphides are present. Cu, Ni and the platinumoid elements increase in the chromitite layers, especially the UG2 chromitite layer. Clinopyroxene is not commonly cumulus and is identified as chromiferous augite. The equilibrium temperature of a coexisting orthopyroxene-clinopyroxene pair was calculated according to the Wood-Banno and Wells modifications to be 1179°C and 1097°C respectively. Cumulus olivine associated with the UG2 pegmatoid and the UG3A chromitite was identified as chrysolite. The compositions of 15 chromite samples were determined and showed similar chemistry to those reported by De Waal (1975). The crystallization temperatures of coexisting olivine and chromite pairs was determined

using the Jackson (1969) and Roeder et al, (1979) geothermometers.

The UG2 chromitite layer contains an average of 8,5 g/t PGE and Au over a width of 0,64 metres in 22 intersections in borehole and underground samples. A study of the distribution of Pt and Pd in the weathered and unweathered zones clearly shows that both, but especially Pd, are mobile and depleted in the surface environment. The sulphide liquid in the UG2 chromitite layer was calculated to have contained 925 ppm Pt and 934 ppm Pd which is 578 and 359 times respectively the calculated levels in early immiscible sulphide liquids (Naldrett and Cabri, 1976). A model is proposed in which the UG2 chromitite layer acted as a physico-chemical barrier to the upward migrating late deuteric fluids and volatiles charged with platinoids, Au, Sb, As and Te. The platinoids were collected by earlier sulphide droplets which separated from the magma during crystallization of the UG2 chromitite layer.

Structures are sub-divided into Class I and Class II features. Class I features are related to viscosity and density contrasts of layers at the time of crystallization of the magma and may be seen as bifurcating and anastomosing layers, folding and slump features, rafting of chromitite blocks, minor faults and potholes. Class II features are associated with tectonic movement which postdates the consolidation of the layering and are sub-divided into three categories; faults, dolerite dykes and pipes. The pipes are pegmatoidal in character, zoned with ultramafic cores and pyroxenite rims, have sharp contacts and cause downwarping and attenuation of the layering towards the pipes to form marginal synclines. It is postulated that

intercumulus material coalesced along structural weaknesses and moved upward until the lithostatic pressure impeded upward movement at which time lateral and outward intrusions occurred. The layers of the intruded rocks bent down to accommodate the outward flowing material and gave rise to the marginal synclines.

The concept of a closed cell cyclic unit is introduced to account for the inherent characteristics and origin of the cyclic units of the upper chromitite group.

## SAMEVATTING

Die plaas Maandagshoek 254 KT is in die oostelike gedeelte van die Bosveldkompleks geleë. Die opeenvolging wat ondersoek is, vorm deel van die Winterveld Noriet-Anortosiet van die kritiese sone en bestaan uit die UG1, UG2, UG3 en UG3A sikliese eenhede. Hierdie sikliese eenhede bestaan uit 'n basale chromitiet, met of sonder olivien, wat opeenvolgend deur melanoriet, noriet, leukonoriet en anortosiet ooreël word. Die sikliese eenhede word gekenmerk deur skerp kontakte en 'n merkwaardige konstantheid langs die strekking en helling.

Die En-inhoud van die ortopirokseen en die An-inhoud van die plagioklaas neem af en vermeerder onderskeidelik opwaarts in die UG1 en UG2 sikliese eenhede. Onderbrekings van hierdie neiging kom voor onder die chromitietlae waar die En-inhoud van die ortopirokseen toeneem en in die anortosietlae aan die bokant van die sikliese eenhede waar die An-inhoud van die plagioklaas toeneem. Die spoorelementstudie van plagioklaas het getoon dat die Rb en die Zr inhoud opwaarts in die UG1 en UG2 sikliese eenhede toeneem. Rb en Sr toon 'n redelike teenoorgestelde verhouding. Cr en Ni in die ortopirokseen vertoon 'n onreëlmatige toename opwaarts in die sikliese eenhede maar die Ni-inhoud verminder waar sigbare sulfied teenwoordig is. Cu, Ni en die platinoïede neem toe in die chromitietlae, veral in die UG2 chromitietlaag. Klinopirokseen is gewoonlik nie kumulus nie en is geïdentifiseer as chroomhoudende ougiet. Die ewewigstemperatuur van 'n saambestaande ortopirokseen-klinopirokseen-paar is volgens die Wood-Banno en Wells metodes bereken en waardes van 1179°C en 1097°C is onderskeidelik bepaal. Kumulus-olivien geassosieer met die pegmatitiese gedeelte van die UG2 chromitietlaag en die UG3A chromitietlaag is geïdentifiseer as chrisoliet. Die samestelling van 15 chromietmonsters is bepaal en die chemie daarvan stem ooreen met dié soos gerapporteer deur De Waal (1975). Die kristallasietemperature van saambestaande olivien en chromietpare is vasgestel met behulp van die geotermometers van Jackson (1969) en Roeder et al. (1979).

Die UG2 chromitietlaag bevat gemiddeld 8,5 g/t PGE en Au oor 'n breedte van 0,64 meter in 22 interseksies in boorgate en ondergrondse monsters. Ontleding van die verspreiding van Pt en Pd in die UG2 chromitietlaag in verweerde en onverweerde sones het getoon dat albei, maar veral Pd, mobiel en verarm is in die verweringsone. Die sulfiedvloeistof in die UG2 chromitietlaag het volgens berekening 925 dpm Pt en 934 dpm Pd bevat, wat onderskeidelik 578 en 359 keer die beraamde hoeveelheid in 'n vroeë onmengbare sulfiedvloeistof (Naldrett en Cabri, 1976) is. 'n Model word voorgestel waarin die UG2 chromitietlaag as 'n fisies-chemiese hindernis opgetree het vir opwaarts-stygende vloeistof en gasse verryk aan platinoïede, Au, Sb, As en Te. Die platinoïede, is vermoedelik versamel deur sulfieddruppels wat vroeg gedurende kristallisering van die UG2 chromitietlaag uit die magma geskei het.

Strukture word onderverdeel in Klas I en Klas II-tipes. Klas I-strukture se oorsprong is verwant aan die viskositeits- en digtheidskontraste van die lae gedurende kristallisering van die magma. Hierdie soort strukture word gekenmerk deur vertakking, opbreking, plooiing en versakking van lae, uitbreek (rafting) van chromitietblokke, klein verskuiwings en kolkgate. Klas II-strukture word geassosieer met tektoniese beweging na die konsolidasie van die lae en word in drie kategorië verdeel, nl. verskuiwings, doleriet-gange en pype. Die pype is pegmatities van aard, gesoneer met ultramafiese kerns en piroksenitiese rande, het skerp kontakte en veroorsaak afskeuring en verdunning van die lae in die rigting van die pype om randsinkliene te vorm.

Daar word gepostuleer dat interkumulus-vloeistof langs swak sones verenig en opwaarts beweeg het totdat die litostatiese druk dit verhoed het en laterale, uitwaartse indringing genoodsaak het. As gevolg hiervan is die lae van die gesteentes wat ingedring is afgebuig om die uitwaartsvloeiende materiaal te akkommodeer.

Die konsep van 'n geslote-sel-sikliese eenheid word voorgestel om die inherente karakteristieke eienskappe en oorsprong van die sikliese eenhede van die boonste chromitietgroep te verklaar.

CONTENTS		Page
1	INTRODUCTION .....	1
1.1	Locality .....	1
1.2	Topography and geomorphology .....	1
1.3	Historical review .....	4
1.4	Past work and purpose of the present investigation .....	5
1.5	Classification, modal analyses, IC numbers and cumulus terminology .....	7
1.6	Determinative methods and analytical techniques ..	8
1.6.1	XRF Spectrometry .....	8
1.6.2	Optical methods .....	10
1.6.2.1	Eulerian angles (plagioclase) .....	10
1.6.2.2	Extinction angles (plagioclase) .....	10
1.6.2.3	Refractive indices of plagioclase glasses .....	10
1.6.3	Microprobe analyses (olivine).....	10
1.6.4	Spectrographic and wet chemical analytical methods (chromite) .....	10
2	GEOLOGY .....	12
2 1	Regional geology .....	12
2.2	Description of lithologies .....	14
2.2.1	Orthopyroxene - plagioclase cumulates .....	14
2.2.2	Clinopyroxene - orthopyroxene - plagioclase cumulates .....	20
2.2.3	Chromite-bearing cumulates .....	22
2.2.3.1	Chromitite layers .....	22
2.2.3.1.1	UG1 chromitite layer .....	22
2.2.3.1.2	UG2 chromitite layer .....	27
2.2.3.1.3	UG3 chromitite layer .....	27
2.2.3.1.4	UG3A chromitite layer .....	27
2.2.3.2	Textural features of chromite in chromite- bearing lithologies .....	29
2.2.4	Olivine-bearing cumulates .....	32
2.2.5	Transgressive pegmatoids/pipes .....	34
2.2.6	Dolerite dykes .....	36



3	DESCRIPTION OF THE CYCLIC UNITS .....	37
3.1	Introduction .....	37
3.2	The UG1 cyclic unit .....	38
3.3	The UG2 cyclic unit .....	40
3.4	The UG3 cyclic unit .....	41
3.5	The UG3A cyclic unit .....	41
4	MINERAL CHEMISTRY .....	43
4.1	Introduction .....	43
4.2	Plagioclase .....	43
4.2.1	Major element analyses .....	43
4.2.2	Trace element analyses .....	44
4.3	Pyroxenes .....	47
4.3.1	Orthopyroxene .....	47
4.3.1.1	Major element analyses .....	47
4.3.1.2	Trace element analyses .....	48
4.3.2	Clinopyroxene .....	51
4.3.2.1	Major element analyses .....	52
4.3.2.2	Trace element analyses .....	52
4.3.3	Wood-Banno geothermometer .....	54
4.4	Olivine .....	56
4.5	Chromite .....	57
4.6	Olivine-chromite geothermometer .....	63
5	PLATINOID GEOCHEMISTRY .....	67
5.1	The distribution and mineralogy of platinoids in the upper group chromitites .....	67
5.2	Platinoid geochemistry .....	73
5.3	The origin of the PGE associated with the UG2 chromitite layer .....	76
6	STRUCTURE .....	82
6.1	Description of structural features .....	82
6.1.1	Class I structural features .....	82
6.1.2	Class II structural features .....	89
6.1.2.1	Transgressive pegmatoids/pipes .....	89
6.1.2.2	Origin of the pegmatoids/pipes .....	94
6.1.2.3	Dolerite dykes .....	100
6.1.2.4	Faults .....	100

7	ORIGIN OF THE CYCLIC UNITS .....	101
7.1	Development of the concept of cyclic units in the Bushveld Complex .....	101
7.2	Setting and features of the cyclic units .....	103
7.2.1	Attitude of layering .....	103
7.2.2	Geology of cyclic units .....	103
7.2.3	Grain size variation .....	103
7.2.4	Mineral composition variations .....	103
7.2.5	Trace element analyses .....	104
7.2.6	Structural features .....	104
7.3	The origin of the cyclic units in the upper part of the critical zone .....	104
7.3.1	Review of proposed hypotheses .....	104
7.3.2	Origin of the chromitite layers .....	107
7.3.3	Cyclic units - Towards a model .....	112
8	CONCLUSIONS .....	120
9	ACKNOWLEDGEMENTS .....	122
10	REFERENCES .....	123
	APPENDICES .....	133

FIGURES	Page
Fig. 1 : Locality map of Maandagshoek 254 KT .....	2
Fig. 2 : The topography of Maandagshoek 254 KT .....	3
Fig. 3 : Geological map of Maandagshoek 254 KT and Driekop 253 KT .....	5
Fig. 4 : Geological column of the critical zone on Maandagshoek 254 KT .....	13
Fig. 5 : Columnar section of the cyclic units and the UG2 chromitite layer in the upper chromitite group of Maandagshoek 254 KT .....	15
Fig. 6 : Poikilitic melanorite located above the UG3 chromitite layer .....	17
Fig. 7 : Anorthosite at the top of the UG3A cyclic unit ...	17
Fig. 8 : Intercumulus bronzite forming irregular tongues in cumulus plagioclase .....	18
Fig. 9 : Strain features, characterised by irregular extinction in intercumulus plagioclase, in melanorites .....	18
Fig. 10 : Large (4mm long) euhedral grain of bronzite displaying thin exsolution lamellae parallel to the (100) plane of orthopyroxene .....	19
Fig. 11 : Large oikocryst of orthopyroxene in "nodular" gabbronorite .....	19
Fig. 12 : Coronophytic halo of clinopyroxene poikilitically enclosing cumulus orthopyroxene grains .....	21
Fig. 13 : Nodular gabbronorite from below the UG1 chromitite layer .....	21
Fig. 14 : Section E/A showing the UG1 chromitite layer and its relationship to the enclosing lithologies ....	23
Fig. 15 : Section E/B showing the UG2 chromitite layer and its relationship to the enclosing lithologies ....	24
Fig. 16 : Section E/C showing the UG3 and UG3A chromitite layers and their relationship to the enclosing lithologies .....	25

Fig. 17 : Interlayered chromitite and anorthosite of the UG1 chromitite layer .....	26
Fig. 18 : The UG2 chromitite layer .....	26
Fig. 19 : The UG3 chromitite layer .....	28
Fig. 20 : Chromite-bearing poikilitic melanorite overlying the UG3 chromitite layer .....	28
Fig. 21 : The two chromitite layers of the UG3A chromitite layer .....	30
Fig. 22 : Coarse-grained aggregate of polygonal chromite in the UG2 chromitite layer .....	30
Fig. 23 : Oikocrysts of bronzite enclosing subhedral chadacrysts of chromite in the UG2 chromitite layer .....	31
Fig. 24 : Chains of subhedral chromite associated with intercumulus plagioclase in melanorites in the UG1 chromitite layer .....	31
Fig. 25 : Unidentified round silicate inclusion in a chromite grain in the UG1 chromitite layer .....	33
Fig. 26 : Serpentinized olivine grain from the UG3A chromitite layer .....	33
Fig. 27 : View of Pipe A from an altitude of approximately 300 metres looking NNE .....	35
Fig. 28 : The distribution of Zr, Sr, Rb, $\frac{Sr}{Rb}$ , $\frac{K}{Ca + Na + K} \times 10^2$ and $\frac{Ca}{Ca + Na + K} \times 10^2$ in plagioclase separates of borehole MDH 7 .....	46
Fig. 29 : The distribution of V, Cu, Cr in the orthopyroxene separates of borehole MDH 7 .....	49
Fig. 30 : Variation of oxides present in chromite samples taken from the UG1, UG2, UG3 and UG3A chromitite layers .....	60
Fig. 31 : Small elongate ilmenite lamellae in a chromite grain .....	61
Fig. 32 : Whole rock analyses for Pt, Pd, total Ni and Cu in the UG2, UG3 and UG3A cyclic units in borehole MDH 6 .....	70

Fig. 33	: Irregular layering in the UG1 chromitite .....	83
Fig. 34	: Interlayered chromitite and anorthosite, in the UG1 chromitite layer .....	83
Fig. 35	: Complex disturbance in the norites and leuconorites below the UG3 chromitite layer .....	84
Fig. 36	: Large lens of chromitite located in the anorthosite below the UG1 chromitite layer ....	86
Fig. 37	: Lens of chromitite located in the gabbro-norites below the UG1 chromitite layer .....	86
Fig. 38	: Minor faulting in the UG1 chromitite layer ....	87
Fig. 39	: Pothole on Maandagshoek .....	87
Fig. 40	: A "pothole" mapped on surface between trenches 2E and 2F .....	88
Fig. 41	: The UG2 layer contours on Maandagshoek 254 KT .	90
Fig. 42	: UG1 and UG2 chromitite layer profiles on Maandagshoek 254 KT .....	91
Fig. 43	: An interpretation of the shape of pipe C .....	93
Fig. 44(a)	: Cross-section of a rigid plate, with a central aperture which is being pressed downwards onto a viscous mass .....	97
Fig. 44(b)	: Pressure distribution in the viscous mass in Fig. 44(a) .....	97
Fig. 45	: Conceptual profiles at the interface of an intruding viscous mass of mafic magma of an incipient pipe and the layered rocks of the Bushveld Complex .....	98
Fig. 46	: Cation norm projection on the join olivine-chromite-quartz after Irvine (1977) illustrating the possible formation of chromitite layers by liquid mixing .....	110
Fig. 47	: Synoptic diagram showing the initial stages in the development of a cyclic unit .....	114
Fig. 48	: Synoptic diagram illustrating the closing stages of crystallization of a cyclic unit ....	116
Fig. 49	: Diagrammatic representation of the formation of a plagioclase matte (A) and the slump features observed below certain of the chromitite layers .....	117

TABLES	Page
Table 1 : Chemical analyses of coexisting clinopyroxene and orthopyroxene used for the temperature calculation .....	53
Table 2 : The distribution of Zn, Cu, Ni, Co, Cr and V in two clinopyroxene separates from borehole MDH 7 .....	52
Table 3 : Chemical analyses and structural formulae of olivines .....	57
Table 4 : Chemical analyses and structural formulae of 15 chromite samples .....	59
Table 5 : The equilibrium temperatures of coexisting olivine-chromite pairs .....	65
Table 6 : The Pd and Pt analyses of the UG1, UG2 and UG3 chromitite layers in surface environment ..	68
Table 7 : The distribution of Pt, Pd, Rh, Ru, Ir, Au, total Ni, sulphide Ni, Cu and Cr <sub>2</sub> O <sub>3</sub> in the UG2 chromitite layer .....	71

APPENDICES		Page
Appendix I	: Chemical analyses and structural formulae of plagioclase separates .....	133
Appendix II	: Anorthite content of plagioclase in the upper critical zone .....	142
Appendix III	: The distribution of Y, Zr, Sr and Rb in plagioclase separates .....	145
Appendix IV	: Chemical analyses and structural formulae of orthopyroxene separates .....	146
Appendix V	: The distribution of Zn, Cu, Co, V, Ni and Cr in orthopyroxene separates .....	155

## 1 INTRODUCTION

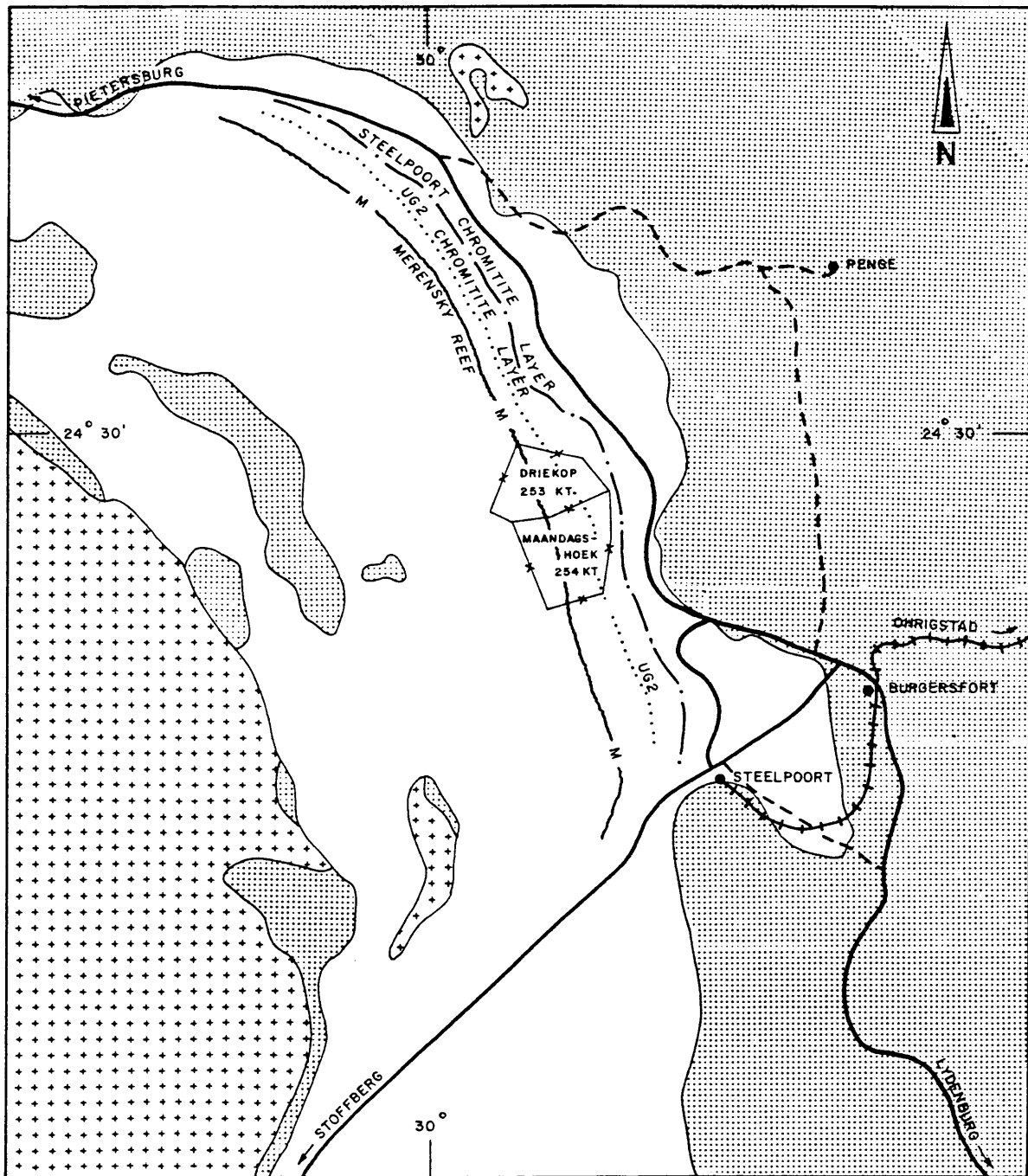
### 1.1 Locality

The farms Maandagshoek 254 KT and Driekop 253 KT are situated about 20 km to the northeast of Steelpoort in South Lebowa, eastern Transvaal (Fig. 1). Both these farms are of considerable economic importance as they are situated firstly, on the platiniferous Merensky Reef and the UG2 chromitite layer and secondly, downdip from the Steelpoort Chromitite Layer (Fig. 1).


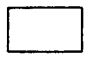
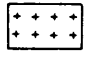
### 1.2 Topography and geomorphology

The topography of the Maandagshoek area is dominated by the steep eastern escarpment of the Leolo Mountains along the western boundary and a series of hills in the east (Fig. 2). These are separated by a wide valley which is attributed, according to Willemse and Frick (1970), to a large river, the headwaters of which are represented by the present day Groot and Klein Dwars Rivers. This river drained in a northerly direction to the Olifants River. Eventual capture of the headwaters by the Steelpoort River caused redirection of the water flow and at present the relatively insignificant Moopetsi River flows to the north from the watershed between the Steelpoort and Olifants drainage systems which is situated along the road to the Maandagshoek Mission Hospital. The escarpment to the west rises rapidly from a height of 960 metres above sea-level at the valley floor to 1 700 metres above sea-level on Garatouw 282 KT and forms a portion of the Leolo Mountains which are made up of main zone gabbro, norite and anorthosite. The hills to the east of this valley consist of gabbronorite, norite and pyroxenite of the critical zone. The wide valley is characterised by deeply incised dongas which in places indicate a soil depth in excess of 10 metres. This depth was ascertained by borehole drilling. The depth of alteration in the bedrock is between 15 and 20 metres from the surface. Soil profiles

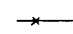

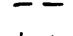





**GEOLOGICAL LEGEND**

-  TRANSVAAL SEQUENCE
-  RUSTENBURG LAYERED SUITE
-  GRANITES / GRANOPHYRES / FELSITES

**LEGEND**

-  FARM BOUNDARIES
-  MAIN ROADS
-  SECONDARY ROADS
-  RAILWAY LINES

KILOMETRES 10 0 10 20 30 KILOMETRES

Figure 1: Locality map of Maandagshoek 254 KT within the eastern limb of the Bushveld Complex.

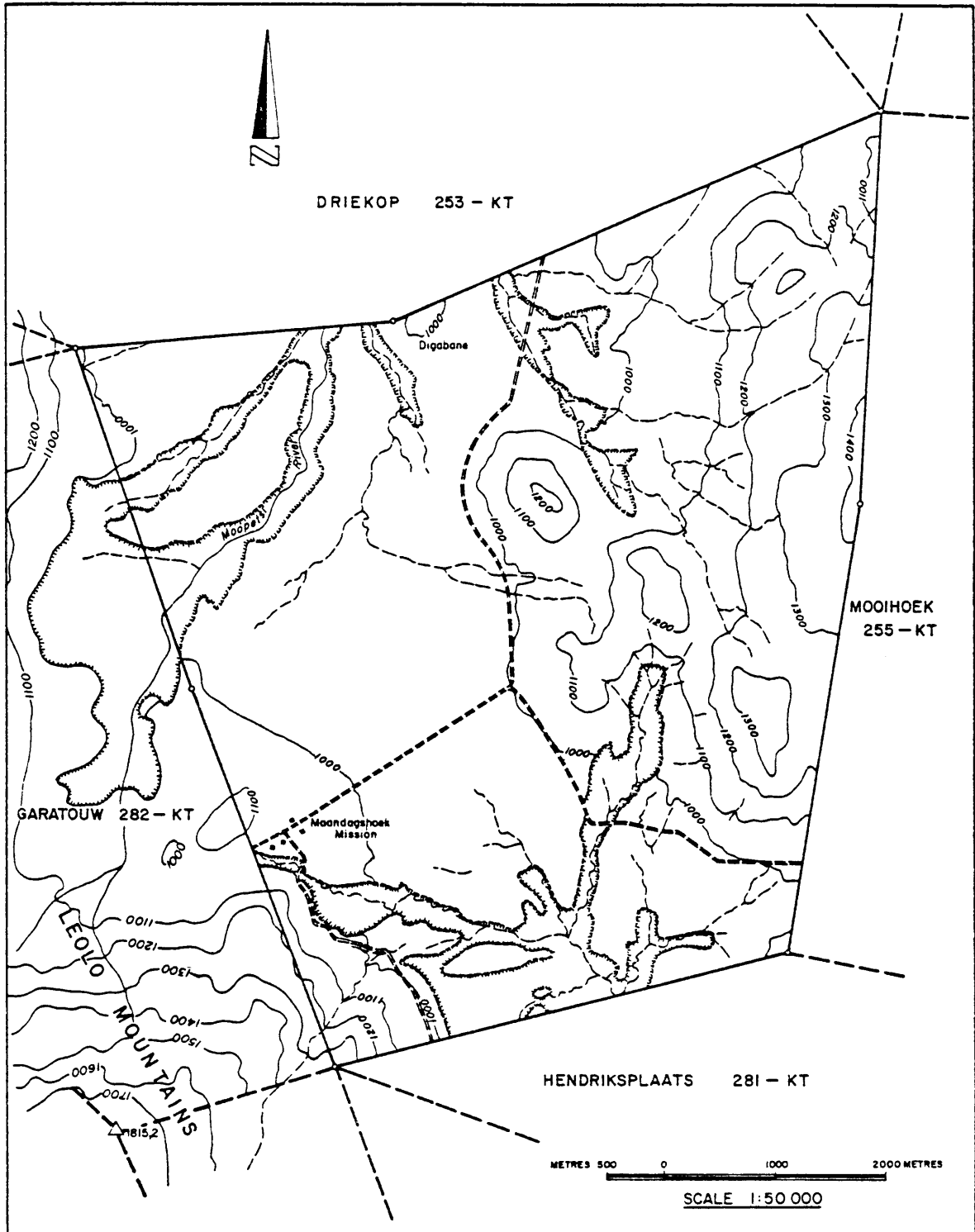


Figure 2: The topography of Maandagshoek 254 KT.

within the black turf show concretions of calcrete and in many places minor stratiform developments of attapulgite-montmorillonite clay. During the initial exploration programme a small deposit of attapulgite-montmorillonite was evaluated which is at present being mined.

### 1.3 Historical review

Maandagshoek was first brought to the attention of the geological and prospecting fraternity in May 1924, when A.F. Lombaard, a prospector-farmer, panned out some alluvial platinum from a dry water course close to the Mooihoek pipe. After the positive identification of the platinum, Dr. Hans Merensky visited Maandagshoek and encouraged A.F. Lombaard and Schalk Schoeman to search for the source rock of the platinum. On 15 August 1924 Dr. Hans Merensky, assisted by Lombaard and the brothers Schalk and Willem Schoeman traced the source of the platinum to a dunite pipe on Mooihoek. After this, A.F. Lombaard, located a coarse-grained layer of pyroxenite with a pronounced iron stain. The discovery site (Folder A) of the "Lombaards Reef" may be seen on a geological sketch map dated 17 December 1925 which shows the sites of the various platiniferous bodies discovered by the above-mentioned prospectors.

Lombaard (1945), in a historical treatise on the discoverers of platinum in South Africa, relates that during late 1924, Jan Schoeman, in the company of Koos and Schalk Schoeman and Dr. C Jansen Weilbach, proposed that the Reef should in future be named after Dr. Hans Merensky because of his scientific background and enthusiasm in searches for platinum. The 'Lombaard Reef' was subsequently also traced to the western Bushveld by Dr. Merensky and others and eventually became known as the Merensky Reef. This work continued throughout 1926 when the Driekop and Onverwacht pipes were discovered. Prospecting work was conducted on Maandagshoek and various adits and trenches from this period,

amongst others the original discovery site (Folder A and Fig 3) now declared a national monument, are still to be found. Fragments of information lodged with the mining commissioner's office at Pietersburg show that the prospectors were well aware of the fact that the UG2 chromitite layer was also enriched in platinoids but by reason of the relatively lower values in the surface environment, and the lack of a co-ordinated exploration effort, the UG2 chromitite layer was not actively prospected until the early fifties.

In 1952 two entrepreneurs, Language and Joubert, mined the UG1 chromitite layer on the eastern flanks of the koppie Legabeng on the farm Driekop (Fig. 3). Several adits were sunk on the layers but marketing and mining problems put a halt to their endeavours.

#### 1.4 Past work and purpose of the present investigation

Because of its difficult metallurgical problems, the UG2 chromitite layer did not become an exploration target for platinum-group elements (PGE) until well into the nineteen seventies. As recently as 1972 only the Merensky Reef was considered as a possible source of economically exploitable platinoids in a review of the mineral potential of the Steelpoort area of the eastern Transvaal (Duke 1972).

Between 1971 and the end of 1977 the Mining Corporation Limited investigated various chromitite layers of the upper chromitite and lower chromitite groups (the UG and LG chromitite layers according to the notation of Cousins and Feringa (1964, p. 186)) on Maandagshoek 254 KT and Driekop 253 KT by means of geological mapping, geophysical investigations and diamond drilling (Fig. 3 and Folder A). During this period particular stress was laid upon the economic evaluation of the UG2 chromitite layer and its associated platinoid, copper and nickel mineralisation. In addition the exploration effort was directed toward the elucidation of structures which disrupt the continuity of the chromitite layers of the upper group, especially in the vicinity of

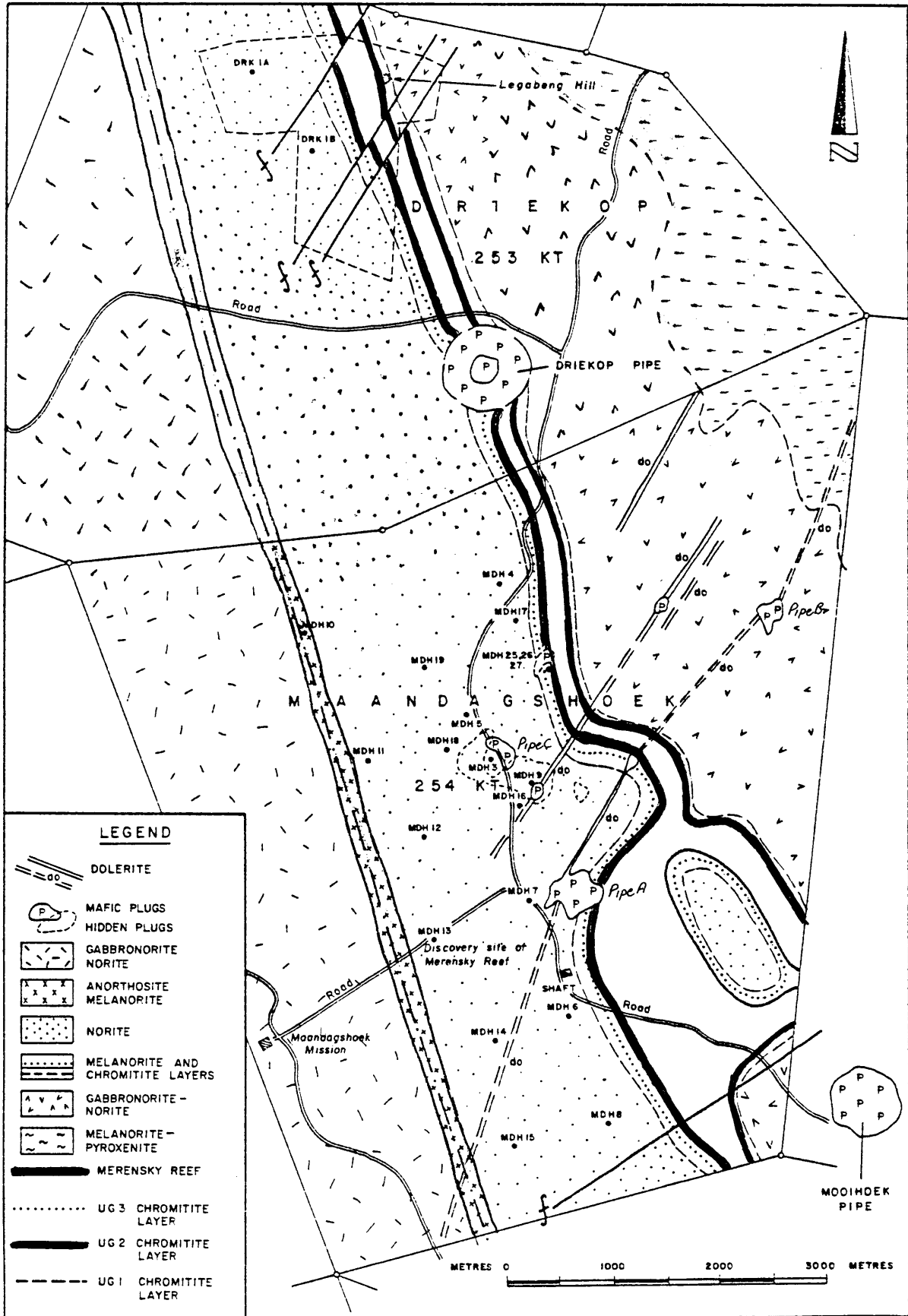


Figure 3 : Geological map of Maandagshoek 254 KT and Driekop 253 KT showing in particular the positions of the Merensky Reef, the upper group chromitite layers, mafic pipes and borehole sites.

pipes and faults. Due to relatively poor surface exposure, especially of the melanorites, pyroxenites and chromitites, in the broad valley on Maandagshoek 254 KT, the geology of the farm (Fig. 3 and Folder A) is to a large extent inferred from borehole information.

The purpose of this study is to supplement the information gained from field mapping and borehole logging with a detailed investigation of the petrography, mineralogy and mineral chemistry of the cyclic units that contain the upper group chromitite layers. For the purpose of the study the centrally situated borehole, MDH 7 (Fig. 3), was selected in order to gain insight into the origin of these cyclic units and their associated platinoid-rich chromitite layers. In addition, attention is given to the influence of the mafic pipes on the layering while the distribution of platinoids, Cu and Ni sulphides in the upper group chromitites is reviewed.

#### 1.5 Classification, modal analysis, I.C. numbers and cumulus terminology

The classification and nomenclature of the rock types are in accordance with the scheme proposed by Streckeisen (1976) and rocks in the geological column and on surface were classified by modal analyses. Modal counts were made by means of the method outlined by Van der Plas and Tobi (1965, p. 87 - 98) on 173 polished sections from borehole MDH 7. The point distance chosen was in almost all cases larger than the largest cumulus grain size and 1 000 points per *thin.* section were measured with the Swift Automatic Point Counter. According to the chart given by Van der Plas and Tobi (1965, p.88) the estimated content is within three per cent by volume of the actual value with a 95 per cent confidence. The results of these analyses may be seen together with the detailed geological column on Folder B.

The IC Numbers (Chayes, 1976, p.72-78) were determined by observing the number of identity changes in a 40 mm traverse (Folder B). The average area of the thin sections was determined as 480 mm<sup>2</sup> and by extrapolation

of the graph given by (Chayes 1956, p.77) it was possible to estimate the standard deviation of the various IC Numbers as :-

IC Numbers	Standard Deviation
10	9
20	6
30	4
40	3,3
50	2,8
100	1,6
200	1,0
300	0,7

The cumulus terminology of Wager et al (1960) is used throughout and is interpreted as follows :-

Cumulus crystals are the primary crystals to precipitate out of a magma. If these cumulus crystals are heavier than the liquid they settle to the floor of the magma chamber as a cumulate rock. In such a rock the liquid found in the interstices of the cumulate crystals is called the inter-cumulus liquid which crystallises to form the intercumulus phase. This later crystallisation takes place during the post-cumulus stage when adcumulus growth can enlarge the initial cumulus crystals and reaction between the crystals and the liquid can take place. Isomodal cumulates are defined as rocks which roughly contain the same proportions of component minerals while monomineralic cumulates contain only one cumulate phase which usually makes up more than 90 per cent of the rock.

## 1.6 Determinative methods and analytical techniques

### 1.6.1 XRF Spectrometry

Borehole core was crushed, pulverised and screened to separate the +80 and -200 mesh fraction. This separate was washed and dried and seventy-nine plagioclase, eighty orthopyroxene and seven clinopyroxene concentrates were obtained by means of a Frantz isodynamic separator. Purity was variable but in most cases an apparent purity of greater

than 99 per cent was observed in grain mounts using a binocular microscope. Problems in separation included the presence of minute specks of intergranular chromite, the poikilitic nature of the orthopyroxene in which plagioclase and clinopyroxene was minutely included, and the intimate association between clinopyroxene and orthopyroxene.

Approximately six grams of the sample was pulverised to about 200 mesh and pressed into 40 mm diameter briquettes. Glass discs were prepared in duplicate using a method developed by the University of Cape Town from that of Norrish and Hutton (1969). Major elements determined with the tube in parenthesis, are as follows : MgO, Al<sub>2</sub>O<sub>3</sub>, SiO<sub>2</sub>, P<sub>2</sub>O<sub>5</sub>, K<sub>2</sub>O and CaO (chromium tube) total Fe as Fe<sub>2</sub>O<sub>3</sub>, MnO, Cr<sub>2</sub>O<sub>3</sub> and NiO (tungsten tube). Trace elements determined were Ni, Cu, Zn (gold tube) Co, Cr, V, Nb, Zr, Y, Sr and Rb in addition to Na<sub>2</sub>O (tungsten tube). All samples were analysed with a Siemens SRS XRF spectrometer.

Average errors in accuracy between ten calibrations and the values given by Flanagan (1969) relative to 11 standards were as follows. Using standards AGV-1, BCR-1, G-2, GSP-1, JB-1, JG-1, MGR-1, NIM-D, NIM-N, NIM-P and PCC-1 errors were at maximum levels of SiO<sub>2</sub> ±0,204, TiO<sub>2</sub> ±0,010, Al<sub>2</sub>O<sub>3</sub> ±0,111, Fe<sub>2</sub>O<sub>3</sub> ±0,104, MnO ±0,002, MgO ±0,032, CaO ±0,032, Na<sub>2</sub>O ±0,073, K<sub>2</sub>O ±0,025, P<sub>2</sub>O<sub>5</sub> ±0,010, Cr<sub>2</sub>O<sub>3</sub> ±0,004, NiO ±0,012 per cent respectively. Trace elements were Co ±3; Cr ±2; V ±4; Zn ±2; Cu ±2; Ni ±3; Nb ±2; Zr ±4; Y ±2; Sr ±3; Rb ±4 ppm respectively. Precision in all cases is better than ±40 per cent of the absolute error.

All analyses are expressed L.O.I. and H<sub>2</sub>O free and the major element chemistry has been normalised to the hydrous total.



## 1.6.2 Optical methods

### 1.6.2.1 Eulerian angles (plagioclase)

Eulerian angles of the first order (Burri et al., 1967, p. 41 - 43 and 117 - 133) were measured on combined albite-Carlsbad twins on cumulus plagioclase crystals and the compositions determined from a chart given by the authors. Eulerian angles were usually measured in duplicate because of the unsuitability of the  $\theta$  curve for compositional determination in the range  $An_{70}$  -  $An_{85}$ . This gave four sets of two angles which allowed eight values per sample to be averaged.

### 1.6.2.2 Extinction angles (plagioclase)

Extinction angles were measured on combined albite-Carlsbad twins and estimated on tables given by Deer et al. (1966, p. 333 and 334).

### 1.6.2.3 Refractive indices of plagioclase glasses

About 0,2 g of feldspar was wrapped in platinum foil and heated to  $1500^{\circ}\text{C}$  in a furnace for 15 minutes. The sample was rapidly removed and quenched. The glassy charge was broken free and the RI determined by the normal oil immersion method using sodium light. The plagioclase compositions were estimated by using plate XVII of Burri et al. (1967).

## 1.6.3 Microprobe analyses (olivine)

Polished sections were prepared from the olivine-rich zones associated with the UG2 and UG3A chromitite layers. Each sample was analysed in duplicate by the ARL SEMQ microprobe at the University of the Witwatersrand using the Wakefield diopside standard. The probe operator was G. Davies.

## 1.6.4 Spectrographic and wet chemical analytical methods (chromite)

The samples were crushed, pulverised and screened to extract the +100 mesh to -200 mesh fraction. After washing to remove dust the samples were passed through the Frantz

isodynamic separator, firstly at low amperage to remove iron particles or magnetite and then at approximately 0,8 amps. Purity at this stage was estimated to be around 99 per cent with only the occasional grain containing adhering silicate. The resulting fraction was left to stand for 48 hours in cold 40 per cent hydrofluoric acid. The chromite was repeatedly cleaned in running water. The silicate-fluoride coating that remained adhering to the grains was abraded off in a magnetic stirrer for about  $\frac{1}{2}$  hour and the resulting crystals cleaned with de-ionised water and dried. The purified chromite separates were analysed in duplicate by the Council for Mineral Technology. MgO, Cr<sub>2</sub>O<sub>3</sub>, SiO<sub>2</sub>, total Fe, Al<sub>2</sub>O<sub>3</sub> and CaO were spectrographically determined while V<sub>2</sub>O<sub>5</sub>, TiO<sub>2</sub>, CaO, MnO, ZnO, CuO, total S, Na, K and the ratio ferrous to ferric iron were determined by wet chemical methods.

## 2 GEOLOGY

### 2.1 Regional Geology

The geology of the critical zone, and the associated chromitite layers in the eastern Bushveld Complex has been described in detail by Cameron (1963, 1964, 1971, 1977 and 1980) and the nomenclature he has used in subdividing this zone is maintained for continuity and correlation purposes.

The geological column, (Fig. 4) shows the relationship between the lower pyroxenite and upper anorthosite subzone of the critical zone as observed in borehole profiles on Maandagshoek.

According to Cameron (1963, p.97) the base of the lower subzone of critical zone (not shown in Fig. 4) is taken at the position where there is a distinct increase in the amount of cumulus chromite and postcumulus plagioclase in the bronzitite. The first chromitite layer of the lower group of layers is developed a short distance above this level in the intrusion. The lower group of chromitite layers, not fully shown on the profile but developed over a vertical distance of approximately 500 m, consist of up to twelve chromitite layers (Cameron 1977, p.1085). The Steelpoort Layer is the best developed of these and has an average thickness of 1,08 m in the seven borehole intersections on Maandagshoek. The appearance of cumulus plagioclase at the base of the F unit (Cameron 1963, p.97), is taken as the top of the lower subzone of the critical zone. The lower subzone of the critical zone is now also referred to as the Swartkoppies Pyroxenite (South African Committee for Stratigraphy (SACS, 1980, p. 226)).

The upper subzone, or the Winterveld Norite-Anorthosite (SACS, 1980, p. 227), is comprised essentially of norites, gabbronorites, anorthosites, and chromitites which display spectacular layering. Included in this subzone are the middle group of chromitite layers which are developed over 35 m and consist of six chromitite layers ranging from

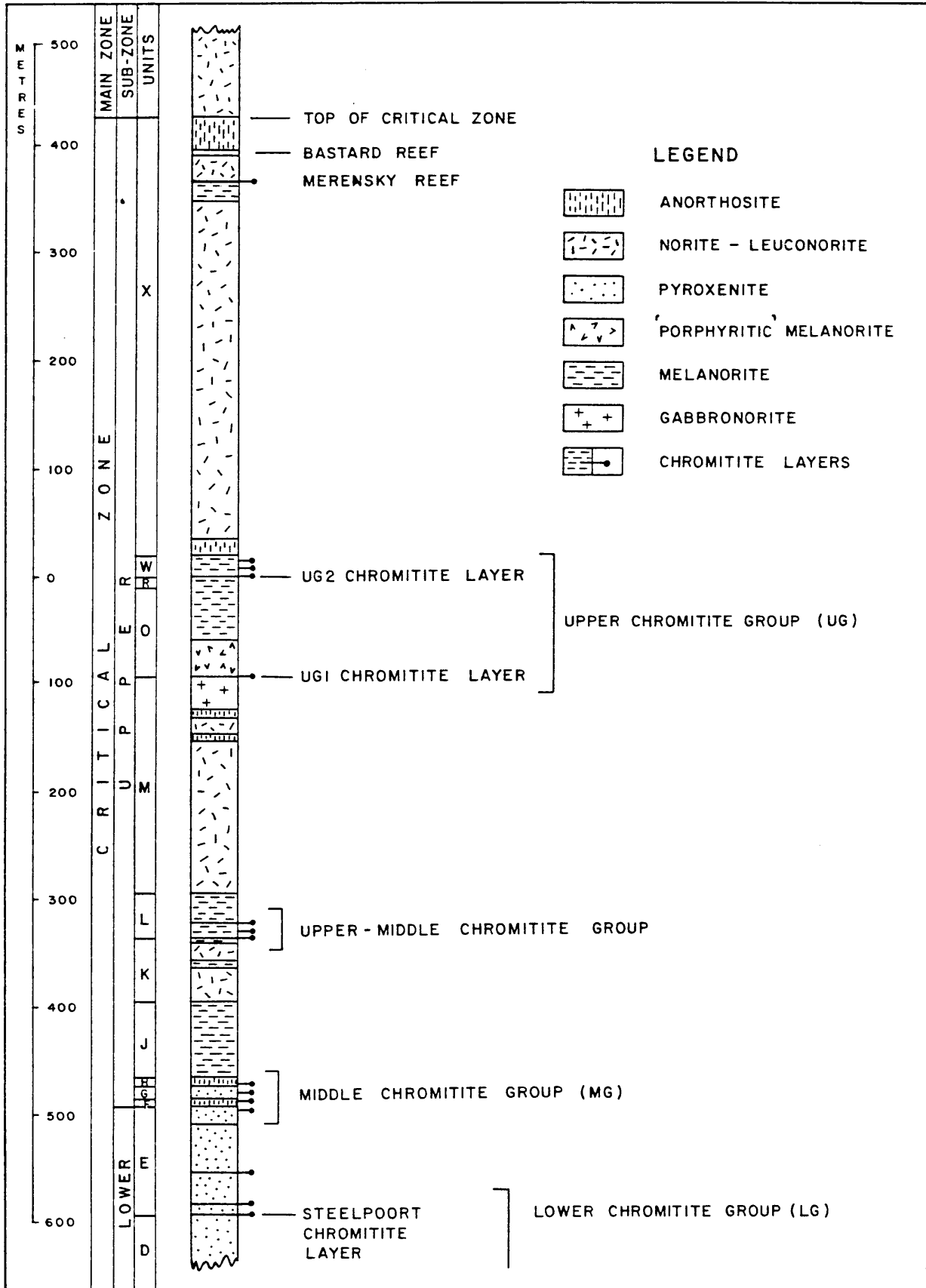


Figure 4 : Geological column of the lower pyroxenite (Swartkoppies Pyroxenite) and the upper anorthosite (Winterveld Norite - Anorthosite) subzones of the critical zone as intersected in boreholes on Maandags-hoek 254 KT.

0,02 to 0,25 m in thickness, the upper-middle group of chromitite layers developed over 18 m and consisting of three chromitite layers ranging in thickness between 0,02 to 0,05 m and the upper group of chromitite layers developed over 125 m and consisting of five layers ranging from 0,10 to 0,60 m in thickness. The top of the upper subzone is located at the top of the very distinctive "giant mottled anorthosite" of the Bastard cyclic unit.

The rocks of the critical zone show evidence of both large and small-scale cyclic layering. The large scale cyclic layering is typified by piles of medium-grained norite, usually over 100 m in thickness. Leuconorites are found in the upper part of such a cyclic unit while in the lower portion orthopyroxene may preponderate over plagioclase to form melanorites. In such layering, contacts tend to be gradational and rock units are essentially isomodal over tens of metres. These monotonous sequences are separated by intervals where cyclicity is more rapidly repeated and in which small-scale layering is developed. Such interruptions in the isomodal crystallisation are accentuated by cyclic units and have produced the chromitite layers and the Merensky Reef. The detailed columnar section, Fig. 5 and Folder B, show among others cyclic units and the distribution of the various rock types as well as their model analyses.

## 2.2 Description of the lithologies

### 2.2.1 Orthopyroxene - plagioclase cumulates

The bulk of the rock types mapped consists of variable proportions of orthopyroxene and plagioclase and are classified according to the nomenclature outlined by Streckeisen (1976) into anorthosites, leuconorites, norites and melanorites.

Local terminology such as poikilitic (mottled) and speckled anorthosites are used to differentiate between the

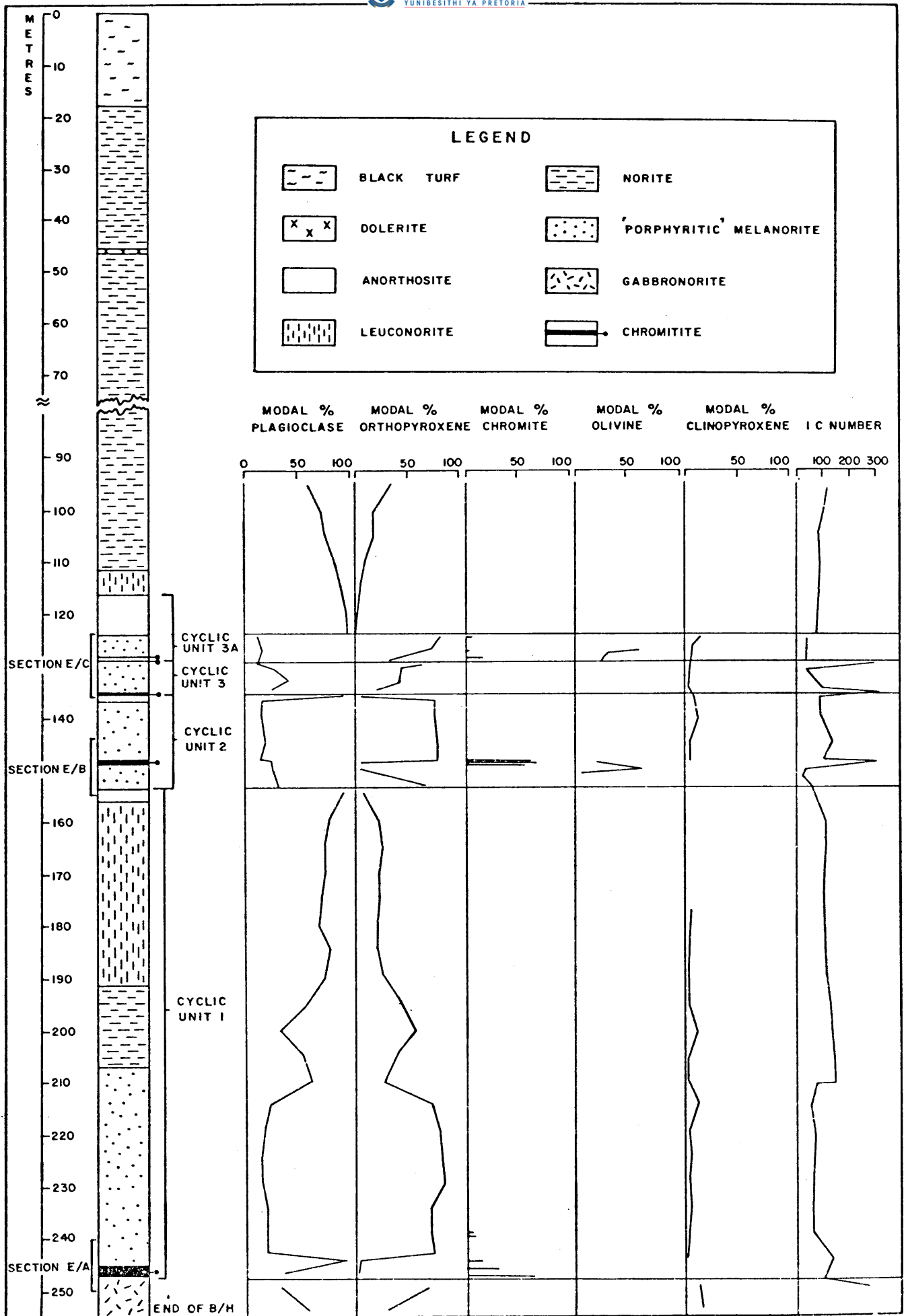


Figure 5 : Columnar section of the cyclic units in the upper critical zone Maandagshoek 254 KT showing the distribution of the major rock forming minerals and IC numbers of these rocks. Note positions of sections E/A, E/B and E/C

types of anorthosite found. The former type contains large poikilitic clots of orthopyroxene which may be up to 50 mm in diameter, while in the latter the orthopyroxene tends to be cumulus but constitutes less than ten per cent by volume of the rock.

The medium-grained melanorites, which generally overlie the UG1, UG2, UG3 and UG3A chromitite layers, commonly contain large, green oikocrysts of clinopyroxene evenly distributed through the rock. Where exposed these rocks display their poikilitic texture extremely well (Fig. 6).

In the plagioclase-rich rocks of the cyclic units the grain boundaries of the plagioclase crystals are commonly curved with well developed triple junctions, which indicates simultaneous adcumulus growth (Fig. 7). In the melanorites the intercumulus plagioclase tends to be anhedral.

Intercumulus bronzite occasionally forms irregular penetration features which squeeze between and occasionally enter the enclosing plagioclase laths (Fig. 8). These features are not due to replacement but probably represent residual liquid squeezed into openings between the crystals by the pressure exerted by the superincumbent crystal mush.

Intercumulus plagioclase in the melanorites is strained and is characterised by irregular extinction. These effects made optical determinations of the anorthite content of intercumulus material difficult (Fig. 9).

The crystals of the plagioclase-rich cumulates sometimes show lamination parallel to the pseudostratification of the layering. This feature is especially apparent in the anorthosite below the UG3 chromitite layer.

Exsolution of augite in cumulus orthopyroxene is frequently observed as fine exsolution striae, elongated blebs or even isolated lensoid shaped bodies parallel to the (100) plane of the orthopyroxene (Fig. 10). These exsolution lamellae commonly disappear close to the margins of the bronzite crystals, a feature that can probably be ascribed

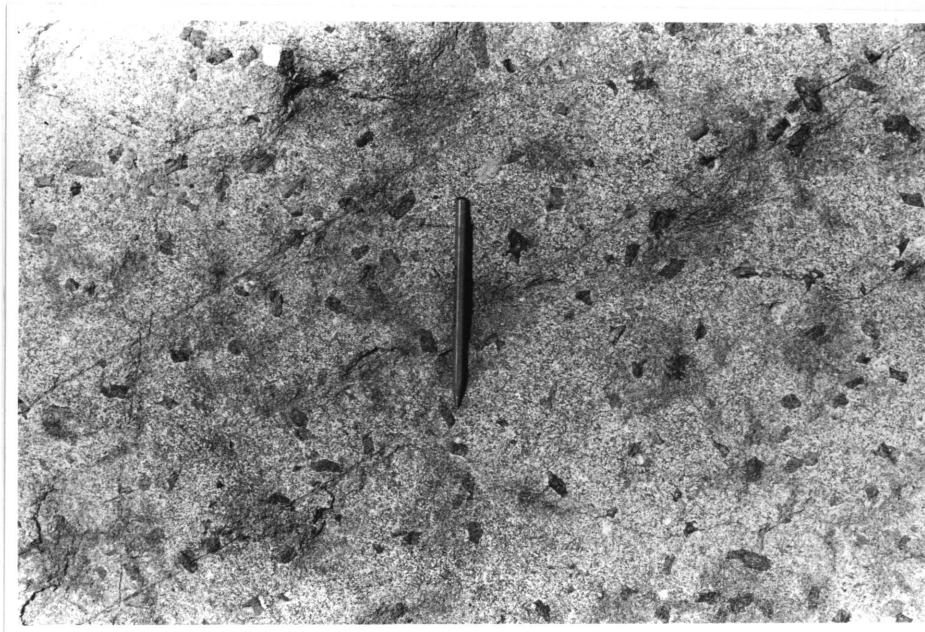


Figure 6 : Poikilitic melanorite above the UG3 chromitite layer in a donga close to the prospect shaft on Maandagshoek 254 KT. The large green oikocrysts of clinopyroxene enclose chromite, plagioclase and orthopyroxene.

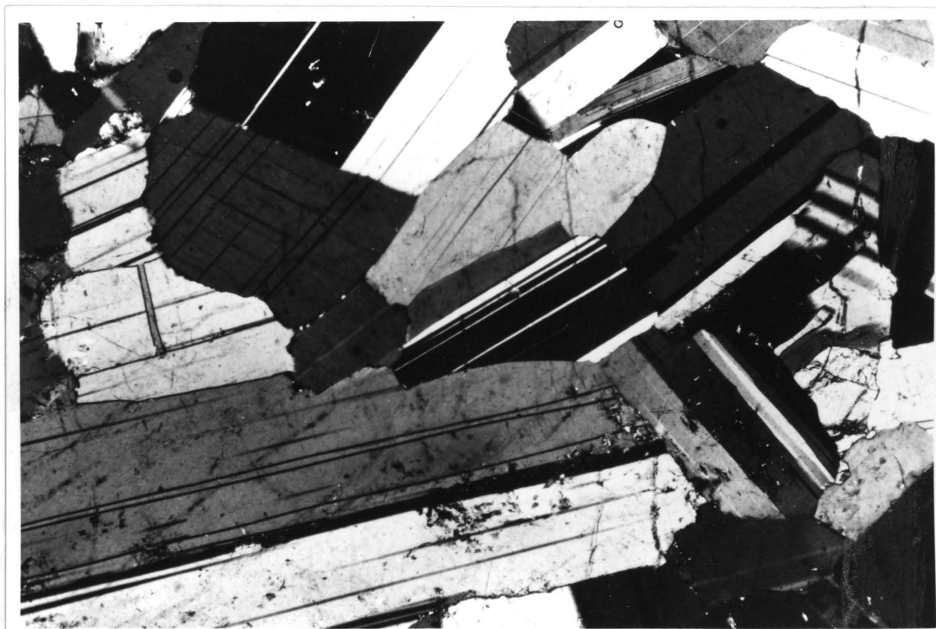


Figure 7 : Anorthosite at the top of the UG3A cyclic unit. Note the curved contact surfaces between the subhedral plagioclase grains which are indicative of simultaneous crystallization. Section A30; Transmitted light; Crossed nicols, 50X.



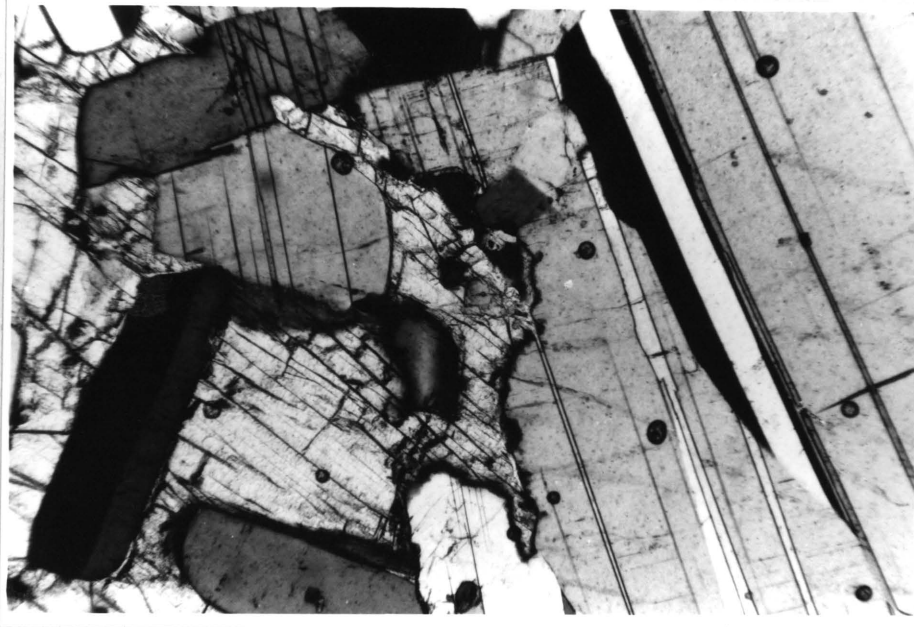


Figure 8 : Intercumulus bronzite forming irregular tongues in cumulus plagioclase. Section E 18; Transmitted light; Crossed nicols, 50X.



Figure 9 : Strain features, characterised by irregular extinction in intercumulus plagioclase, in a melanorite. Section B4; Transmitted light; Crossed nicols, 150X.

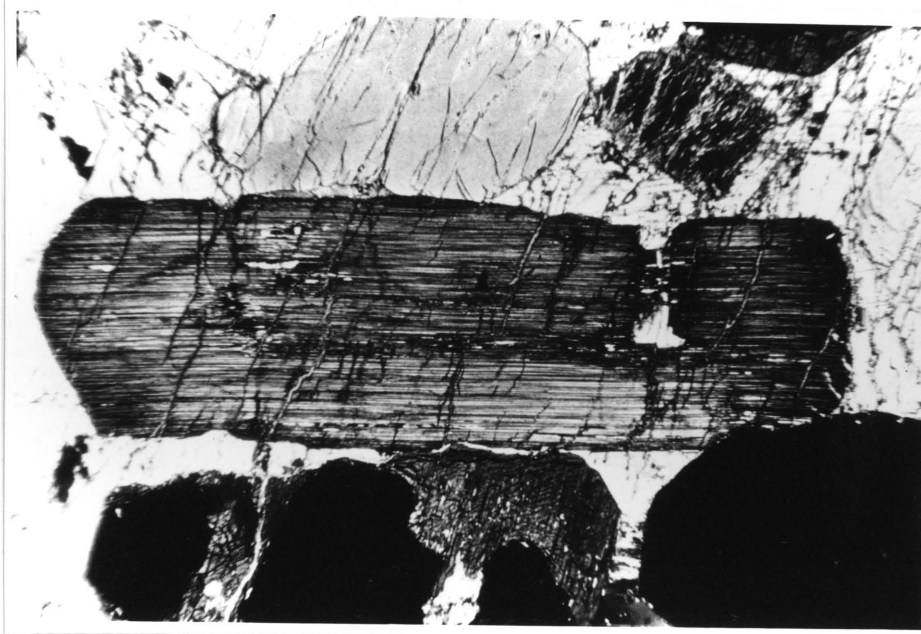


Figure 10 : Large (4mm long) euhedral grain of bronzite displaying thin exsolution lamellae parallel to the (100) plane of the orthopyroxene. Section E32; Transmitted light; Crossed nicols, 50X.

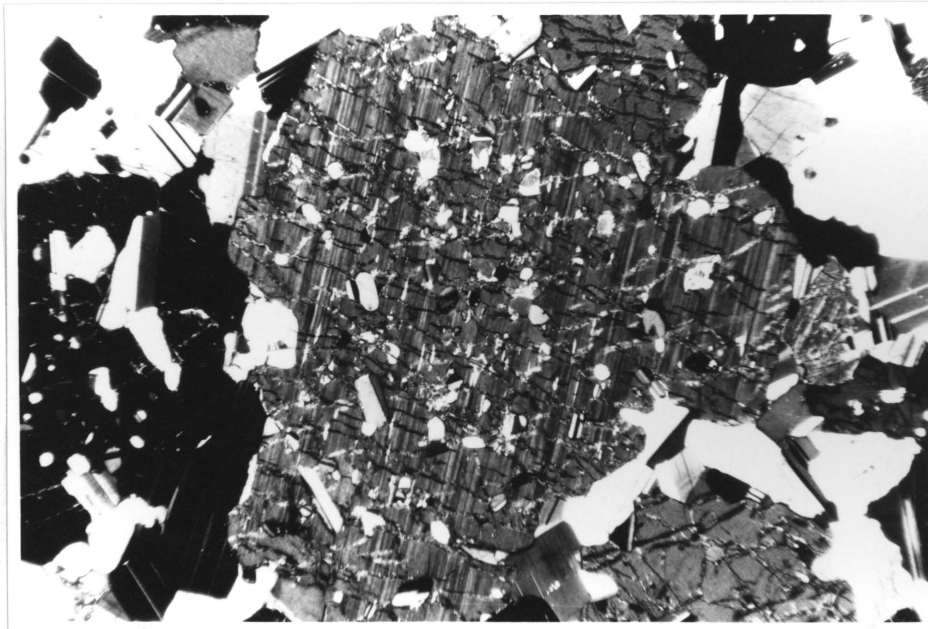


Figure 11 : Large oikocryst of orthopyroxene, 5mm in diameter, in a nodular gabbronorite, enclosing minute anhedral grains of plagioclase and clinopyroxene, below the UG1 chromitite layer. Section F5; Transmitted light; Crossed nicols, 50X.

to adcumulus overgrowth of less calcic orthopyroxene or it could indicate that Ca migrated out of the orthopyroxene close to the margin of the grain.

Clinopyroxene is sometimes seen to poikilitically enclose cumulus orthopyroxene (Fig. 12). Such features, termed coronophytic by Wells (1952, p. 919 - 921), are interpreted to represent reaction between the intercumulus liquid and the orthopyroxene.

Poikilitic clinopyroxenes, evenly distributed in the melanorites, are found in the rock sequences immediately overlying the chromitite layers (Fig. 6). The clinopyroxene, which is ubiquitous within the melanorites, was studied in detail and the type and proportion of enclosed minerals noted. Poikilitic clinopyroxene above the UG1 chromitite layers contains subhedral laths of plagioclase and bronzite, with sparse grains of included chromite. The clinopyroxenes above the UG2 chromitite layer contain little or no plagioclase and chromite but abundant rounded laths of bronzite, whereas those of the melanorites directly above the UG3 chromite layer contain abundant and evenly distributed chromite. The chromite grains included within the clinopyroxene are smaller and more rounded than those found in the associated cumulus bronzite and intercumulus plagioclase. In some instances the clinopyroxene contains chains or clusters of chromite. In the rocks above the UG3 chromitite layers there is a systematic upward decrease of chromite within the rock and within the clinopyroxene. None of the clinopyroxene above the UG3A chromitite layer contained chromite.

#### 2.2.2 Clinopyroxene - orthopyroxene - plagioclase cumulates

Two different types of gabbronorites are developed below the UG1 chromitite layer, viz., a fine grained variety and a "nodular" variety. In hand specimen the "nodular" gabbro-norite contains small bulbous forms which protrude above the surface of the rock (Fig. 13). On fresh surfaces the nodules

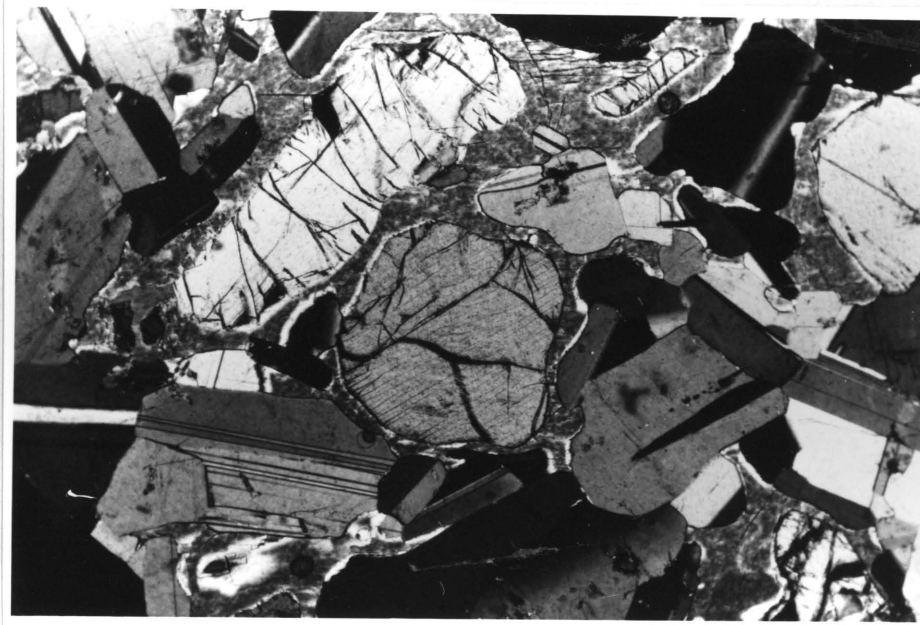


Figure 12 : Coronophytic halo of clinopyroxene poikilitically enclosing cumulus orthopyroxene grains. Section A4; Transmitted light; Crossed nicols, 50X.



Figure 13 : "Nodular" gabbro-norite from below the UG1 chromitite layer on Maandagshoek 254 KT. The nodules consist of orthopyroxene oikocrysts which include clinopyroxene and plagioclase. (See Fig. 11).

are brown while the matrix is light apple-green in colour. The fine-grained gabbronorite is interlayered with the coarser variety, but generally individual layers cannot be followed for great distances along strike. The relationship of both types of rock to each other is not consistent and thus in core logging and field mapping they were considered as one unit.

The "nodular" gabbronorites consist of large oikocrysts of anhedral orthopyroxene enclosing minute anhedral crystals of plagioclase and clinopyroxene (Fig. 11). These oikocrysts are commonly surrounded by a selvage of coarser-grained plagioclase feldspar. The fine-grained variety consists of cumulus plagioclase, orthopyroxene and clinopyroxene. The latter commonly constitutes more than 10 per cent of the mode. Chromite is not present in these rocks.

### 2.2.3 Chromite-bearing cumulates

#### 2.2.3.1 Chromitite layers

Four composite layers namely the UG1, UG2, UG3 and UG3A chromitite layers are present in the upper chromitite group. The positions of these layers within the cyclic units are illustrated in Figure 5. Sections E/A, E/B and E/C in Figures 14, 15 and 16 respectively show these layers in more detail.

##### 2.2.3.1.1 UG1 chromitite layer

The UG1 chromitite layer is typified by a complex interlayering of chromitite, anorthosite and melanorite (Fig. 17). Another distinctive characteristic is the association of green garnet (uvarovite?) with this layer (Cousins and Feringa 1964, p. 196). The UG1 chromitite layer does not have a consistent thickness and is usually made up of several layers of variable thickness (Fig. 17). The average cumulative thickness of the chromitite layers measured in four borehole intersections is 1,46 m.

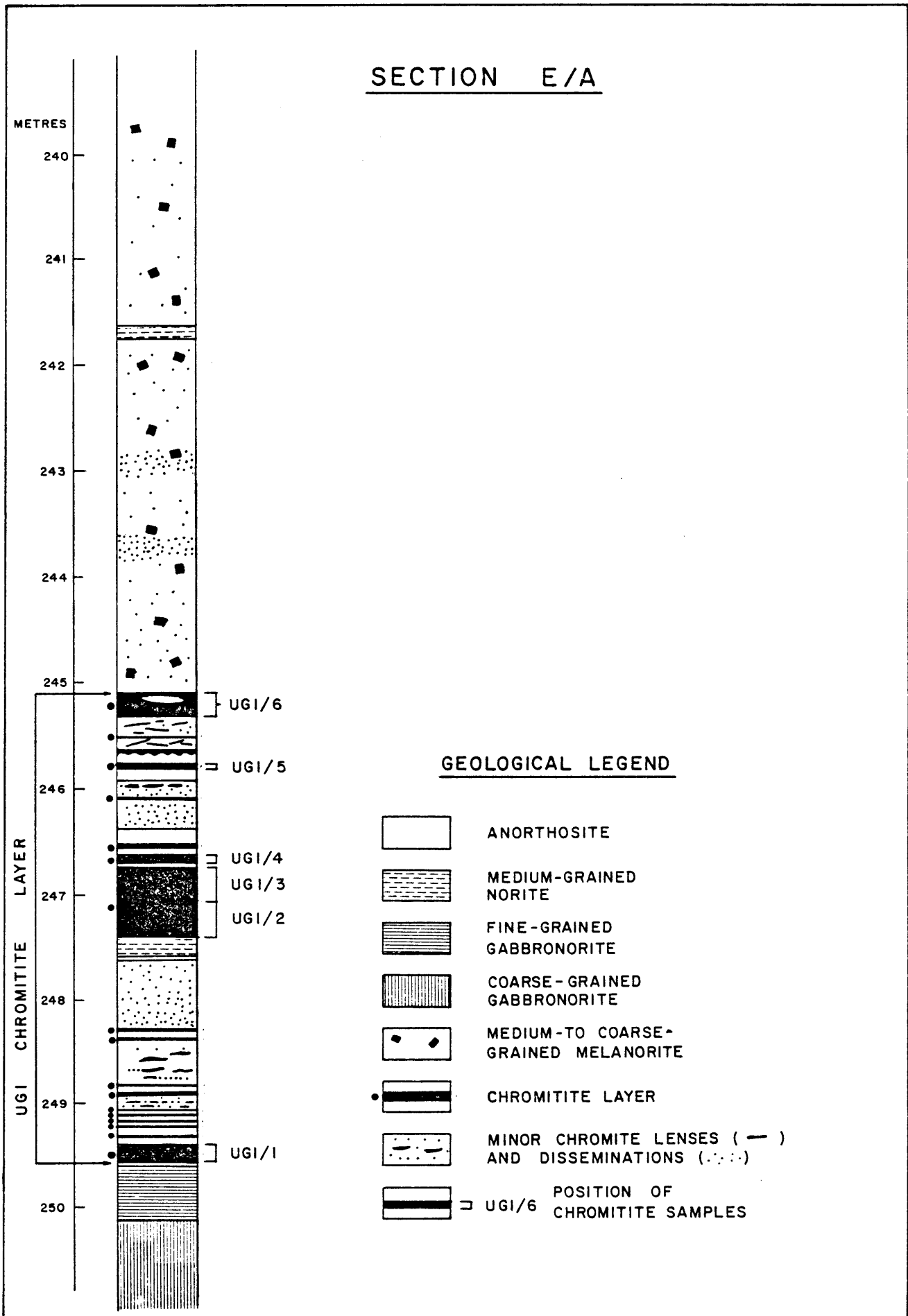


Figure 14 : The UG1 chromitite layer and its relationship to the enclosing lithologies.

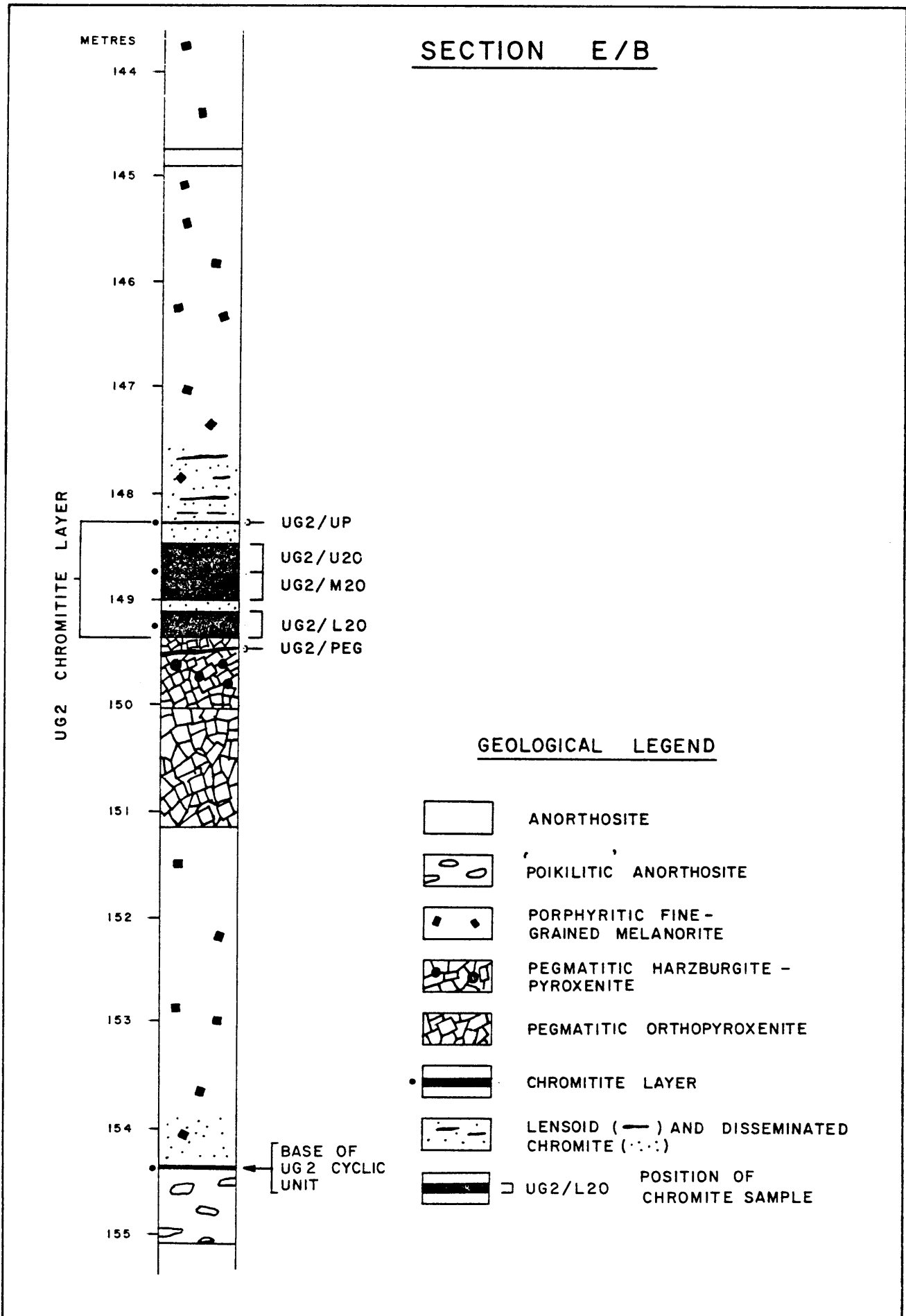


Figure 15 : The UG2 chromitite layer and its relationship to the enclosing lithologies.

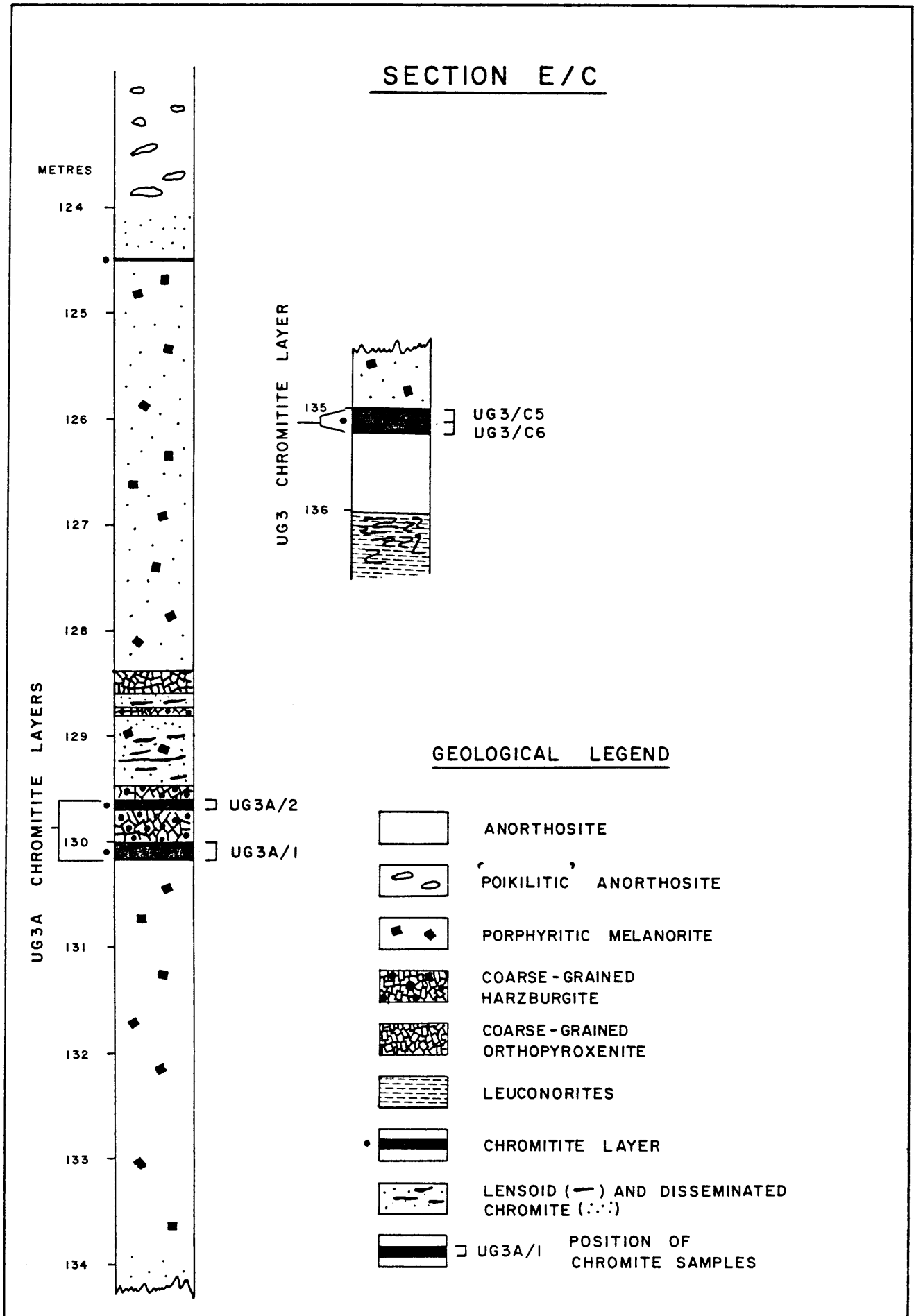


Figure 16 : The UG3 and UG3A chromitite layers and their relationship to the enclosing lithologies.





Figure 17 : Interlayered chromitite and anorthosite of the UG1 chromitite layer on Maandagshoek 254 KT.

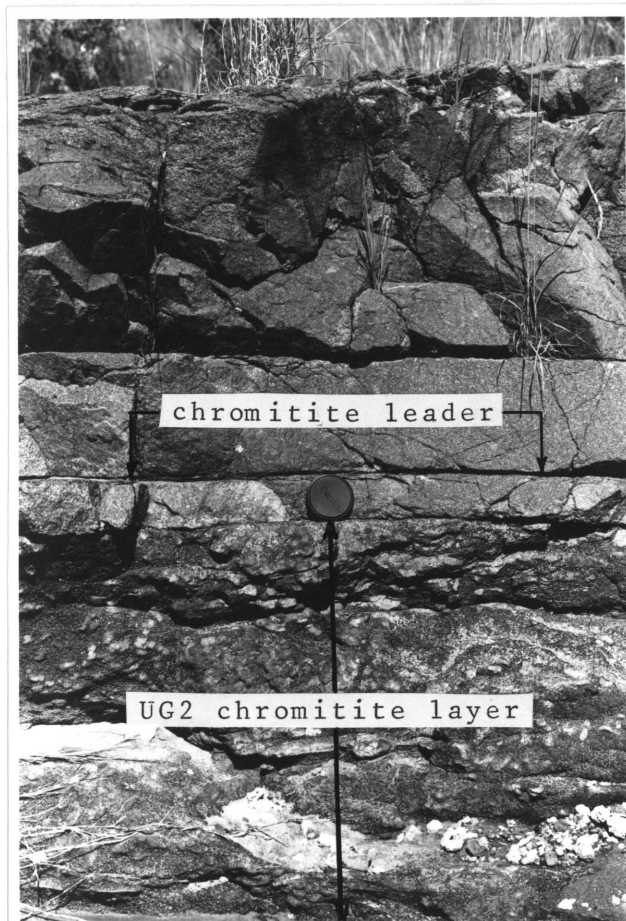


Figure 18 : The UG2 chromitite layer on Maandagshoek 254 KT. Note the competent fine-grained melanorite in the hanging-wall of the layer, the upper chromitite leader and the mottled nature of the chromitite layer.

The contacts between the anorthosite and chromitite layers are generally sharp but more gradational at the contact between melanorite and chromitite. The anorthosite associated with the UG1 chromitite layer typically contains trains of chromite parallel to the layering. The scale of such layering, and the modal proportions of chromite and plagioclase are variable. The structures associated with the UG1 chromitite layer will be described in some more detail in Chapter 5.

#### 2.2.3.1.2 UG2 chromitite layer

The UG2 chromitite layer is underlain by a mafic pegmatoid 0,20 to 0,50 m thick which usually contains an irregular chromitite layer 10 to 30 mm thick and about 0,10 m below the main chromitite layer. The main chromitite layer is 0,50 to 0,60 m thick and is overlain by a fine grained melanorite that contains a distinctive 5 to 10 mm thick chromitite layer some 0,10 to 0,15 m above the main layer (See Fig. 18). The UG2 chromitite layer is usually recognised in the field by its thickness and, when exposed, by its dirty and spotted appearance which is due to oikocrysts of bronzite (Fig. 18).

#### 2.2.3.1.3 UG3 chromitite layer

The UG3 chromitite layer is between 0,19 to 0,32 m thick, has a very dirty appearance in the oxidised zone and is seldom seen in outcrop. An anorthosite footwall with distinctive lenses of chromite forms a resistant pavement, however, which helps define the footwall of the UG3 chromitite layer in the field (Fig. 19). It is overlain by a very characteristic chromite-bearing poikilitic melanorite (Fig. 20).

#### 2.2.3.1.4 UG3A chromitite layers

The two layers which usually constitute the UG3A chromitite only outcrop at two localities on Maandagshoek.



Figure 19 : The UG 3 chromitite layer sandwiched between an anorthosite pavement in the footwall and a poikilitic melanorite in the hangingwall in the river section close to the prospect shaft on Maandagshoek 254 KT.



Figure 20 : Chromite-bearing melanorite overlying the UG3 chromitite layer ( Same locality as Figure 19 ).

The UG3A chromitite layers vary in thickness, but generally consist of a 0,15 m thick lower layer and a 0,10 m thick upper layer set in coarse-grained chromitiferous orthopyroxenite and harzburgite (Fig. 21).

#### 2.2.3.2 Textural features of chromite in chromite-bearing lithologies

Chromite generally has an heterogenous modal distribution within the chromitite layers as is evidenced by the range in modal percentage. The average percentage range is given in parentheses :-

UG1 chromitite layer, 65(52 - 90) per cent

UG2 chromitite layer, 70(60 - 95) per cent

UG3 chromitite layer, 54(50 - 55) per cent

UG3A chromitite layer, 50(40 - 60) per cent.

The bimodal distribution of grain size of the chromite is evidenced by fine-grained chromite locked in intercumulus plagioclase and bronzite, interspersed by irregular aggregates of coarse-grained chromitite. Microscopically these irregular patches are composed of tightly interlocking polygonal chromite with hardly any interstitial minerals (Fig. 22).

The UG2 and UG3A chromitite layers commonly show a mottled texture in surface exposures, due to oikocrysts of bronzite. These intercumulus bronzites enclose numerous chromite grains that are much smaller than the surrounding chromite grains (Fig. 23). Cameron (1969 p. 762 - 766) considers that these smaller chromite crystals represent settled chromite crystals that were trapped by in situ nucleation and growth of postcumulus bronzite and shielded by overgrowth. He concludes that it is thus possible to compare the approximate size of the initial grain size with those after postcumulus enlargement.

Chromite is also found as disseminations, chains and minor chromitite layers in the rocks of the upper critical zone. Chains of subhedral chromite, usually with intercumulus plagioclase, are found within the melanorites (Fig. 24) of

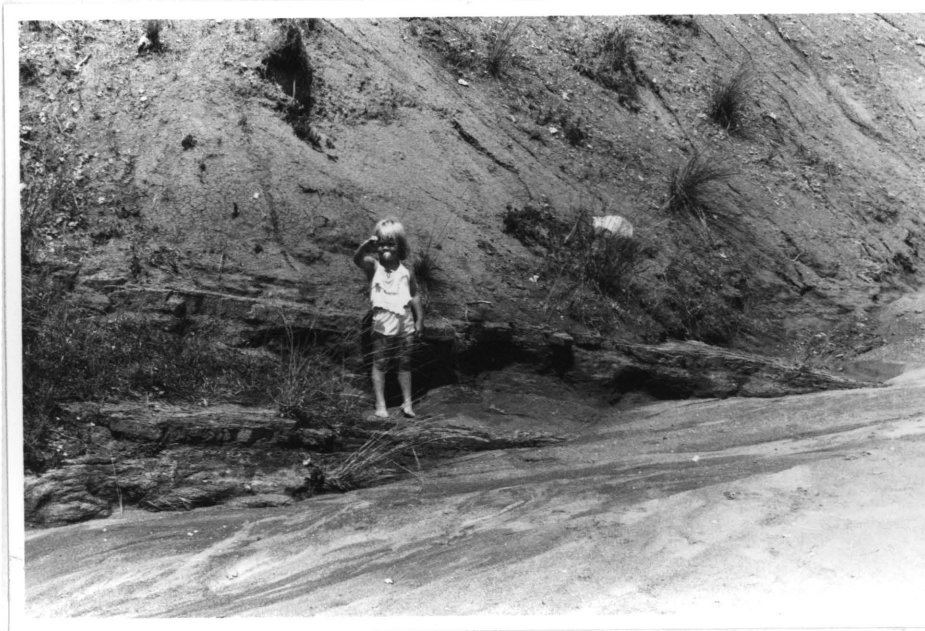


Figure 21 : Two resistant chromitite layers which make up the composite UG3 chromitite layer located in a stream section close to the prospect shaft on Maandagshoek 254 KT.

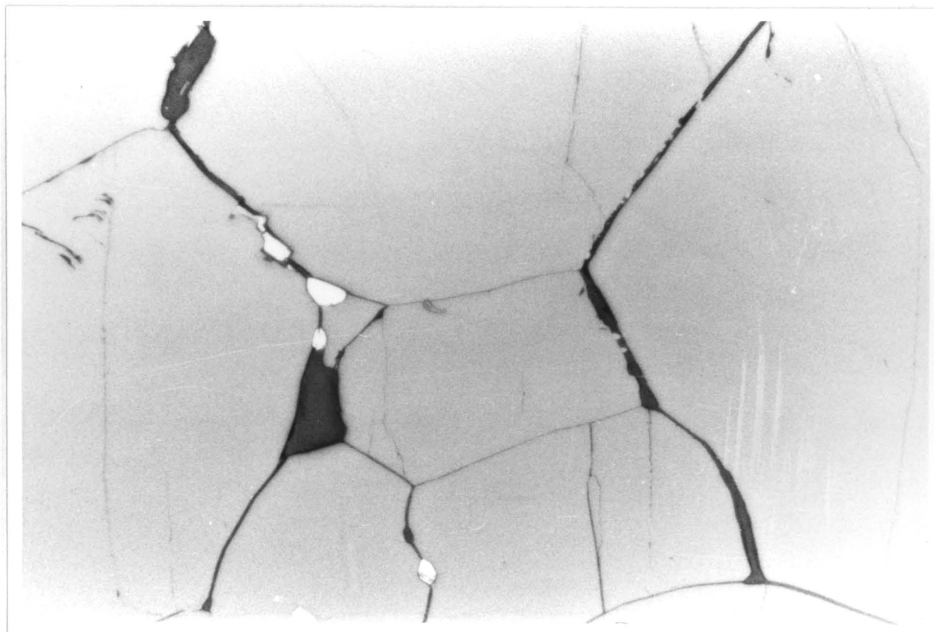


Figure 22 : Coarse-grained aggregate of polygonal chromite enclosing minor intergranular silicate pyrrhotite and chalcopyrite. Section MDH5/UG2/27; Reflected light, 60X.

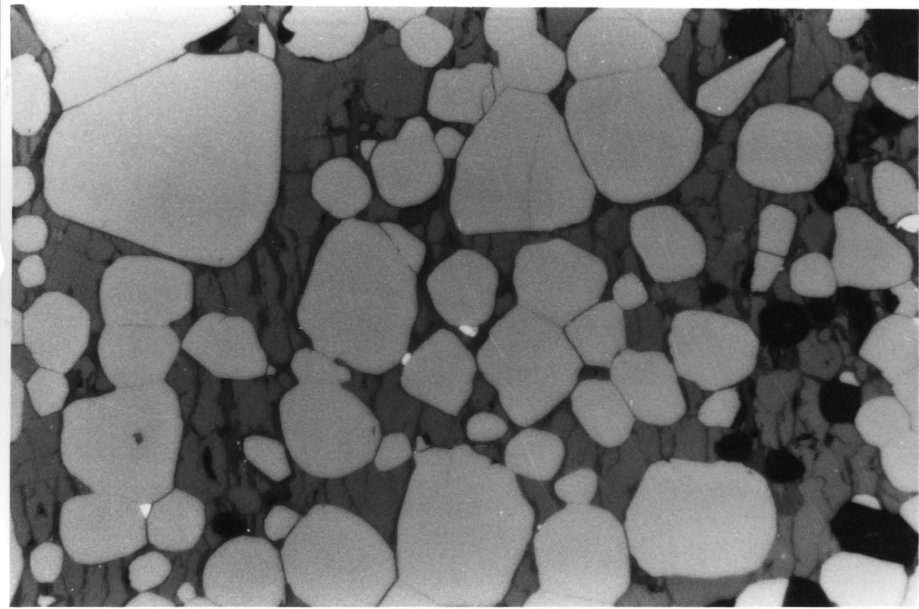


Figure 23 : Oikocryst of bronzite enclosing subhedral chromite crystals in the UG2 chromitite layer. Small sulphide grains are pyrrhotite. Specimen MDH7/UG2/3; Reflected light, 60X.

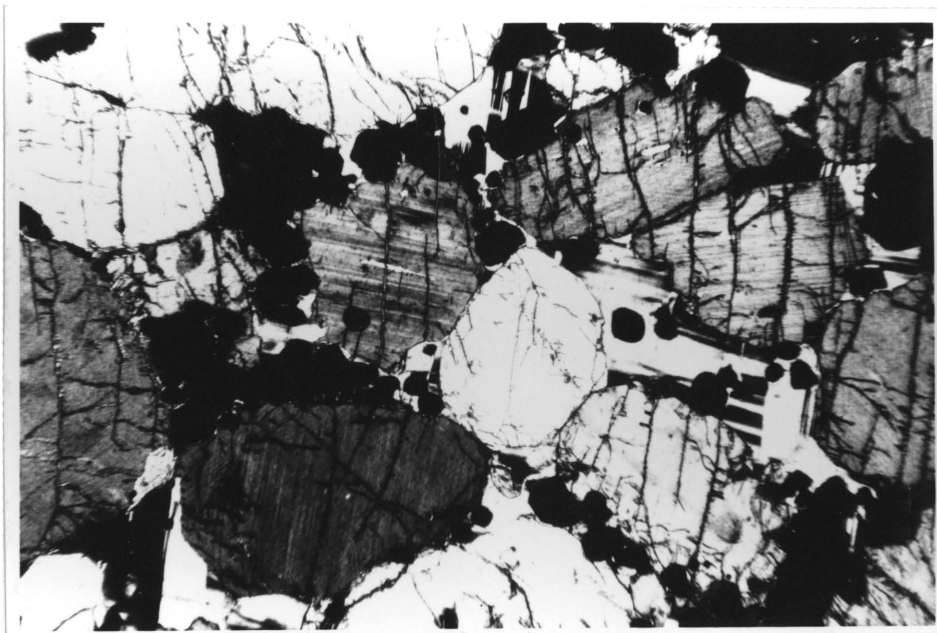


Figure 24 : Chains of subhedral chromite associated with intercumulus plagioclase in melanorites of the UG1 chromitite layer. Section E92; Transmitted light; Crossed nicols, 50X.

the UG1 chromitite layer and are also located within the olivine-rich layers of the UG2 and UG3A chromitite layers.

Minute, rounded silicate inclusions are occasionally found in the chromite grains (Fig. 25). The compositions of these inclusions have not been determined. Hulbert and Von Gruenewaldt (1980, p. 19 - 20) have described such features from chromitite layers at Grasvally and Zoetveld.

Chromite is present as a minor accessory component (0,2 to 0,4 per cent of the mode) throughout the cyclic units and is commonly found as euhedral crystals within the intercumulus material. These crystals are commonly rimmed by biotite which indicates a reaction relationship with the intercumulus liquid.

#### 2.2.4 Olivine-bearing cumulates

Olivine is the least abundant cumulus mineral studied in the cyclic units and is developed in the pegmatoid below the UG2 chromitite layer and in the rocks associated with the UG3A chromitite layer. Cumulus olivine usually occurs in small irregular lensoid bodies which have their long axes coplanar to the layering.

The olivine grains are euhedral and their presence in the rocks is usually accompanied by an increase in the amount of cumulus chromite. Cumulus chromite generally comprises more than 5 per cent of the mode of these rocks and may even reach 40 per cent, especially in the vicinity of the UG3A chromitite layer. In such environments chromite commonly forms chains, set in intercumulus plagioclase and orthopyroxene, which drape over the rounded grains of olivine.

No totally fresh olivine was observed and it has in all cases been almost completely altered to serpentinite (Fig.26)

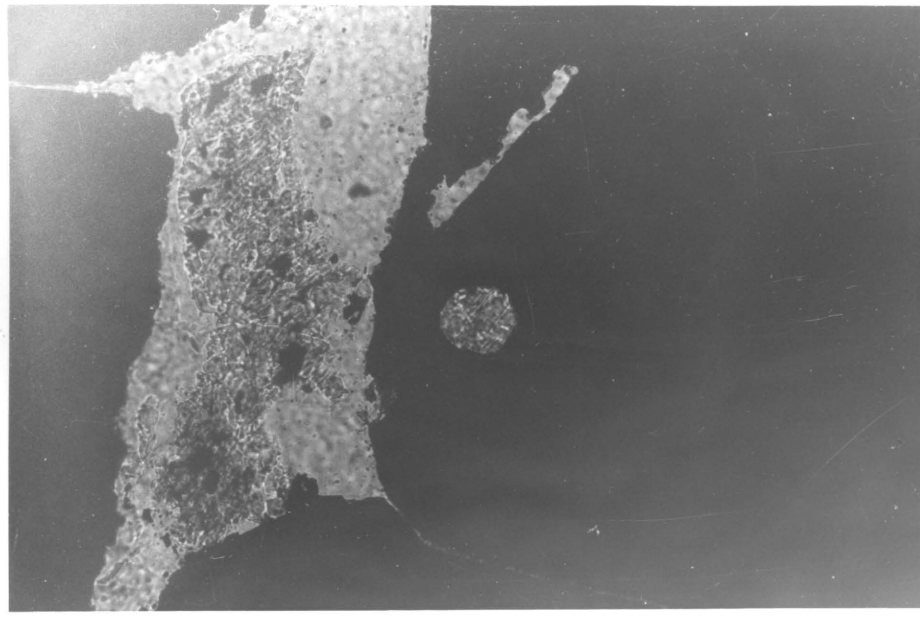


Figure 25 : Unidentified round silicate inclusion in a chromite grain of the UG1 chromitite layer. Section E 89; Transmitted light; Uncrossed nicols, 600X.

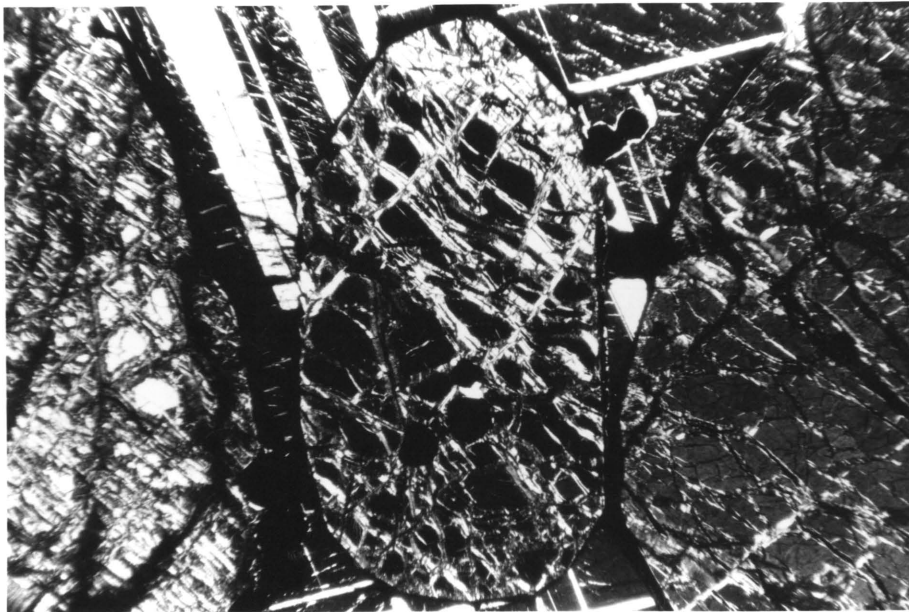


Figure 26 : Serpentinized olivine grain from the UG3A chromitite layer. Section B9; Transmitted light; Crossed nicols, 50X.



and typified by an irregular lattice work of magnetite. Occasional grains contain clear, *angular* islands of unaltered olivine which were analysed by means of the microprobe.

#### 2.2.5 Transgressive pegmatoids/pipes

Three large mafic pipes, indicated as A, B, C on Figure 3 and Folder A, outcrop on Maandagshoek while four other pegmatoids were inferred and subsequently intersected by drilling. Apart from these larger pipes, many smaller pegmatoids were mapped on surface.

The three main pipes were not thoroughly investigated. The first pipe, pipe A, crops out on the top of a prominent hill west of the turn-off to the Maandagshoek Mission (Fig. 27). The main body of the pipe is approximately 300 metres in diameter with the outer contacts covered by scree. The pipe consists of a core of olivine altered to highly magnetic, bluish-grey serpentinite, surrounded by a rim of coarse-grained peridotitic rocks.

Pipe B lies on a small plateau close to the eastern boundary of Maandagshoek 254 KT. Both pipes A and B are cut by the same dolerite dyke. No olivine, or its alteration products were seen in hand specimen but the geochemical sampling showed a core of opaline gossan (berberite) to contain more Ni than the surrounding pegmatoidal pyroxenites. The pipe appears to have a sharp contact with the surrounding layered rocks. Slabs of chromitite have been mapped in pipe B. Analyses show them to have very low PGE values. Of interest is that the chromitite contains a little uvarovite and intercumulus plagioclase, both typical of the UG1 chromitite layer.

The third pipe, Pipe C, is located 1,4 kilometres from the turn-off to the mission station on the road to Driekop. The pipe consists of a small harzburgite core and an outer zone of orthopyroxenite that contains irregular pegmatoidal patches. Borehole MDH 3, drilled to investigate



Figure 27 : View of Pipe A from an altitude of approximately 300 m looking NNE. Note the circular outline of the pipe, the position of the prospect shaft and spoil dump in the foreground.

pipe C, intersected coarse-grained orthopyroxenite that contains small quantities of sulphides. Borehole MDH 9 intersected an apophysis of Pipe C consisting of coarse-grained pyroxenite, peridotite and highly magnetic serpentinite. A surface magnetometer survey has shown pipe C to be 800 m long and 400 m wide (see Folder A). Contacts between the pipe and the layered rocks are sharp.

#### 2.2.6 Dolerite dykes

Three major and many minor dolerite dykes cut the critical zone. The general trend is from 30 to 45°. The pipes are also aligned along this trend and are commonly cut by the dolerite dykes (Fig. 3 and Folder A). Outcrops of fresh dolerite are particularly scarce, but when found display spheroidal weathering, are bluish-black in colour with a reddish-brown oxidised surface. Smaller dolerite dykes weather to form blocky fragments.

### 3 DESCRIPTION OF THE CYCLIC UNITS

#### 3.1 Introduction

Portions of the upper critical zone on Maandagshoek 254 KT consist of a sequence of rocks in which fractional crystallization has resulted in the cyclic repetition of lithologies ideally consisting of chromitite and harzburgite at the base and changing upwards through melanorite, norite, leuconorite to anorthosite at the top of the unit. As such, this repetitive sequence of lithologies satisfies the requirements of a cyclic unit which was defined by Jackson (1961) as "a sequence of particular isomodal and mineral graded layers that are repeated a number of times". If such a sequence of rocks fails to complete a cyclic unit it is called a beheaded cyclic unit (Jackson 1961).

The above cyclicity is not ubiquitously developed in the mafic portion of the Bushveld Complex, although Vermaak (1976, p. 1284) recognises the Merensky Unit as a cyclic unit. Cameron (1978, p. 439 - 444) has described a few cyclic units near the top of the harzburgite subzone of the basal zone consisting of dunite, with accessory chromite, at the base followed by harzburgite with bronzitite at the top. Hulbert (personal communication) has identified cyclicity in the lower zone of the Potgietersrus compartment.

Microscopic investigations of the cyclic layers in the upper critical zone entailed modal analyses and changes in the grain sizes (IC Numbers). Regarding the modal variations, Jackson (1961) described problems he encountered in correlating individual layers and cyclic units of the Stillwater Complex due to changes in the bulk composition and the mineral proportions. Such work led him to differentiate between the cumulus minerals and the intercumulus mesostasis in which the cumulus minerals such as olivine and pyroxene became a superb aid in stratigraphic correlation. Such problems were not encountered on Maandagshoek due to the extremely good lateral continuity of the individual layers and by using the

modal classification of Streckeisen (1976). A total of 213 *thin* sections were inspected and the results are shown on the detailed geological column (Folder B).

Jackson (1961), Cameron and Emerson (1959), Hawkes (1967), and McDonald (1967) used grain size variations, or other closely related parameters, in examining textural and other variations through the cyclic layers. Both Jackson (1961) and Irvine and Smith (1969) found sharp grain size variations at the top and bottom of cyclic units and also sharp increases in the size of the minerals below the chromitite layers in the Stillwater and the Muskox Complexes. Cameron (1969, p. 770 - 771) doubted the usefulness of such investigations as he feels that cumulus grains have undergone postcumulus growth and that they are therefore not indicative of their original size. Grain size variations were, however, measured in terms of IC Numbers and the results are portrayed in Folder B.

### 3.2 The UG1 cyclic unit

The UG1 cyclic unit is poorly exposed but four boreholes intersected the sequence. The average vertical thickness of the unit, from the UG1 chromitite layer to the anorthosite at the top of the unit is 90 m (Fig. 5, p. 15). The section shown in Folder B is based on modal counts of 95 thin sections while the synoptic diagram, section E/A shows the lower portion of the UG1 cyclic unit (Fig. 14, p. 23).

The UG1 chromitite layer lies at the base of the UG1 cyclic unit. The complex interrelationships between discrete anorthosite, chromitite and melanorite layers within the UG1 chromitite layer are illustrated in Figure 14. The measured cumulative thickness of the chromitite components of this layer ranges between 0,96 to 2,11 m in the four borehole intersections. Chromite stops as a major cumulus phase approximately 3 m above the uppermost chromitite layer and is only present in trace amounts above this level. The UG1 chromitite layer is underlain by rocks which contain cumulus orthopyroxene, clinopyroxene, plagioclase and chromite and is *overlain* by a 33 m thick layer of poikilitic melanorite. Bronzite is

the only cumulus phase and forms up to 80 per cent of the rock while intercumulus bytownite and chromiferous augite respectively constitute between 10 to 25 per cent and 5 to 10 per cent of the rock. This sequence does contain minor layers of norite-leuconorite, up to one metre in thickness, the positions of which may be seen in the detailed profile (Folder B).

Seven metres of interlayered norites and leuconorites with minor chromitite layers overly the melanorite. Both bytownite and bronzite are cumulus and apart from two chromitite layers, 0,12 m thick with 12 per cent chromite at the base and a 5 mm thick stringer with 40 per cent chromite at the top, the leucocratic rocks contain less than 0,1 per cent chromite. For the next 19 metres upwards the melanorites become progressively more leucocratic. Both bronzite and bytownite are cumulus while chromite never forms more than 0,2 per cent of the mode. The vast majority of the observed chromite crystals are rounded and found enclosed close to the core of bronzite.

A mottled anorthosite layer, two metres thick, defines the top of the UG1 cyclic unit. It is invariably parted by a 10 to 20 mm thick layer of chromitite about 1,2 m above the base of the anorthosite and is usually overlain by a thin one millimetre thick chromitite marker at the base of the overlying melanorites of the UG2 cyclic unit.

The gabbronorites below the UG1 chromitite layer contain discrete populations of IC numbers, one of 140 to 150 associated with "nodular" gabbronorites, and the other of 210 to 280 for the fine-grained gabbronorites. The multicomponent nature of the UG1 chromitite layer, on the other hand, is reflected in large fluctuations ranging from 100 to 220. The average IC number within the UG1 chromitite layer of 150 rapidly decreases to 60 four metres above the layer while the poikilitic melanorite layer has an average number of 65. The norite and leuconorite gradually decreases

to 100 six metres below the top of the cyclic unit. Where plagioclase becomes the sole cumulus mineral, at the top of the UG1 cyclic unit, the IC number increases to 125.

### 3.3 The UG2 cyclic unit

The UG2 cyclic unit has been intersected by 17 diamond drill-holes during the diamond drilling programme of Mining Corporation. The average thickness of the UG2 cyclic unit is 16,5 m (Folder B and Fig. 15, p. 24) with a tendency to increase slightly in a down-dip direction.

A medium-grained melanorite, underlain by a fine hair-line layer of chromitite, lies at the base of this cyclic unit. The melanorite consists of 70 to 80 per cent cumulus orthopyroxene, with intercumulus plagioclase and clinopyroxene forming the balance of the mode. It gradually coarsens upwards to a footwall pegmatoid below the UG2 chromitite layer, the thickness of which varies between 0,5 to 1,0 m. In the pegmatoid a variety of rock types may be found due to fluctuations in the proportions of the cumulus minerals pyroxene, olivine and chromite. Large intercumulus oikocrysts of clinopyroxene impart a "porphyritic" texture to these rocks. In the prospect shaft, the footwall pegmatoid is parted by an irregular chromitite layer which lies about 0,1 m below the main UG2 chromitite layer. The footwall contact of the UG2 chromitite layer is dimpled. These dimples average 10 mm in height. The main chromitite layer is 0,50 m thick and is separated from a 0,5 - 1,0 cm thick leader chromitite layer by 0,10 - 0,15 m of fine-grained melanorite.

Small lenses and disseminations of chromite (0,6 per cent) are found for about a metre in the overlying fine-grained melanorite. Two thin anorthosite markers are developed about three metres above the UG2 chromitite layer in the poikilitic melanorite. These anorthosite layers are commonly capped by thin chromitite lenses. The melanorite

changes upwards through norite, leuconorite to a thin anorthosite layer at the top of the cyclic unit. The IC numbers in the anorthosite at the top of the UG1 cyclic unit, and the melanorite at the base UG2 cyclic unit change from 125 to 70 and decrease upwards to 16 in the pegmatoid directly below the UG2 chromitite layer. Within the UG2 chromitite layer the average IC number is just under 300. The upward increase in cumulus plagioclase is reflected in an upward increase in IC numbers in the melanorite which change from 70 to 140 and eventually to 200 in the overlying anorthosite.

#### 3.4 The UG3 cyclic unit

This unit, only some 6 m thick, is very poorly exposed, and the following observations are essentially confined to the interpretation of borehole data and observations in the prospect shaft (Fig. 16, p. 25). The UG3 chromitite layer, at the base of the cyclic unit, has sharp lower and upper contacts and an average thickness of 0,22 m. The hanging wall of the UG3 chromitite layer consists of a 5,5 m thick layer of poikilitic melanorite, with less than 0,2 per cent chromite and in which the intercumulus oikocrysts of clinopyroxene comprise 5 - 10 per cent of the rock. No upward increase in the percentage of plagioclase was noted. The IC numbers of the UG3 chromitite layer range between 310 to 350. Above this layer the IC numbers of the poikilitic melanorites decrease rapidly to 50 which changes to 40 at the top of the cyclic unit.

#### 3,5 The UG3A cyclic unit

This unit is rarely seen on surface but was intersected in 17 boreholes and in a prospect shaft. The UG3A cyclic unit has two chromitite layers (Figs. 16 and 21) enclosed in coarse-grained chromite-rich harzburgite at the base. This is overlain by a five metre thick layer of poikilitic melanorite of which the lower two metres contain large green oikocrysts of clinopyroxene. About 4,5 per cent cumulus chromite is present in the melanorite for about a metre



above the chromitite layer. A hairline thick chromitite layer defines a contact between the melanorite and an overlying 12 metre thick sequence of poikilitic anorthosites which gradually change upwards through leuconorites to norites (Folder B).

The lower 2 metres of the UG3A cyclic unit displays a series of rapid reversals in the IC numbers which range from 100 to 270 with an average of 150. The porphyritic melanorites have a constant IC number of 40 while the overlying sequence of anorthosites-leuconorites show an upward increase in IC number from 75 to 110 which reflects the increase of modal orthopyroxene. (See folder B).

## 4 MINERAL CHEMISTRY

### 4.1 Introduction

The major and minor element chemistry of plagioclase, orthopyroxene and clinopyroxene were determined to define if regular compositional changes took place in the cyclic units. The compositions of coexisting clinopyroxene - orthopyroxene and chromite - olivine pairs were determined and used as geothermometers to measure their respective temperatures of crystallization.

The preparation of samples and the analytical techniques used have been described in Chapter 1.

### 4.2 Plagioclase

#### 4.2.1 Major element analyses

In the assessment of the XRF spectrographic results (Appendix 1) it should be noted that this method allows only for the determination of the average composition of both cumulus and intercumulus portions of the plagioclase separates. Because of the uncertainty of the influence of the intercumulus portion of the composition, the anorthite content of the plagioclase was also determined with the aid of optical methods essentially Eulerian angles and optic axial angles as well as with the aid of refractive index determination on glass beads. Wavy extinctions in many of the samples often made precise optical measurements impossible. Comparison of the results showed (Appendix II) that determinations by the Eulerian angles gave An values of 1,5 to 2,0 per cent lower, and the 2V method 1,0 to 1,5 per cent lower than the XRF method. The weighted average of four different methods was used to plot variations in the anorthite content through the various cyclic units (Folder B).

In the gabbro-norites below the UG1 chromitite layer the plagioclase averages  $An_{77,4}$ . At the base of the UG1 cyclic unit, in plagioclase associated with the UG1 chromitite layer,  $An_{77,5}$  was determined. There is an abrupt increase in the An-content of the plagioclase in the poikilitic melanorites above the UG1 chromitite layers up to  $An_{83,9}$

which gradually drops to  $An_{76,0}$  at the top of the melanorites and increases slowly to  $An_{80,8}$  at the top of the cyclic unit.

Cumulus plagioclase in the UG2 cyclic unit generally shows a very regular composition of  $An_{78,0}$ . The composition however, increases at the top of the UG2 cyclic unit where analyses of the plagioclase shows an anorthite content in excess of  $An_{85,0}$  (Folder B). Plagioclase is not commonly found in the UG3 and UG3A cyclic units. In the sequence of anorthosites overlying the UG3A cyclic unit the An content increases progressively from  $An_{79,3}$  at the base, to  $An_{81,5}$  at the top. The anorthite content of the plagioclase in the overlying sequence of leuconorite to norite drops with some fluctuations from  $An_{81,5}$  to  $An_{77,5}$  at the top of the investigated succession.

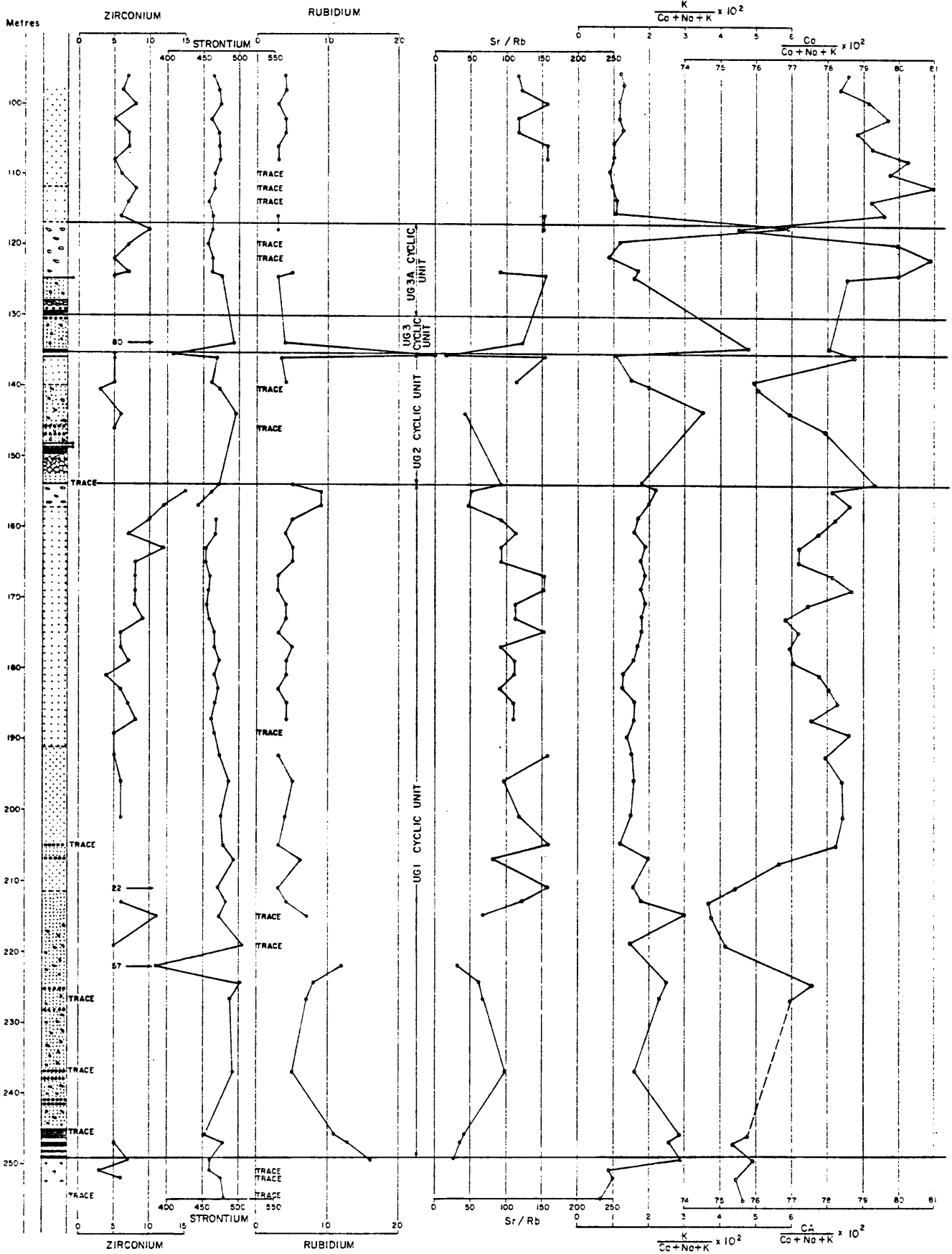
#### 4.2.2 Trace element analysis

Sixty-four plagioclase separates were analysed for the trace elements Y, Zr, Sr and Rb ( Appendix III) in an effort to determine whether the plagioclase displays regular changes in these components in the cyclic units. The mean concentration of Y within the 64 plagioclase analysed is four ppm with a standard deviation of one ppm. Values are low throughout the investigated succession and there is no indication of any Y enrichment in the upper parts of the cyclic units (Fig. 28). The observed concentrations are slightly lower than the six ppm reported for the Bushveld by Frey et al. (1968, p.6088), while Wedepohl (1972) reports values of one ppm Y in plagioclase with a composition of ( $An_{55}$ ) and eight ppm Y in plagioclase ( $An_{20}$ ). Similarly, very little information is available in the distribution of Zr in plagioclase feldspars. The mean of Zr in the suite of the plagioclase investigated is six ppm if the two samples C4 and E62 are ignored. It is tentatively suggested that the high values in the latter two samples are due to the presence of zircon in the plagioclase separates. Because of its ionic potential and ionic radius

(0,79Å), Zr is not readily incorporated into silicate structures and tends to concentrate in the residual liquids during fractional crystallization (Ahrens, 1965, p. 40). It is therefore expected that the Zr content of the plagioclase <sup>separates</sup> could provide good evidence of cyclicity and it can readily be seen that Zr does show an upward enrichment in both the UG1 and UG3A cyclic units.

The mean Rb content in the plagioclase feldspars studied is seven ppm. The low concentration of Rb within the plagioclase may be explained by the fact that the large cation Rb (1,49Å) does not easily substitute for the smaller cations Na (0,98Å) and Ca (1,06Å). An increase in Rb does, however, correlate with the increase in K as may be seen in samples UG3B and UG3C as the two singly charged cations K<sup>+</sup> and Rb<sup>+</sup> have radii that are very similar, 1,33Å and 1,49Å respectively and that Rb is substituted for K in the plagioclase structure (Heier, K.S. 1962, p427). Smith (1972, Fig. 14-8) who has plotted the Rb content of feldspars against major element concentration, found that, in general, the Rb content for a plagioclase of An<sub>80</sub> can lie between one to eight ppm which correlates well with the results of this study. There is a pronounced increase in Rb at the top of the UG1 cyclic unit where plagioclase is the major cumulus mineral present. The antipathetic relationship between Rb and Sr is also evident (Fig. 28).

The mean of 460 ppm Sr is 40 - 130 ppm lower than the plagioclase analysed by Ferguson and Wright (1970, p. 79) in roughly the same position in the critical zone in the western Bushveld Complex. Although the Sr ion has the same charge as the Ca ion, its radius of (1,12Å) is about halfway between that of Ca (0,98Å) and K(1,33Å). Consequently the substitution of Sr into feldspars is not simple even on the ionic model. Ferguson and Wright (1970, p.64) found that the distribution coefficient between Sr and Ca is greater than that between Sr and K in cumulate plagioclases (Fig. 28).



NOTE  
FOR EXPLANATION OF  
GEOLOGY SEE FOLDER B

Figure 28 : The distribution of Zr, Sr, Rb, Sr/Rb,  $K/Ca+Na+K \times 10^2$ ,  $Ca/Ca+Na+K \times 10^2$  in plagioclase separates in borehole MDH7.

Smith (1972, Table 14 - 14) has plotted the relationship between Sr content and major element content of feldspars from coarse-grained rocks from available published data and noticed an extremely complex relationship. There is, however, a fairly regular trend from approximately 400 ppm Sr at An<sub>80</sub> to about 1100 ppm Sr at An<sub>40</sub>. This decrease in the amount of Sr with an increase in the amount of the anorthite component in the plagioclase is also evident at the top of the UG2 cyclic unit.

The Sr/Rb ratio is lower in the plagioclase-rich cumulates which in turn all display a slightly higher K/Ca + Na + K ratio. (Fig. 28).

### 4.3 Pyroxenes

#### 4.3.1 Orthopyroxene

##### 4.3.1.1 Major element analyses (Appendix IV)

Seeing that the composition of cumulus orthopyroxene in chromite-rich cumulates is modified by post-cumulus equilibration between chromite and orthopyroxene (Cameron 1970, p. 52 - 54 and Cameron 1980, p. 855) and hence a function of the modal proportions of these two phases, only orthopyroxenes from rocks with less than 2 weight per cent Cr<sub>2</sub>O<sub>3</sub> were analysed and used to construct the compositional trend (Folder B). It should also be noted that throughout the sequence, but especially in the melanorites, small primocrysts of chromite are found in the centre of the orthopyroxene grains and hence inhibit a clean magnetic separation.

The bronzites contain approximately 1,5 weight per cent CaO. The CaO appears to be present in the form of a calcium-rich monoclinic pyroxene, exsolved parallel to the (100) plane (Hess and Philips, p. 454, 1940) and also in the form of a coronophytic halo of clinopyroxene around the bronzite.

The compositional trends of the orthopyroxene are expressed in terms of the ratio Mg/Mg + Fe (where Fe = Fe<sup>2+</sup> + Mn) (Folder B). In the gabbronorites below the UG1

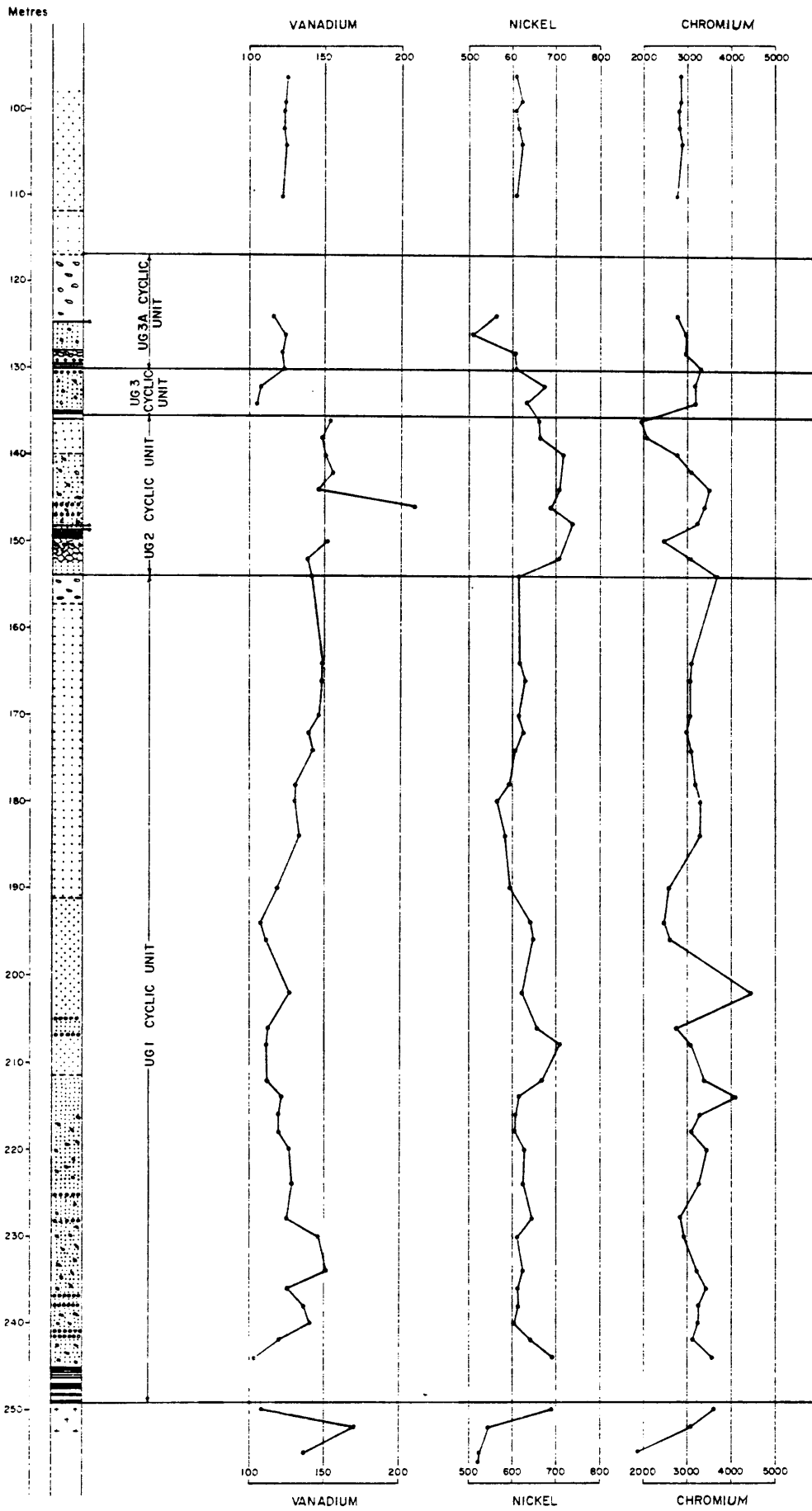
chromitite layer the En content of the bronzites increases from En<sub>77</sub> to just under En<sub>81</sub> close to the layer. In the poikilitic melanorites above the UG1 chromitite layer the composition of the bronzite drops to En<sub>77</sub> ten metres above the layer, but then slowly increases to En<sub>81</sub> in the norites in the middle of the UG1 cyclic unit. Above this the composition of the bronzite drops to En<sub>76</sub> in the leuconorites close to the top of the UG1 cyclic unit. There is a rapid increase to En<sub>82</sub> in the pegmatoid below the UG2 chromitite layer. Within the sequence of poikilitic melanorites - norites - leuconorites - anorthosites above the UG2 chromitite layer the composition of the bronzite steadily decreases from En<sub>81</sub> to En<sub>78</sub>. No significant trends were observed in the UG3 cyclic unit where the bronzite composition averages En<sub>78,5</sub>. Microprobe data of bronzite within the harzburgites enclosing the UG3A chromitite layer showed the composition of the bronzites to be En<sub>76,3</sub> and En<sub>77,8</sub>.

Above the UG3A chromitite layers the En composition of the bronzite was found to be En<sub>78</sub> and to increase to En<sub>79,5</sub> at the top of the melanorite sequence. In the norites above the UG3A cyclic unit the composition of the bronzite averages En<sub>78</sub>.

#### 4.3.1.2 Trace element analyses

Fifty-five orthopyroxene separates were analysed for Zn, Cu, Co, V, Ni and Cr (Appendix V). The distributions of V, Ni and Cr were plotted on a diagram in an attempt to illustrate features of cyclicity in the cyclic units (Fig. 29).

If sample OPX - C23 is deleted from the calculations the bronzite has a mean of 101 ppm Zn with a low standard deviation of the population of 11 ppm Zn (Appendix V). Due to the strong chalcophile tendency of Zn the high value of 1233 ppm in sample OPX - C23 is probably due to some sulphide impurity in the mineral separate. The abundance of Zn in orthopyroxenes in this study is approximately twice that reported by Wedepohl (1972). No cyclicity of Zn in the



NOTE

FOR EXPLANATION OF GEOLOGY  
 SEE FOLDER B

Figure 29 : The distribution of V, Cu and Cr in the orthopyroxene separates of borehole MDH 7. Digitised by the Department of Library Services in support of open access to information, University of Pretoria, 2021



cyclic units was noted but it is clear that the bronzite closer to the chromitite layers and those in the melanorites of the UG2, UG3 and UG3A cyclic units are depleted in Zn relative to the more leucocratic sequences. The probable reason for the depletion is the presence of chromite and sulphide minerals which take Zn into their lattices. The mean of 11 ppm Cu is low and probably represents a fraction which can be taken up into the orthopyroxene lattice. Ferguson (1969, p. 74) reports values of 6 to 16 ppm Cu in orthopyroxenes in the critical zone of the western Bushveld and feels that because of the similar electronegativity and ionic radii that  $\text{Cu}^{2+}$  may be camouflaged by  $\text{Fe}^{2+}$  within the orthopyroxene lattice. Because of the relative weakness of the Cu-O bonds compared to the Mg-O and Fe-O bonds in orthopyroxene it is expected that the amount of Cu in the orthopyroxene will be low. No distinct trends are present in the distribution of Cu in the orthopyroxenes within the cyclic units of the upper group. The anomalous values of 100 and 97 ppm Cu in orthopyroxene samples OPX - D24 and OPX - E64 respectively are probably due to contamination by minute grains of Cu sulphide minerals. Whole rock analyses for Cu in the top three cyclic units show that Cu may be present in quantities up to 560 ppm in the chromitite layers, over 150 ppm in the pegmatite below this layer and over 100 ppm above the UG3A chromitite layers (Fig. 32, p. 70).

The mean content of Co in the orthopyroxenes is 110 ppm with a standard deviation of the population of 4 ppm. No trends were observed.

If Ni content of samples OPX - D10 of 1003 ppm and OPX - D19 of 1436 ppm are ignored the mean content of the samples is 630 ppm, with a standard deviation of population of 45 ppm. Ferguson (1969) found the concentration of Ni in cumulus orthopyroxene to lie between 375 - 650 ppm.

Whole rock analyses for total Ni through the upper three cyclic units showed that the Ni content ranges

between 250 to 400 ppm (Fig. 32). There is also a strong correlation between high Ni content and the chromitite layers. The tendency for Ni to increase in the vicinity of the chromitite layers in whole rock analyses (Fig. 32) is also reflected in the distribution of Ni of the orthopyroxene separates (Fig. 29). A steady decrease in the amount of Ni in the orthopyroxenes above the UG2 chromitite layer through to the top of the UG3A cyclic unit can probably be explained by the separation of small quantities of sulphides during the crystallization of this sequence which depleted the silicate liquid in Ni.

Cr is found in extremely variable amounts in orthopyroxenes with Ferguson (1969, p.74) reporting a variation from 150 ppm to 1500 ppm in Bushveld pyroxenes. The similar ionic radii of  $\text{Cr}^{3+}$  (0,638Å) and  $\text{Fe}^{3+}$  (0,64Å) and the lower electronegativity of  $\text{Cr}^{3+}$  allows it to substitute for  $\text{Fe}^{3+}$  in the orthopyroxene lattice. It should, however, be borne in mind that chromite primocrysts are commonly found in the bronzite crystals and the analytical data therefore does not always reflect the amount of chromium in solid-solution in the bronzite. The mean value of Cr in the orthopyroxene in this study is 3039 ppm. Cr has a similar distribution trend to Ni in that it also increases close to the UG1 chromitite and shows a tendency to increase upwards in this cyclic unit (Fig. 29).

V is generally present in magmas as  $\text{V}^{3+}$  and is largely removed from the magma by oxides such as magnetite, ilmenite and chromite. It was expected that the concentration of V in the orthopyroxenes would be low and that it would correlate with chromium. This correlation was not recognised. There is, however, apart from the initial depletion in the melanorites of the UG1 unit, a slight enrichment of V upwards through the cyclic units (Fig. 29).

#### 4.3.2 Clinopyroxene

#### 4.3.2.1 Major element analyses

The clinopyroxenes are inherently intercumulus and extreme difficulty was encountered in obtaining clean mineral separates for chemical analyses. Cumulus clinopyroxene was only found in the gabbronorites below the UG1 chromitite layer and even these were much smaller in grain size than the associated plagioclase and orthopyroxene and were consequently difficult to purify.

The chemical composition of separate C1 determined by XRF spectrometry may be seen in Table 1. The average atomic percentages of this clinopyroxene is 47,8 per cent Mg, 8,8 per cent Fe and 43,4 per cent Ca. This composition falls within the endiopside field, close to the augite field, of the pyroxene quadrilateral (Poldervaart and Hess, 1951, p. 474).

Variations in the  $Al_2O_3$  content from 6,5 per cent to 2,15 per cent in sample C1 (not shown in Table 1) are caused by impurities, especially included plagioclase. Cr is present in significant amounts, ranging from 0,44 to 0,93 per cent.

#### 4.3.2.2 Trace element analyses

Co, Cr, V, Cu, Ni and Zn were determined in two clinopyroxene samples (Table 2).

Table 2

The distribution of Zn, Cu, Ni, Co, Cr and V in clinopyroxene separates from borehole MDH 7.

Sample No.	Zn	Cu	Ni	Co	Cr	V
C1C	33	22	406	61	6033	312
F5C	52	19	380	82	2799	232

Sample C1C was taken from the UG3 cyclic unit (intercumulus) and sample F5C from the gabbronorites just below the UG1

TABLE 1 Chemical analyses of coexisting clinopyroxene (CIC) and orthopyroxene (CIP) used for the temperature calculation.

	<u>Clinopyroxene (CIC)</u>	<u>Orthopyroxene (CIP)</u>
SiO <sub>2</sub>	52,97	54,18
TiO <sub>2</sub>	0,36	0,23
Al <sub>2</sub> O <sub>3</sub>	2,16	1,16
FeO	6,63	14,08
MnO	0,17	0,28
MgO	16,85	27,41
CaO	19,95	1,57
Na <sub>2</sub> O	0,30	0,09
K <sub>2</sub> O	0,03	0,01
P <sub>2</sub> O <sub>5</sub>	0,03	0,01
Cr <sub>2</sub> O <sub>3</sub>	0,93	0,45
NiO	0,07	0,09
TOTAL	<u>100,45</u>	<u>99,56</u>

chromitite layer. Clinopyroxene separates from the gabbro-norites below the UG1 chromitite layer have a Cr content of 595 ppm while the clinopyroxenes within melanocratic rocks of the cyclic units have 810 ppm. Both clinopyroxenes have similar major element chemistry and contain similar amounts of Cu, Zn, Co and Ni. Sample F5 has less V and Cr than sample C1.

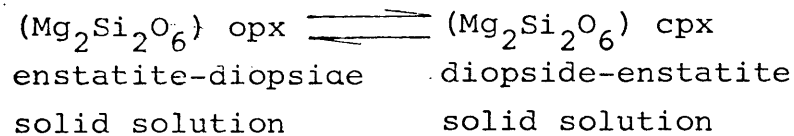
#### 4.3.3

##### Wood-Banno geothermometer

Wood and Banno (1973) calculated the equilibrium temperature of two-pyroxene assemblages by treating the solubility of enstatite in diopside ( $\text{CaMgSi}_2\text{O}_6$ ) which co-exists with orthopyroxene ( $\text{Mg}_2\text{Si}_2\text{O}_6$ ) as an ideal solution model. By applying an empirical approach to account for the  $\text{Fe}^{2+}$  on the orthopyroxene-clinopyroxene miscibility gap in natural systems greater accuracy in calculating equilibrium temperatures was established by Wells (1977).

Davis and Boyd (1966) investigated the miscibility gap between diopside and enstatite at 30 kb and applied a geothermometer for orthopyroxene-clinopyroxene assemblages that were low in  $\text{FeO}$  and  $\text{Al}_2\text{O}_3$ .

The reaction investigated by Davis and Boyd (1966) is



for which the condition of equilibrium is

$$\begin{array}{ccc}
 \text{Cpx} & = & \text{Opx} \\
 \mu \text{ Mg}_2\text{Si}_2\text{O}_6 & & \mu \text{ Mg}_2\text{Si}_2\text{O}_6 \\
 \text{where } \mu = \text{chemical potential}
 \end{array}$$

By assuming that both pyroxene phases act as two-site solutions the relationship between activity and composition is

$$a_{\text{Mg}_2\text{Si}_2\text{O}_6}^{\text{Cpx}} = \left( X_{\text{Mg}}^{\text{M2}} \cdot X_{\text{Mg}}^{\text{M1}} \right) \text{Cpx}$$

$$a_{\text{Mg}_2\text{SiO}_6}^{\text{Opx}} = \left( X_{\text{Mg}}^{\text{M2}} \cdot X_{\text{Mg}}^{\text{M1}} \right) \text{Opx}$$

In which  $a$ =activity and M1 and M2 = pyroxene structural sites.

From the above the idealised activities of  $\text{Mg}_2\text{Si}_2\text{O}_6$  components of orthopyroxene-clinopyroxene pairs may be calculated.

The above, however, does not conform to natural systems as the addition of  $\text{Ca}^{2+}$ ,  $\text{Na}^+$ ,  $\text{Mn}^{2+}$ ,  $\text{Al}^{3+}$ ,  $\text{Cr}^{3+}$ ,  $\text{Ti}^{4+}$  and  $\text{Fe}^{3+}$  will effect the solubility of the two pyroxene phases within each other.

The ratio

$$\left[ \frac{a_{\text{Mg}_2\text{Si}_2\text{O}_6}^{\text{cpx}}}{a_{\text{Mg}_2\text{Si}_2\text{O}_6}^{\text{opx}}} \right]$$

was thus formulated by (Wood and Banno 1973) using the equation  $a_{\text{Mg}_2\text{Si}_2\text{O}_6} = X_{\text{Mg}}^{\text{M1}} \cdot X_{\text{Mg}}^{\text{M2}}$  and assuming that the large ions present in the ortho- and clinopyroxene structures occupy M2 sites while the smaller of the octohedrally co-ordinated ions occupy M1 sites. The ions were assigned to the two sites as follows :

<u>M2</u>	<u>M1</u>
$\text{Ca}^{2+}$	$\text{Al}^{3+}$
$\text{Na}^+$	$\text{Cr}^{3+}$
$\text{Mn}^{2+}$	$\text{Ti}^{4+}$
	$\text{Fe}^{3+}$

The activities were thus calculated by

$$a_{\text{Mg}_2\text{SiO}_6} = \left( \frac{\text{Mg}^{2+}}{\text{Ca}^{2+} + \text{Mg}^{2+} + \text{Fe}^{2+} + \text{Mg}^{2+} + \text{Mg}^{2+}} \right)_{\text{M2}}$$

$$\cdot \left( \frac{\text{Mg}^{2+}}{\text{Fe}^{3+} + \text{Fe}^{2+} + \text{Al}^{3+} + \text{Ti}^{4+} + \text{Cr}^{3+} + \text{Mg}^{2+}} \right)_{\text{M1}}$$

By using the above activities and plotting against temperature a straight line eventuated and an expression in T (in °K) was obtained.

$$T = \frac{-10202}{\ln \left[ \frac{a_{\text{cpx}}^{\text{Mg}_2\text{Si}_2\text{O}_6}}{a_{\text{opx}}^{\text{Mg}_2\text{Si}_2\text{O}_6}} \right] - 7,65 x_{\text{Fe}}^{\text{opx}} + 3,88 \left( x_{\text{Fe}}^{\text{opx}} \right)^2 - 4,6}$$

$$\text{where } x_{\text{Fe}}^{\text{opx}} = \left( \frac{\text{Fe}^{2+}}{\text{Fe}^{2+} + \text{Mg}^{2+}} \right)_{\text{opx}}$$

Because of the impurities in the clinopyroxene separates it was only possible to calculate the equilibrium temperatures of samples CIC and CIP (Table 1).

The following equilibrium temperatures were obtained

Wood-Banno geothermometer 1179°C

Wells Modification 1097°C

#### 4.4 Olivine

Cumulus olivine is associated with the pegmatoid below the UG2 chromitite layer and with the enclosing rocks of the UG3A chromitite layer. Pervasive serpentinisation and associated magnetite made separation of the olivines impossible. Occasional small angular islands of clear olivine, however, remained and their compositions were obtained by the electron microprobe. Two to three points per slide were determined and averaged (Table 3). The olivine was identified as chrysolite. Samples OL/7/1 and OL/7/2 were taken 0,30 metres apart in the UG2 pegmatoid and the composition was found to range from Fo<sub>78,4</sub> to Fo<sub>80,7</sub> while the averages of samples OL/7/3 and OL/7/4, taken 20 cm apart in the UG3A unit, were Fo<sub>76,9</sub> to Fo<sub>75,9</sub>. Although an upward iron enrichment is indicated, the range in compositions between nearby olivines prohibits any meaningful interpretation of the limited data available.

Table 3 : Chemical analyses and structural formulae of olivines in the pegmatoid below the UG2 chromitite layer and associated with the UG3A chromitite layer

	UG2 PEGMATITE		UG3A CHROMITITE LAYER	
SAMPLE NO.	OL 7/1	OL 7/2	OL 7/3	OL 7/4
SiO <sub>2</sub>	39,54	39,57	38,45	39,29
TiO <sub>2</sub>	0,01	0,01	0,0	-
FeO	19,21	18,11	21,64	21,78
MgO	39,14	42,50	40,41	38,48
CaO	0,03	0,02	0,02	0,02
Total	97,93	100,21	100,52	99,57
	Number of ions on the basis of 4 oxygens			
Si	1,030	1,004	0,991	1,019
Ti	-	-	-	-
Fe	0,419	0,384	0,466	0,473
Mg	1,520	1,607	1,552	1,488
Ca	0,001	0,001	0,001	0,001
Total	2,970	2,996	3,010	2,981
	Atomic Ratios			
Mg	78,39	80,71	76,91	75,88
Fe	21,61	19,29	23,09	24,12



#### 4.5 Chromite

Fifteen samples from portions of the chromitite layers (Figures 14, 15 and 16) were selected for chemical analyses. The samples were purified as outlined in Chapter 1 and subsequently analysed at The Council for Mineral Technology (Table 4). The extremely low  $\text{SiO}_2$  and  $\text{CaO}$  values (not reported) are a measure of the purity of the specimens prepared for chemical analysis. The cell formulae and pertinent cation ratios, listed in Table 4, were calculated by using the Bosch 1 programme (De Waal and Oosthuizen, 1974).  $\text{Cr}_2\text{O}_3$  and  $\text{FeO}$  show a slight upward increase and while  $\text{Al}_2\text{O}_3$  remains constant and  $\text{Fe}_2\text{O}_3$  shows an upward decrease in the UG1 and UG2 chromitite layers. The Cr/Fe ratio of the UG2 chromitite layer is lower than that of the UG1 chromitite layer (Fig. 30). This conforms to the normal differentiation trend expected in the sequence. Samples do show reversals in the above trend but this can be accounted for by the fact that the samples were either taken from thin chromitite layers or disseminated chromite-rich zones. For example sample UG2/Peg was taken from an irregular chromitite layer that is located in a pegmatoid below the UG2 chromitite layer, sample UG2/UP was taken from a small layer found above the main layer. Sample C6 was taken from a rock with disseminated chromite just above the UG3 chromitite layer while sample UG3 A/1 was taken from a chromitite associated with cumulus olivine in the UG3A chromitite layer.

The concentration of minor elements show that the chromites are not simple  $\text{M}^{2+}\text{M}_2^{3+}\text{O}_4$ -type spinels but that they contain between 2,69 and 1,38 per cent ulvospinel component (Ti-rich)  $\text{M}_2^{2+}\text{M}^{4+}\text{O}_4$  in solid solution or as an impurity. Cameron (1977, p1084) accounts for the  $\text{TiO}_2$  present as being due to inclusions of rutile within the chromite grains.

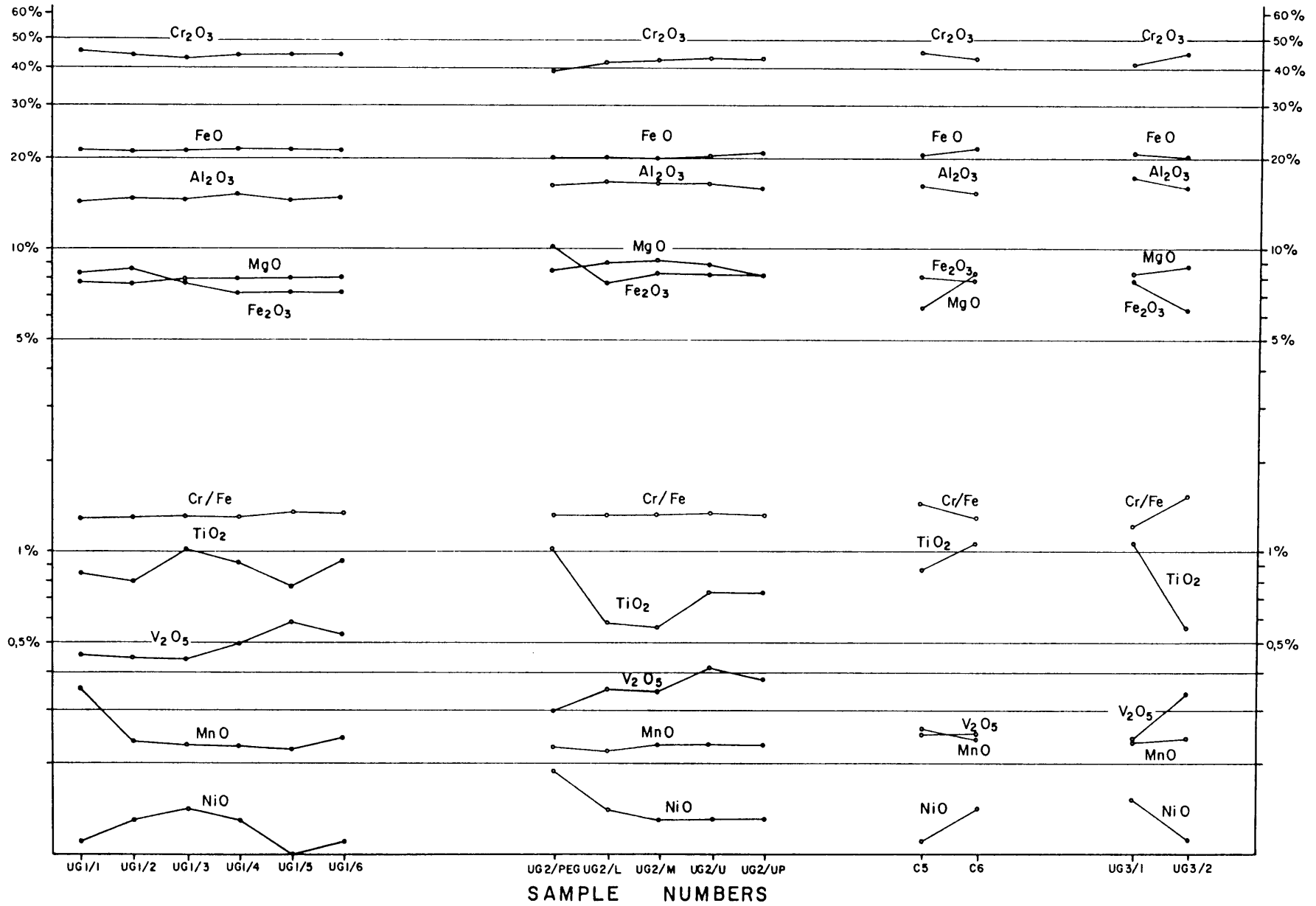
Polished sections of the UG2 chromitite layer show that rutile occurs as lamellae which have exsolved from the chromite crystals (Fig. 31), from which it may be concluded that most of the Ti in the analyses is present in the form of rutile.

Table 4 : Chemical analyses and structural formulae of 15 chromite samples (analysed in duplicate) from the UG1, UG2, UG3 and UG3A chromite layers

	UG1/1	UG1/2	UG1/3	UG1/4	UG1/5	UG1/6	UG2/PEG	UG2/L20	UG2/M20	UG2/U20	UG2/UP	UG3/C5	UG3/C6	UG3A/1	UG3A/2
Al <sub>2</sub> O <sub>3</sub>	14,80	14,85	14,90	15,20	14,90	14,90	16,30	16,90	16,60	16,40	15,80	16,10	15,40	17,05	16,00
Cr <sub>2</sub> O <sub>3</sub>	45,00	44,40	43,90	44,10	44,10	44,20	39,60	42,00	42,85	43,10	43,30	45,50	43,10	41,10	45,40
Fe <sub>2</sub> O <sub>3</sub>	8,49	8,64	7,72	7,16	7,11	7,13	10,19	7,78	8,44	8,32	8,28	6,42	8,11	7,99	6,36
V <sub>2</sub> O <sub>5</sub>	0,45	0,45	0,44	0,49	0,59	0,54	0,30	0,35	0,35	0,41	0,37	0,25	0,25	0,23	0,34
TiO <sub>2</sub>	0,84	0,80	1,03	0,92	0,77	0,93	1,03	0,58	0,57	0,73	0,73	0,87	1,08	1,07	0,56
MgO	7,60	7,70	8,00	8,10	8,00	8,05	8,60	9,00	9,15	8,90	8,20	8,10	7,90	8,30	8,80
NiO	0,11	0,13	0,14	0,13	0,09	0,11	0,18	0,14	0,13	0,13	0,13	0,11	0,14	0,15	0,11
CoO	0,04	0,03	0,04	0,04	0,03	0,04	0,05	0,04	0,04	0,04	0,04	0,04	0,04	0,04	0,04
FeO	22,50	22,10	22,30	22,80	22,40	22,60	21,60	20,80	20,30	20,50	21,70	21,40	22,40	22,50	21,00
ZnO	0,11	0,10	0,10	0,11	0,10	0,11	0,10	0,09	0,09	0,09	0,09	0,10	0,10	0,10	0,10
MnO	0,24	0,24	0,23	0,23	0,22	0,24	0,23	0,22	0,23	0,23	0,23	0,26	0,24	0,23	0,24
TOTAL	100,18	99,44	98,80	99,28	98,31	98,85	98,18	97,90	98,75	98,85	98,87	99,15	98,76	98,76	98,95
Al	4,5954	4,6376	4,6759	4,7465	4,7000	4,6768	5,1007	5,2691	5,1326	5,0743	4,9273	4,9911	4,8262	5,2971	4,9612
Cr	9,3726	9,3011	9,2413	9,2376	9,3327	9,3063	8,3123	8,7839	8,8872	8,9453	9,0579	9,4616	9,0605	8,5653	9,4431
Fe <sup>3+</sup>	1,6830	1,7227	1,5468	1,4275	1,4321	1,4288	2,0358	1,5487	1,6661	1,6435	1,6486	1,2707	1,6227	1,5848	1,2591
V	0,0951	0,0956	0,0939	0,1041	0,1266	0,1153	0,0639	0,0742	0,0736	0,0863	0,0785	0,0527	0,0533	0,0486	0,0717
Ti	0,1664	0,1594	0,2062	0,1833	0,1550	0,1863	0,2057	0,1154	0,1124	0,1441	0,1453	0,1721	0,2160	0,2121	0,1108
Mg	2,9844	3,0412	3,1751	3,1989	3,1920	3,1956	3,4035	3,5488	3,5780	3,4827	3,2341	3,1757	3,1311	3,2612	3,4510
Ni	0,0233	0,0277	0,0300	0,0277	0,0194	0,0236	0,0384	0,0298	0,0274	0,274	0,0277	0,0233	0,0299	0,0318	0,0233
Co	0,0085	0,0064	0,0085	0,0085	0,0064	0,0085	0,0106	0,0085	0,0084	0,0084	0,0085	0,0084	0,0085	0,0085	0,0084
Fe <sup>2+</sup>	4,9570	4,8970	4,9655	5,0517	5,0142	5,0332	4,7959	4,6014	4,4535	4,5005	4,8016	4,7071	4,9809	4,9599	4,6202
Zn	0,0214	0,0196	0,0197	0,0215	0,0198	0,0216	0,0196	0,0176	0,0174	0,0174	0,0176	0,0194	0,0196	0,0195	0,0194
Mn	00,0536	0,0539	0,0519	0,0516	0,0499	0,0541	0,0517	0,0493	0,0511	0,0511	0,0515	0,0579	0,0541	0,0514	0,0535
TOTAL	23,9606	23,9621	24,0148	24,0589	24,0489	24,0502	24,0381	24,0467	24,0078	23,9812	23,9986	23,9399	24,0028	24,0400	24,0217
Cr/Fe <sup>2+</sup> + Fe <sup>3+</sup>	1,3142	1,3082	1,3212	1,3274	1,3480	1,3409	1,1329	1,3298	1,3522	1,3556	1,3075	1,4737	1,2775	1,2185	1,4954
Cr/Al	2,0396	2,0056	1,9764	1,9462	1,9854	1,9899	1,6296	1,6671	1,7315	1,7629	1,8383	1,8957	1,8773	1,6170	1,9034
Mg/Mg + Fe <sup>2+</sup>	0,3758	0,3831	0,3900	0,3877	0,3889	0,3883	0,4151	0,4354	0,4455	0,4362	0,4025	0,4028	0,3860	0,3967	0,4276
Cr/Cr + Al + Fe <sup>3+</sup>	0,5988	0,5938	0,5976	0,5994	0,6034	0,6038	0,5380	0,5630	0,5666	0,5711	0,5793	0,6017	0,5841	0,5545	0,6029
Al/Cr + Al + Fe <sup>3+</sup>	0,2936	0,2961	0,3024	0,3080	0,3039	0,3034	0,3302	0,3377	0,3272	0,3239	0,3152	0,3174	0,3112	0,3429	0,3167
Fe <sup>3+</sup> /Cr + Al + Fe <sup>3+</sup>	0,1075	0,1099	0,1000	0,0926	0,0926	0,0927	0,1318	0,0992	0,1062	0,1049	0,1054	0,0808	0,1046	0,1026	0,0804

Figure 30 : Variation of oxides in chromite separates taken from the UG1, UG2, UG3 and UG3A chromite layers, For positions see Figures 14, 15 and 16.

WEIGHT PERCENTAGE OF OXIDES



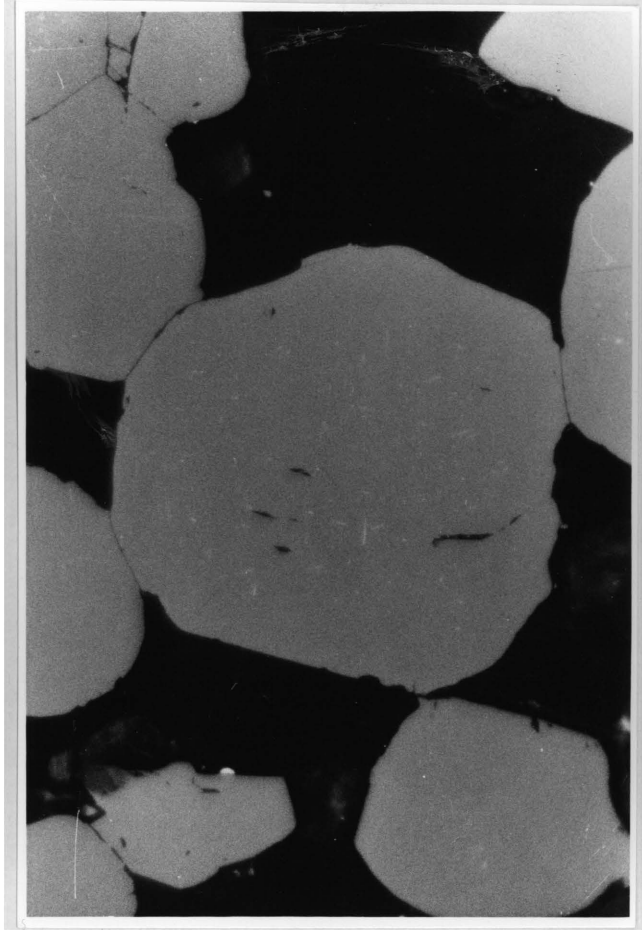


Figure 31 : Small elongate rutile lamellae (white) exsolved parallel to the (111) planes of a chromite crystal (grey) in borehole MDH 12. Section MDH1 2/UG2/2; Reflected light, 200X.

Sample UG2/Peg contains 1800 ppm Ni and 500 ppm Co which are the highest Ni and Co values of all the samples analysed. The high values may be due to discrete sulphide minerals locked within the chromite grains but it should be noted that chromite from the UG2 chromitite layer contains less Ni and Co. It is possible that the sulphides present in this layer could have taken these chalcophile elements into their lattices during crystallization.

An upward increase in  $V_2O_5$  has been noted in both the UG1 and UG2 chromitite layers although the overall  $V_2O_5$  content decreases from the UG1 to the UG3A chromitite layer.

Analyses of the UG1 and UG2 chromitite layers in this study compare favourably with those reported by De Waal (1975). The UG2 samples have a significantly similar composition which is exemplified by the  $Mg/R^{2+}$  ratio of 0,44 at Maandagshoek compared with an average of 0,45 in De Waal's suite of UG2 samples (De Waal 1975, p. 22).

All discussion and interpretation of variations of the chromite compositions depend on whether the composition of the chromite is representative of the early accumulated chromite or if its composition has been modified by postcumulus equilibration with the intercumulus liquid. Cameron (1977, p. 1085 - 1090) has described variations in the major cation proportions in the main chromitite layers of the critical zone in the eastern lobe, and finds a decrease in  $Cr/Fe$ ,  $Mg/Fe^{2+} + Mg$  and an increase in  $Fe/Cr + Al + Fe^{3+}$  upwards. He has, however, noted that the upper critical zone shows unordered trends. Cameron (1977) also found that the disseminated chrome spinels of the silicate rocks are usually lower in  $Cr/Fe$ ,  $Mg/Mg + Fe^{2+}$  and  $Al/R^{3+}$  and higher in  $Fe^{3+}/R^3$  and  $Cr/R^{3+}$  than chromite in nearby chromitite layers.

Irvine, (1967, p. 84), explained the decrease in  $Mg/Fe^{2+}$  in disseminated chromites, in terms of the distribution coefficient for Mg and  $Fe^{2+}$  between silicate and spinel which increases with falling temperature. Consequently, the chrome spinel is enriched in ferrous iron on cooling. In

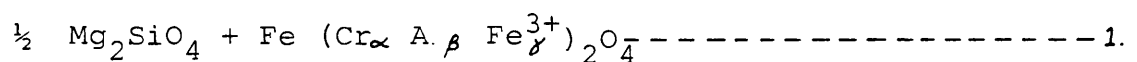
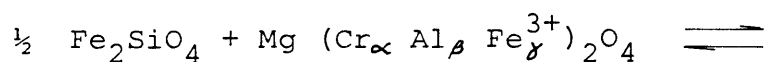
the situation where chromite is the primary constituent and constitutes the bulk of the rock, such as in a chromitite layer, the  $K_D$  between coexisting chromite and orthopyroxene dictates that the intercumulus silicates be significantly enriched in Mg as a result of equilibration while the chromite composition remains relatively constant.

Hamlyn and Keays (1979, p. 81) have conducted a systematic study of the compositional differences between chromite in the intercumulus material (intergrain chromite) and chromite grains enclosed by cumulus olivine in the Panton Sill. The data showed that the intergrain chromite was relatively enriched in the  $MgAl_2O_4$  component compared with adjoining grains enclosed by the cumulus olivine. The authors conclude that the intergrain chrome spinels were enriched in the  $MgAl_2O_4$  component during post-cumulus overgrowth and equilibration with the intercumulus liquid. They also found that the larger chromite crystals generally have higher Mg and Al cation fractions.

From the above it is clear that the composition of disseminated chromite in silicates is a function of the amount of silicate liquid with which it can react and thus only chromite from massive chromitites can be used as an index of the fractionation of the magma (Cameron, 1977).

#### 4.6 Olivine - chromite geothermometer

If crystallisation of olivine and chromite crystals occurred close together it can be assumed that the concentration of some of the co-existing elements in the olivine and chromite should reflect the chemical potential of these elements at the particular temperature at which crystallization took place. The distribution of  $Fe^{2+}$  and Mg between olivine and chromite in equilibrium may be expressed as follows :-



where  $\alpha, \beta$  and  $\gamma$  are the atomic fractions of the trivalent cations.

This reaction was demonstrated by Irvine (1965, p.654 - 660) to be sensitive to changes in temperature and that analyses of these two phases could be used as a geothermometer.

Jackson (1969) measured the modal proportions and the concentrations of the major cations in olivine and chromite in 35 layers from the Stillwater Complex. From this work he found that there was a clear relationship between the proportions of the two minerals and their chemical compositions. Jackson (1969) substituted various thermodynamic data including the standard Gibbs free energy of formation for the end members of olivine and chromite and a gas constant into Eq(1) and, assuming ideal solid solution, derived the following expression :-

$$(K^O) = \frac{5580\alpha + 1018\beta - 1720\gamma + 2400}{0,90\alpha + 2,56\beta - 3,08\gamma - 1,47 + 1987 \ln K_{D_{Mg-Fe^{2+}}}} \quad (2)$$

where  $\alpha = Cr/Cr + Al + Fe^{3+}$  (olivine)

$\beta = Al/Cr + Al + Fe^{3+}$  (olivine)

$\gamma = Fe^{3+}/Cr + Al + Fe^{3+}$  (olivine)

$$\text{and } K_{D_{Mg+Fe^{2+}}} = \frac{X_{Mg}^{Ol} \times X_{Fe^{2+}}^{Chr}}{X_{Fe^{2+}}^{Ol} \times X_{Mg}^{Chr}} \quad (3)$$

where X = mole fraction in solid solution ( $Mg/Mg + Fe^{2+}$  and  $Fe^{2+}/Mg + Fe^{2+}$ ).

Jackson (1969) was aware of a multitude of problems that could radically change the above and lists five major problem areas :

- . Olivine and chromite must be in equilibrium.
- . The assumption that the end members of olivine and chromite as regards unit activity coefficient is ideal.
- . The free-energy values for end member spinel and olivine are correct.
- . The assumption that pressure has no effect on the free-energy values.
- . The precision and accuracy of chemical analyses.

Irvine (1967) also drew attention to the fact that the distribution coefficient (Eq(3)) increases as the temperature drops. Thus in rocks where chromite is relatively sparse it would become richer in the ferrous iron as the rock cools while the silicate would essentially remain the same and vice versa when olivine is the minor constituent in a chromite layer. He considers that subsolidus re-equilibration may occur for several hundred degrees below their original crystallisation temperature and thus recommends that the best samples to use should be taken from co-existing layers in which olivine and chromite occur in maximum concentration rather than from co-existing grains from the same sample.

Roeder et al (1979, p. 331 - 333) have experimentally shown that such subsolidus re-equilibration does occur and have questioned the Jackson (1969) geothermometer and suggested that if a different free energy value of  $\text{FeCr}_2\text{O}_4$  is used, a more realistic temperature of formation may be obtained.

If the new free energy data is used Eq (2) becomes :

$$t(^{\circ}\text{K}) = \frac{3480\alpha + 1018\beta - 1720\gamma + 2400}{2,23\alpha + 2,56\beta - 3,08\gamma - 1,47 + 1,987 \ln_{K_D}} \text{-----(4)}$$

Data from the UG2 pegmatoid in the UG3A chromitite layer were substituted into both equations (Table 5).

Table 5

The equilibrium temperatures of co-existing olivine-chromite pairs calculated by using thermodynamic data of Jackson (1969) and Roeder et al (1979).

Sample No.		Layer No.	Temperature ( $^{\circ}\text{C}$ )	
Olivine	Chromite		Jackson (1969)	Roeder et al. (1979)
OL 7/3	UG3A/2	UG3A	2015	1100
OL 7/4	UG3A/1	UG3A	1824	1036
OL 7/1	UG2/PEG	UG2	1772	1012
OL 72	UG2/PEG	UG2	1577	913



The results obtained when using the Roeder method are geologically more reasonable than those of Jackson but variations of 200°C with the former method indicates that the olivine-chromite geothermometer is not very meaningful in determining temperatures of crystallisation of the upper group chromitites. In this regard it is possible that the lower temperatures obtained for the olivine-chromite pairs in the pegmatoid below the UG2 chromitite layer could be due to post-cumulus equilibration of the cumulates during the formation of the pegmatoid. The high Fe<sup>3+</sup> content of chromite from this layer could also be related to such a postcumulus process. It is also possible that incipient serpentinization could have affected the Fe-ratio of the olivine and caused the unexpected results.

## 5 PLATINOID GEOCHEMISTRY

### 5.1 The distribution and mineralogy of platinoids in the upper group chromitites

Although the platinoids of the UG2 chromitite layer have been analysed extensively and detailed mineralogical and metallurgical studies have been conducted by a number of mining houses, very little of this information has been published to date.

Wagner (1929, p.94) has recorded values of up to 19,7 g/t platinoids and Au in the chromitite layers of the upper group in the eastern Bushveld Complex while McLaren (1978) has published preliminary results of a comparative study of the chemical analyses, the mineralogy and the mode of occurrence of platinoid minerals and alloys at various localities in the Bushveld Complex. Hiemstra (1979, p. 471) published the average analyses of samples taken from several localities in the Bushveld Complex, but care should be employed in the interpretation of such results as lateral variations in the distribution and grade of the various platinoids have been recognised by McLaren (1981).

Analyses of surface samples in trenches (Folder A) established that both Pt and Pd are present in the UG1, UG2 and UG3 layers (Table 6). Wagner (1929, p.190) already recognised that the Pt/Pd ratio in the oxidised environment was higher than in the primary ore, an observation that was substantiated by analytical data from samples taken in the UG2 chromitite layer in which the Pt/Pd ratio in surface and unoxidised environments were 1,77 and 0,99 respectively (Tables 6 and 7). This also agrees with Fuchs and Rose's (1974, p. 344) findings that Pd was much more mobile than Pt under weathering conditions and with Cousins' (1973, p. 80) estimated order of resistance to chemical attack of Ir>Os>Ru>Rh>Pt>Pd.

A series of whole rock samples through the top three cyclic units of borehole MDH 19, were analysed for Cu, total

Table 6 : Pt and Pd analyses of the UG1, UG2 and UG3 chromitite layers in the surface environment. (For location of the trenches see Folder A)

UG 1 CHROMITITE LAYER						UG2 CHROMITITE LAYER						UG3 CHROMITITE LAYER					
Sample No	Pd	Pt	Pd+Pt	Pt/Pd	Width	Sample No	Pd	Pt	Pd+Pt	Pt/Pd	Width	Sample No	Pd	Pt	Pd+Pt	Pt/Pd	Width
	g/t	g/t	g/t		meters		g/t	g/t	g/t		meters		g/t	g/t	g/t		meters
1W1	0,12	0,30	0,42	2,50	0,14	2A	0,30	0,98	1,28	3,27	0,80	3I2	0,14	0,46	0,60	3,28	0,20
1W2	0,20	0,26	0,46	1,30	0,71	2B	0,10	1,60	1,70	1,60	0,61	3R2	0,17	0,62	0,79	3,64	0,25
1Y1	0,11	0,46	0,57	4,18	0,70	2C2	1,34	3,64	4,98	2,72	0,70	3U	0,26	0,60	0,86	2,31	0,32
1QQ	0,28	0,28	0,56	1,00	1,00	2D	0,70	1,64	2,34	2,34	0,62	3Z	0,16	0,74	0,90	4,62	0,23
1VV	0,16	0,44	0,60	2,75	0,50	2E1	1,09	3,60	4,69	3,30	0,61	3CC	0,10	1,55	1,65	15,5	0,30
1DA	0,09	0,32	0,41	3,55	1,00	2E2	0,72	1,36	2,08	1,89	0,62	3DD1	0,19	0,80	0,99	4,21	0,41
						2F	0,90	3,58	4,48	3,98	0,60	3DD2	0,22	0,85	1,07	3,86	0,18
						2G	1,32	3,78	5,10	2,86	0,59	3EE	0,18	0,70	0,88	3,89	0,20
						2H	2,60	3,20	5,80	1,23	0,55	3HH1	0,26	1,00	1,26	3,85	0,30
						2K1	1,78	1,62	3,40	0,91	0,65	3HH2	0,26	0,80	1,06	3,07	0,21
						2L	1,66	4,12	5,78	2,48	0,70	3II	1,38	0,80	2,18	0,58	0,23
						2M1	2,40	3,64	6,04	1,52	0,80	3LL	0,24	0,87	1,11	3,62	0,11
						2O1	1,72	1,90	3,62	1,10	0,60	3NN	0,25	0,65	0,90	2,60	0,18
						2P	1,50	1,90	3,40	1,27	1,05	3PP	0,08	0,66	0,74	8,25	0,25
						2Q	1,80	2,00	3,80	1,11	0,65	3SS	0,22	0,74	0,96	3,36	0,32
						2S	0,94	2,12	3,06	2,25	0,80	3TT1	0,26	0,66	0,92	2,54	0,32
						2T	2,74	3,60	6,34	1,31	0,85	3TT2	0,22	0,70	0,92	3,18	0,28
						2BB	1,50	3,55	5,05	2,37	0,70						
						2FF	2,74	3,32	6,06	1,21	0,60						
						2GG	2,92	4,70	7,62	1,61	0,78						
						2OO	0,92	1,05	1,97	1,14	0,55						
						2RR	1,50	1,98	3,48	1,32	0,92						
						2UU	1,40	3,26	4,66	2,33	0,54						
						2WW	1,90	3,59	5,49	1,89	0,80						
						2YY	2,20	3,80	6,00	1,73	0,50						
						2JJ	2,58	3,87	6,45	1,50	0,85						
Aver.	0,16	0,34	0,50	2,12	0,67	Aver.	1,59	2,82	4,41	1,77	0,69	Aver.	0,27	0,78	1,05	2,89	0,28

Ni, Pt and Pd (Fig. 32). All four elements display a rough upward enrichment from the base of the UG2 cyclic unit towards the UG2 chromitite layer and all reach a maximum in the layer. The platinoid and base metal values decrease sharply in the melanorites directly above the UG2 chromitite layer and remain low to the base of the UG3 chromitite layer. There is a rapid rise in Ni and Pt in the UG3 layer but Cu and Pd do not show an appreciable increase. Few sulphide minerals have been seen in this layer and the increase in Ni is partially attributed to the presence of chromite. There is a drop in Ni and Pt above the UG3 chromitite layer and a small peak of Pt, Pd and Ni at the top of the melanorite in the UG3A cyclic unit where visible sulphides are observed. A slight peak of Pt and Pd occurs in the UG3A layers with a concomitant increase of total Ni. Small quantities of sulphides are associated with the UG3A chromitite layer and the increase in Ni content is attributed to the presence of olivine and chromite. In summary there is a strong correlation between high Pt and Pd associated with high modal chromite except in the UG3 layer where Pd remains depleted. Cu and Ni follow the platinoids except in the UG3 layer which is depleted in Cu.

The results of assays of 17 borehole intersections, a bulk sample from the prospect shaft and four channel samples from the old adit are presented in Table 7.

Analyses for Cu, Ni, Pt, Pd, Rh, Ru, Ir and Au in the UG2 chromitite layer in boreholes MDH 5, 6, 7 are given by McLaren (1981). The distribution of the various platinoids show a relatively consistent pattern in which Pt and Pd are enriched near the bottom and top of the layer while the average Pt/Pd ratio in MDH 5 and 7 is 1,1 and 1,02 respectively compared with 1,49 in MDH 6. In all the boreholes both Pt and Pd increase toward the upper and lower contacts while Rh, Ru and Ir show an upward decrease through the layer. This feature is exemplified by the upward increase in the Pt/Ru and Pt/Rh ratios. Au generally increases towards the

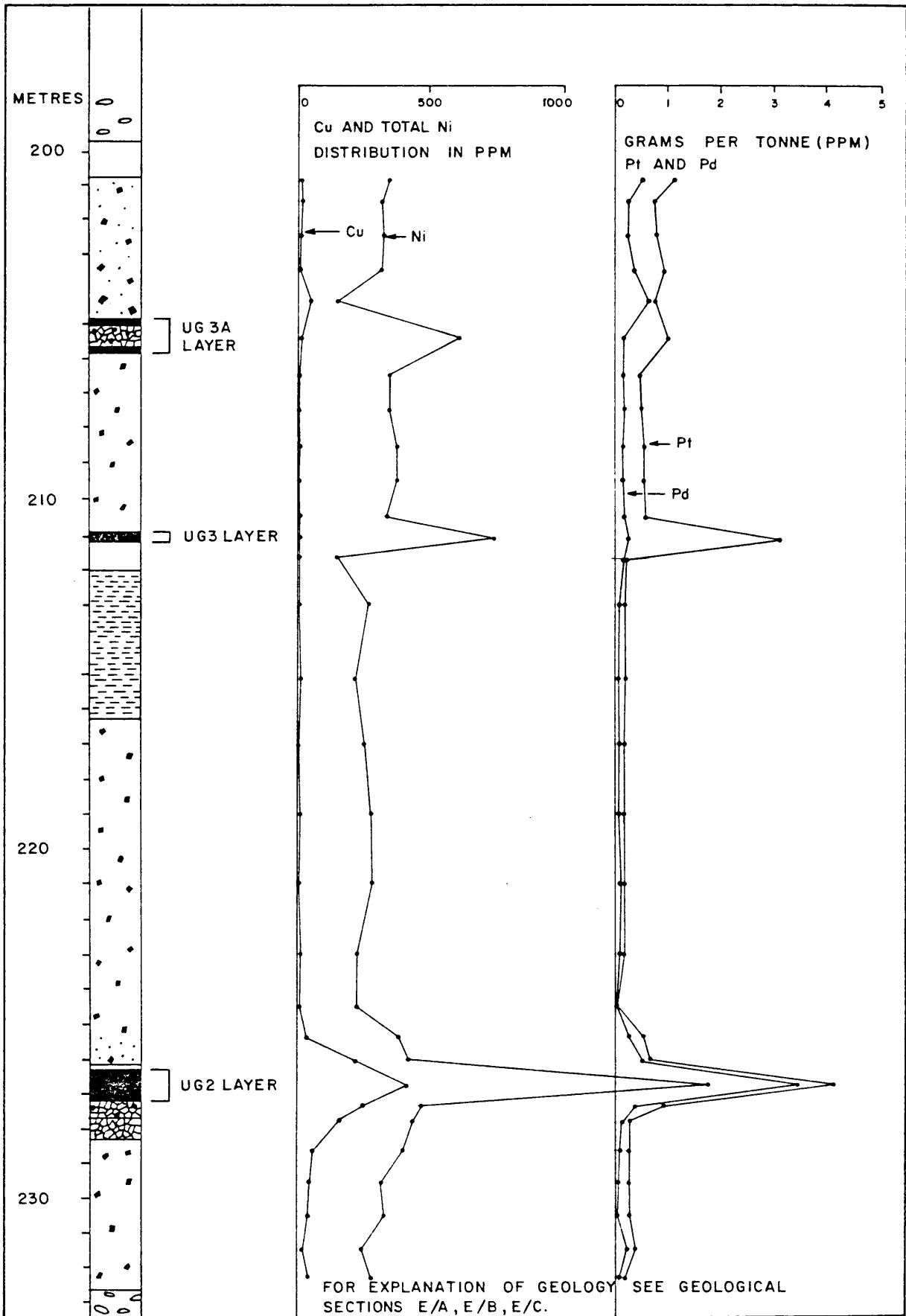


Figure 32 : Whole rock analyses for Pt, Pd, total Ni and Cu in the UG2, UG3 and UG3A cyclic units in borehole MDH 6.

Table 7 : Distribution of Pt, Pd, Rh, Ru, Ir, Au, total Ni, sulphide Ni, Cu and Cr<sub>2</sub>O<sub>3</sub> in the UG2 chromitite layer in 17 borehole interseptions, a shaft and an adit. (For positions of samples see Folder A).

MDH B/H NO.	UG LAYER NO.	Tot PGE + Au	Pt	Pd	Ru	Rh	Ir	Au	Tot Ni	Sulph. Ni	Cu	Cr <sub>2</sub> O <sub>3</sub>	Width	Pt+Pd	Pt/Pd	Cu/Ni	Pt+Pd Tot PGE + Au
			g/t	g/t	g/t	g/t	g/t	g/t	ppm	ppm	ppm	%-age	m				
4	2	*8,20	nd	nd	nd	nd	nd	nd	nd	nd	nd	@34,7	0,70	-	-	-	-
5	2	10,65	4,33	3,92	1,22	0,95	0,16	0,07	nd	796	272	nd	0,56	8,25	1,10	0,34	0,77
6	2	8,88	4,11	2,77	1,10	0,57	0,33	nd	nd	839	489	nd	0,83	6,88	1,48	0,58	0,77
7	2	7,32	2,69	2,65	0,83	0,69	0,38	0,08	nd	897	460	+42,65	0,79	5,34	1,01	0,51	0,73
8	2	8,06	3,10	3,65	0,60 <sup>+</sup>	0,42 <sup>+</sup>	0,21 <sup>+</sup>	nd	1600	nd	460	nd	0,52	6,75	0,85	-	0,84
10	2	6,15	3,05	1,50	0,83 <sup>+</sup>	0,52 <sup>+</sup>	0,25 <sup>+</sup>	nd	1600	nd	130	nd	0,63	4,55	2,03	-	0,74
11	2	7,14	3,80	1,95	0,75 <sup>+</sup>	0,45 <sup>+</sup>	0,22 <sup>+</sup>	nd	1600	nd	100	nd	0,55	5,75	1,95	-	0,80
12	2	5,0	2,3	1,4	0,7	0,4	0,20	nd	1400	nd	60	nd	0,50	3,70	1,64	-	0,74
13	2	8,45	3,0	3,6	1,0	0,6	0,25	nd	1800	nd	220	nd	0,63	6,6	0,83	-	0,78
14	2	9,18	3,1	3,8	1,3	0,7	0,28	nd	1700	nd	370	nd	0,71	6,9	0,81	-	0,75
15	2	8,19	2,7	3,3	1,1	0,7	0,39	nd	1900	nd	390	nd	0,97	6,0	0,82	-	0,73
16	2	9,73	3,9	3,5	1,3	0,8	0,23	nd	1400	nd	560	nd	0,58	7,4	1,11	-	0,76
17	2	8,20	3,5	4,1	0,3	0,1	0,20	nd	1400	nd	320	nd	0,51	7,6	0,85	-	0,95
18	2	7,70	3,7	3,4	0,3	0,1	0,20	nd	1300	nd	330	nd	0,51	7,1	1,09	-	0,92
19	2	5,55	2,3	2,7	0,2	0,1	0,25	nd	1500	nd	460	nd	0,62	5,0	0,85	-	0,91
26	2	8,77	3,5	3,9	0,64 <sup>+</sup>	0,40 <sup>+</sup>	0,33 <sup>+</sup>	nd	1700	nd	270	nd	0,49	7,4	0,90	-	0,84
28	2	9,89	3,4	4,7	0,92 <sup>+</sup>	0,58 <sup>+</sup>	0,29 <sup>+</sup>	nd	1800	nd	500	nd	0,70	8,1	0,72	-	0,82
Shaft	2	*10,62	3,41	3,50	1,21	0,85	0,3	nd	nd	967	331	nd	0,74	6,91	0,97	0,34	0,74
Adit 1	2	7,62	2,7	3,2	0,89 <sup>+</sup>	0,56 <sup>+</sup>	0,27 <sup>+</sup>	nd	1200	nd	430	nd	0,68	5,9	0,84	-	0,77
" 2	2	7,10	2,8	2,8	0,77 <sup>+</sup>	0,49 <sup>+</sup>	0,24 <sup>+</sup>	nd	1600	nd	300	nd	0,59	5,6	1,00	-	0,79
" 3	2	9,27	3,5	4,2	0,81 <sup>+</sup>	0,51 <sup>+</sup>	0,25 <sup>+</sup>	nd	1600	nd	450	nd	0,62	7,7	0,83	-	0,83
" 4	2	7,81	2,8	3,4	0,84 <sup>+</sup>	0,52 <sup>+</sup>	0,25 <sup>+</sup>	nd	1600	nd	80	nd	0,64	6,2	0,82	-	0,79
AVER.		8,21	3,21	3,24	0,87	0,54	0,27	0,07	1570	875	332		0,64	6,46	0,99 (1,07)	0,38	0,79 (0,78)

nd - not determined

\* - total PGE and Au determined by lead collection method

@ - chromitite assay (JCI)

+ - cleaned chromite (average of 3 samples) (NIM)

All assays by McLachlan & Lazar except MDH 5.6.7 and the shaft sample which were assayed by NIM.

contacts. In addition to the work on Maandagshoek 254 KT, McLaren (1978, p.24) has also studied the UG2 chromitite layer from various other localities in the western Bushveld. He found the platinoid and Au values to be high in the basal and middle portions of the layer at these localities while the Pt/Pd ratios are low close to the base of the UG2 layer and higher close to the top in the western Bushveld. In contrast, the Pt/Pd is low and fairly constant throughout the layer at the locality to the south of Maandagshoek.

The sulphides and associated platinum group minerals (PGM) in polished sections from borehole MDH 5 and the prospect shaft have also been studied by McLaren (1981, p.171). The PGM present in MDH 5, which is located close to a mafic pipe, differ radically from those investigated at other localities on Maandagshoek and the Complex as a whole, in that they are chiefly alloys of the type Pt - Fe; Pd - Pb; Pd - Cu; Pd - Te; Pd - Hg, which comprise 75 per cent of total PGM present, while numerous bismuthides, tellurides, antimonides, arsenides, PGE - Pb alloys and laurite (8 per cent) comprise the balance. The associated sulphides are primarily pentlandite, pyrrhotite, chalcopyrite and bornite with minor amounts of chalcocite, covellite and millerite. In contrast, the PGM in the UG2 chromitite layer of the prospecting shaft and other cores investigated by McLaren are essentially sulphides.

Major base metal sulphides present in the shaft material are pentlandite, chalcopyrite, pyrrhotite with subordinate amounts of pyrite. McLaren (1978, p.23 - 24) has calculated that 81 per cent of the PGM in the MDH 5 borehole intersection of the UG2 chromitite layer are associated with base metal sulphides, while the rest are found along grain boundaries (11 per cent), in chromite (3 per cent) and in the gangue (5 per cent). Similarly samples from the shaft showed the PGM also to be associated with base metal sulphides (BMS) and along grain boundaries, and rarely to be enclosed in the chromite.

## 5.2 Platinoid geochemistry

The geochemical affinity of platinoids with sulphides in mafic to ultramafic rocks is well documented in the literature (Wright and Fleischer, 1965; Mertie, 1969; Razin, 1976) and their strong chalcophile tendency is exemplified by numerous examples of high platinoid concentrations in association with Ni-Cu sulphides in mafic to ultramafic rocks of the Bushveld Complex (Wagner, 1929; Liebenberg, 1970; Brynard et al. 1976; McLaren, 1978 and Von Gruenewaldt, 1979). In both the Merensky Reef and the UG2 chromitite layer the platinoids are primarily associated with sulphides although the S content of the latter is in the order of six times lower than the former.

The close association between sulphides and platinoids has resulted in numerous researchers suggesting that sulphides act as a collector of platinoids. Naldrett and Cabri (1976) have questioned the simple model of platinoids being collected in an immiscible sulphide liquid during crystallisation of stratiform disseminated platiniferous deposits because of the enormous gap between the calculated concentrations of platinoids in sulphide melts and those found in mineralised layers such as the Merensky Reef. Calculations by Naldrett and Cabri (1976, p. 1152 - 1154) have shown the Pt and Pd concentrations in early, immiscible sulphide liquid to be in the order of two and three ppm respectively in contrast to the 260 ppm of Pd and 110 ppm of Pt in the Merensky Reef and 500 to 2 000 ppm in the Stillwater. Although precise determinations of the distribution coefficient for Pt and Pd between sulphide and silicate liquid for Pt and Pd have not been observed Naldrett and Duke (1980, p. 1 421) quote the best available estimates as being 1 000 for Pt and 1 500 for Pd.

Hiemstra (1979, p. 471), using results obtained from the analyses of samples from the UG2 chromitite layer (McLaren, 1978), has calculated the Pt and Pd values in the



sulphides to be 5835 ppm and 3574 ppm respectively. Work in this study has shown that the S content of the UG2 chromitite layer used by Hiemstra (1979) was unrealistically low. If the concentration of platinoids in the initial sulphide liquid is calculated according to the average Pt and Pd concentrations found in the UG2 layer on Maandagshoek (Table 7) using an S content of 1300 ppm,<sup>\*</sup> then the sulphide liquid on Maandagshoek must have contained 925 ppm Pt and 934 ppm Pd. This would imply levels of Pt and Pd enrichment in the sulphide liquid, which separated at the time of the formation of the UG2 chromitite layer of 578 and 359 times the calculated levels for sulphides separating from a normal basaltic liquid (Naldrett and Cabri (1976)).

The above exercise only serves to slightly close the aforementioned gap between calculated concentration of platinoids in sulphide liquids and the concentrations encountered in economic platinoid deposits. Unless there are some radical miscalculations in the partition coefficient of the platinoids between silicate and sulphide liquids some other carrier or collector must be sought to concentrate the platinoids into ore deposits.

In addition to the strong partitioning of the platinoids into the sulphide liquid there seems to be a strong affinity of these elements for chromite. Wagner (1929, p.69) has reported the occurrence of large slabs of chromitite from the Onverwacht Pipe which contained up to 1877 g/t of platinoids. He describes the chromitite xenoliths as acting like "great sponges" which concentrated platinoids within themselves. Crocket et al. (1976, p.1313 - 1322) quote whole rock analyses through sections of the Merensky Reef on Middelkraal, finding a strong enrichment of Pt, Pd and Au immediately above the upper chromitite marker layer. Detailed studies of the distribution of individual separated chrome-spinels did not conclusively demonstrate that the association of chrome spinel with platinoids was due to

<sup>\*</sup>Unpublished work conducted by Mining Corporation.

lattice substitution in the spinels or due to minute, discrete PGM or PGE-alloys within the chromite grains. Grimaldi and Schnepfe (1969) approached the problem of lattice substitution of platinoids in the chrome spinel progressively dissolving chromite in sodium peroxide and compared original analytical results with the proportions of total Pt, Pd and Rh remaining within the chromite at various stages during its decomposition. The final interpretation revealed that Rh and Pt could be accommodated within the chrome spinel lattice, while Pd was found outside. The authors supported their above findings by pointing out that the ionic radii of  $Rh^{4+}$ ,  $Pt^{4+}$  and  $Cr^{3+}$  are close enough for ionic substitution.

The possibility of diadochic substitution of metallic cations of the PGE was also proposed by Razin and Komenko (1969, p.555) and Razin et al. (1965, p.122) who suggested  $Pt^{4+}$  may be accommodated in chromite. The above authors also considered that the platinoids may even have lithophile tendencies and that they could form isomorphous admixtures in silicates. Gijbels et al. (1974) studied the distribution of Os, Ru and Ir in orthopyroxene, plagioclase and chromite separates in relation to differentiation processes in the Bushveld Complex. They found a strong correlation between Os, Ru, Ir and chromite and postulated that platinoids may be collected by high-temperature cumulus chromite and subsequently expelled during the cooling process.

From the above evidence it appears as though ionic substitution of the platinoids within the chromite lattice is a distinct possibility, although serious questions may be raised as to whether the authors have demonstrated conclusively that the mineral separates are free from discrete sulphides and associated platinoid minerals.

Cousins and Vermaak (1976, p.294) questioned ionic substitution of platinoids in chromite and cite data gathered by mineralogists of Johannesburg Consolidated Investment

Company in which the chrome spinels were found to contain minute inclusions of sulphides and associated platinoid minerals. Cousins (1973) presented data from the Merensky Reef in which the Pt and Pd and total platinoids show a strong correlation with S but a negative correlation with chromite.

Detailed mineralogical studies of the UG2 chromitite layer by McLaren (1978 and 1981) has shown the presence of very small amounts of platinoid alloys, platiniferous sulphides and base metal sulphides <sup>in the</sup> chrome spinels of the UG2 chromitite layer.

Hiemstra (1979) succinctly summarised the problems involved in concentrating platinoids in the UG2 chromitite layer and has called upon the siderophile nature of platinoids to account for their unusually high concentrations. Metallic alloys of iron, nickel and copper, which are stable under very low oxygen fugacity conditions, are considered as the primary concentrators of platinoids. No evidence is presented in his treatise, however, that such low oxygen fugacities could have existed during the crystallisation of the Bushveld magma.

### 5.3 Origin of the PGE associated with the UG2 chromitite layer

The following facts emerge from the work conducted on the chromitites of the upper group and must be taken into account in any hypothesis to explain the origin of the platinoid enrichment within the UG2 chromitite layer :-

The PGE and Au of the UG2 chromitite layer are associated with base metal sulfides; and the presence of discrete platinoid sulphides such as laurite (Ru, Os, Ir, S), braggite (Pt, Pd, Ni, S) cooperite (Pt, S) and an unnamed platinoid mineral (Pt, Rh, Cu, S) in most of the UG2 chromitite layer occurrences in the Bushveld Complex.

The relative depletion of sulphur in the UG2 chromitite layer when compared to the Merensky Reef which leads to

- calculated concentrations of Pt and Pd in the sulphide melt of 925 and 934 ppm respectively.
- . The different PGM assemblage found close to the mafic pipes which are essentially platinoid alloys and associated tellurides, bismuthides, stibnides and arsenide complexes with minor amounts of laurite.
  - . The unmistakable association of platinoids with the chromitite layers which is well demonstrated by the distribution of platinum and palladium in the upper three cyclic layers on Maandagshoek (Fig. 3)
  - . The gradual upward enrichment of Pt, Pd, Cu and Ni in the footwall pegmatoid below the UG2 chromitite layer and a rapid decrease in platinoids within the rocks directly above the layer.
  - . The relative enrichment in Rh in the UG2 chromitite layer compared with the other mineralised layers in the complex.
  - . The distribution of PGM in the UG2 chromitite layer in which 90 per cent are either hosted by sulphides or form discrete platinoid sulphides or alloys along inter-grain boundaries of the silicate or oxide grains.
  - . The enrichment of Pt and Pd near the bottom and top, and the upward decrease of Rh, Ir and Ru, in the UG2 chromitite layer.

Intracratonic volcanic rocks have been shown by Crockett (1979) to give rise to the magmas that are relatively enriched in platinoids. Most workers agree that during crystallisation of a sulphur saturated magma the platinoids tend to partition strongly into early immiscible sulphide liquid and that this accounts for the origin of many platinoid-base metal sulphide ore deposits at the base of mafic and ultramafic complexes.

PGE and Au can, however, also become enriched in a mafic magma by normal processes of fractional crystallization if the magma is not saturated with sulphur. Sulphur

saturation at a late stage and the separation of an immiscible sulphide liquid may then give rise to disseminated stratiform deposits such as the UG2 chromitite layer and the Merensky Reef. Such a mechanism cannot, however, account for the extensive enrichment of PGE and Au in the sulphides.

Factors which can explain the disparities in the above are :-

- . The amount of PGE and Au in the magma may vary.
- . The calculated  $K_D$  of Naldrett and Cabri (1976) may be too low.
- . Sulphide may not be the only collector of platinoids.
- . Post magmatic processes may concentrate the platinoids.

To overcome the above problem of the abnormal concentration of platinoids Hiemstra (1979) points out that platinoids have strong siderophile tendencies and that an iron alloy, stable only under exceptionally low oxygen fugacities, could act as a primary collector of PGE and Au. Subsequently, with more elevated oxygen fugacity conditions, the iron alloys could have lost their iron to ferro-magnesium minerals and the platinoids could have become concentrated in sulphides associated with the chromite of the UG2 chromitite layer. The sulphides were too small to settle independently and Hiemstra (1979, p. 472) proposes that the sulphide droplets preferentially adhered to the chromite crystals, as opposed to the silicate grains, as they settled to form the UG2 chromitite layer. The above author proposed that this mechanism be called "pepa settling".

Vermaak (1976, p. 1290 - 1296) accounts for the deposition of platinoids in the Merensky Reef to the entrapment of upward-migrating intercumulus liquid, enriched in volatile constituents, S, platinoids, Au, Cu and Ni, below an impermeable matte of plagioclase crystals. The packet of magma that was trapped below this plagioclase matte became enriched in the ferro-magnesian components and subsequently chromite. Removal

of FeO into silicates and chromite lowered the sulphur-carrying capacity of the magma and provided an immiscible sulphide liquid which acted as a suitable collector for the PGE and Au in the Merensky Reef. Vermaak (1976) also attributes the association of platinoids with sulphides of the upper group chromites to the decrease in the FeO content during the crystallization of the chromitite layers. Vermaak (1976, p.1291 - 1292) postulated that the mineralising fluids which formed the Merensky Reef were derived by fractionation of a single pulse of magma.

The concept of a physico-chemical barrier forming a trap for upward migrating, intercumulus fluids could account for the platinoids and base metals associated with the UG2 chromitite layer, but it is suggested that the differentiation of a single magma is not acceptable because many chromitite layers with extremely low proportions of platinoids and sulphides occur in the middle and lower group chromitites. It is felt that magma batches were intermittently intruded into the magma chamber and it is tentatively suggested that such a replenishment could have occurred between the middle and upper group chromitite layers. It is not beyond the bounds of credibility to suggest that this magma batch may have been slightly more enriched in platinoids relative to the earlier magmas and thus would account for the fact that platinoids have not been discovered in exceptional quantities below the upper group.

It is thus agreed with the conclusions of Von Gruenewaldt (1979, p. 253) that the platinoids of the chromitite layers were derived from upward migrating, PGE enriched intercumulus liquids which percolated through the chromitite. Initially precipitation of relatively iron-rich chromites in the UG2 chromitite layer brought about a decrease in the FeO content of the magma causing the precipitation of sulphides. The immiscible sulphide liquid blebs, which thus formed in the interstitial spaces of the chromitite layer, could be called upon to act as collectors of the platinoids as the later PGE and Au enriched intercumulus liquid slowly migrated upwards through this layer as a result of compaction.

The capacity of high-temperature chrome spinels to collect platinoids in addition to the sulphide liquids, however, is not known, and it is tentatively suggested that they could form a primary collector of platinoids at high temperatures which could have exsolved on cooling. The similarity in ionic radii of the elements present in chrome spinels indicate that the platinoids could preferentially replace Cr, V, Ti and Fe. Heterovalent replacement of  $V^{3+}$  and  $Cr^{3+}$  with the tetravalent platinum-group metals or heteroisomorphism with  $Fe^{2+}$  by  $Rh^{3+}$  and  $Ir^{3+}$  are suggested by Razin and Khomenko (1969) as possible ways in which such isomorphism can occur. If high temperature chromites are able to take platinoids into their lattices it could account for the fact that the UG2 chromitite layer is more enriched in  $Rh^{4+}$  than the Merensky Reef.

Platinoid alloys found in borehole MDH 5 may be related to their proximity to pipe C. Tarkian and Stumpfl (1975) have investigated the composition of various platinoid minerals associated with the Driekop Pipe and found that the PGM association is dominated by native platinum, arsenides, antimonides and sulpharsenides. Peyerl (1982, in press) has found that the UG2 chromitite layer close to the Driekop Pipe contains a platinoid assemblage dominated by ferro-platinum and As - Sb alloys which changes progressively away from the pipe to the more normal Pt - Pd sulphide mineralisation. Peyerl explains the above trends to be caused by emanations of  $CO_2$ , carbonated waters, and other volatiles such as As and Sb, from the Driekop Pipe and alteration of the PGM assemblage in the UG2 chromitite layer while still in a semi-solid state. The fact that platinoids and Au are not enriched in the UG2 chromitite layer closer to the pipe indicates that the platinoids in the layer were not derived from the pipes.

In summary it is thus proposed that the incipient chromitite layer acted as a physical barrier, due to the

tightly packed chromite grains, and a chemical barrier to the upward migration of late deuteric fluids and volatiles charged with Au, Sb, As, Te and platinoids. The platinoids were collected by sulphide droplets already in the UG2 chromitite layer. At present no satisfactory explanation has been found to explain the observed distribution of the PGE in the UG2 chromitite layer.



## 6 STRUCTURE

### 6.1 Description of structural features

Underground exposures and surface outcrop of the layers on Maandagshoek 254 KT are limited. The available exposures have allowed a classification of two classes of structural features.

#### 6.1.1 Class 1 structural features

Such features are related to the time of crystallisation of the magma and the formation of layers, and include the effects of viscosity and density contrast between the liquid and the crystals settling under the influence of gravity. These features are usually located close to the interface of rocks rich in chromite, plagioclase and orthopyroxene and are normally found at the top and bottom of the cyclic units.

The UG1 chromitite layer consists of a series of chromitite layers that anastomose and bifurcate at low angles in general concordance with the layering (Figs. 33 - 34). Lee (1981) is of the opinion that the structures seen in the UG1 chromitite layer are primarily caused by vertical or horizontal plastic deformation which is principally caused by variations in the viscosity rather than density contrasts between the anorthosite and chromitite layers. In the above model the less viscous chromitite layers indicate mobility relative to anorthosite and explains some of the layering relationships seen in the UG1 chromitite layer. The cumulative width of the various chromitite layers of UG1 chromitite is not constant but varies from 0,96 metres in MDH 4, 1,48 metres in MDH 7, 2,11 metres in MDH 5 and 1,29 metres in MDH 23.

The leuconorites below the anorthosite layer at the top of the UG2 cyclic unit in the prospect shaft display slump structures. This type of feature is not well exposed on Maandagshoek but may be seen in a donga close to the shaft (Fig. 35). The intensity of this disturbance in the



Figure 33 : Irregular layering in the UG1 chromitite from a locality on the eastern side of the Legabeng Hill on Driekop 253 KT.



Figure 34 : Inter-layered chromitite with intercumulus plagioclase and almost pure anorthosite in the UG1 chromitite layer on Driekop 253 KT. (Same locality as Figure 33).

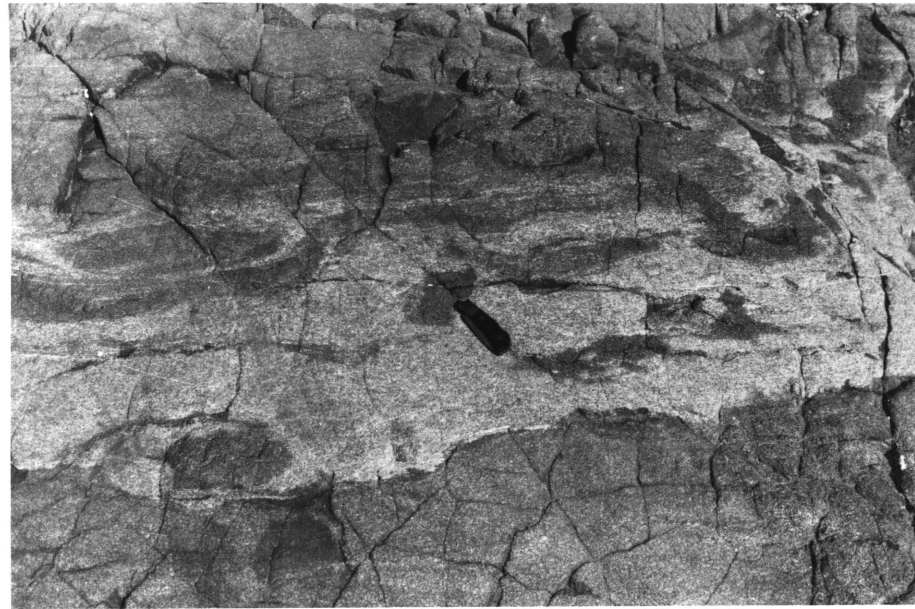


Figure 35 : Complex disturbance in the norites and leuconorites below the UG3 chromitite layer in a river section close to the prospect shaft on Maandagshoek 254 KT.

layering increases upwards and reaches a maximum just below the anorthosite layer.

At the contact between the anorthosite and the overlying chromitite at the top of the UG2 cyclic unit the style of folding is completely different and is characterised by dimpling and low amplitude dome and basin folding. Such features are interpreted as incipient flame structures as described and illustrated by Lee (1981). In the model proposed by Lee (1981) the underlying crystal mush is less viscous than the crystal mush in the overlying layer and, due to this contrast, low amplitude folds begin, which are progressively elongated under the influence of gravity to form cusped structures. Cusped structures have been documented at the base of the UG2 chromitite layer (Lee, 1981), but have not as yet been observed on Maandagshoek. Although Lee feels that viscosity plays the predominant role in the formation of such features it is considered that density contrasts could also have been of importance.

Large elongated fragments of chromitite are found in the gabbro-norites below the UG1 chromitite layer (Fig. 36). The host rocks generally display foliation around these bodies (Fig. 37) in a manner which is not unlike the features that are observed below load casts in sedimentary rocks.

Minor faults, typically in the form of horst and graben faulting along planes at right angles to the layering are confined to the UG1 chromitite layer (Fig. 38). Because of the contrast between the chromitite and anorthosite layers the small faults are clearly visible. In places, chromite has been remobilised along the fault planes. These fault zones commonly contain uvarovite (Cousins and Feringa, 1964, p.196).

A "pothole" was mapped on the surface between trenches 2E and 2F where the UG3 chromitite layer and its footwall anorthosite have transgressed the horizontal layering to about four metres below their normal elevation (Figs. 39 and 40). Features of note are the boundinaged and attenuated nature of the UG3 chromitite layer and the footwall

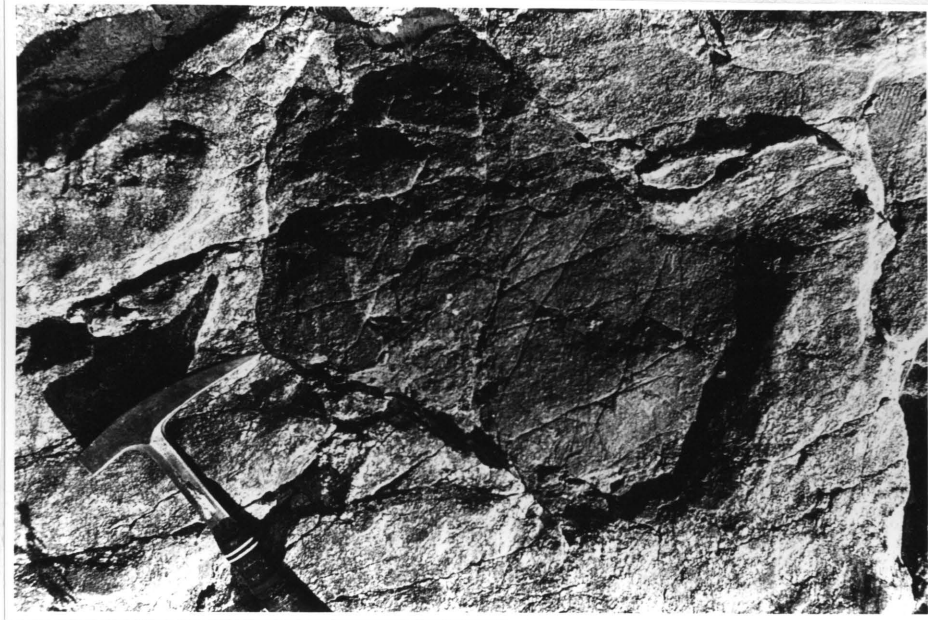


Figure 36 : Plan view of a large lens of chromitite found in anorthosite below the UG 1 chromitite layer to the east of Trench JJ on Maandagshoek 254 KT.



Figure 37 : Lens of chromitiferous melanorite found in the gabbro norites below the UG 1 chromitite layer to the east of Trench RR on Maandagshoek 254 KT.



Figure 38 : Minor faulting in the UG1 chromitite layer. Rock specimen was found close to the outcrop of the UG 1 layer to the east of Trench RR on Maandagshoek 254 KT.

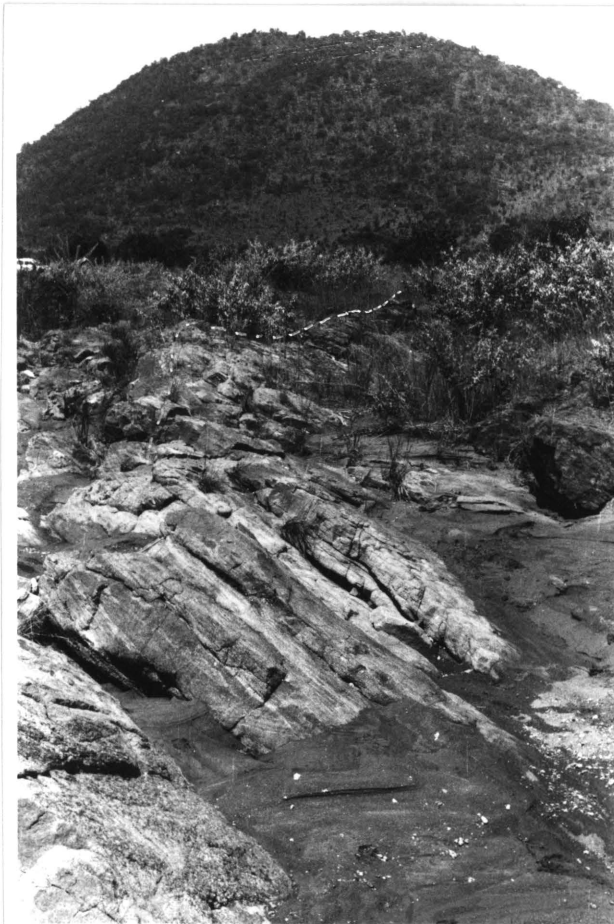


Figure 39 : Pothole on Maandagshoek 254 KT. Note the folding and stretching features in the norites below the anorthosite layer. A plan of this feature is shown in Figure 41.

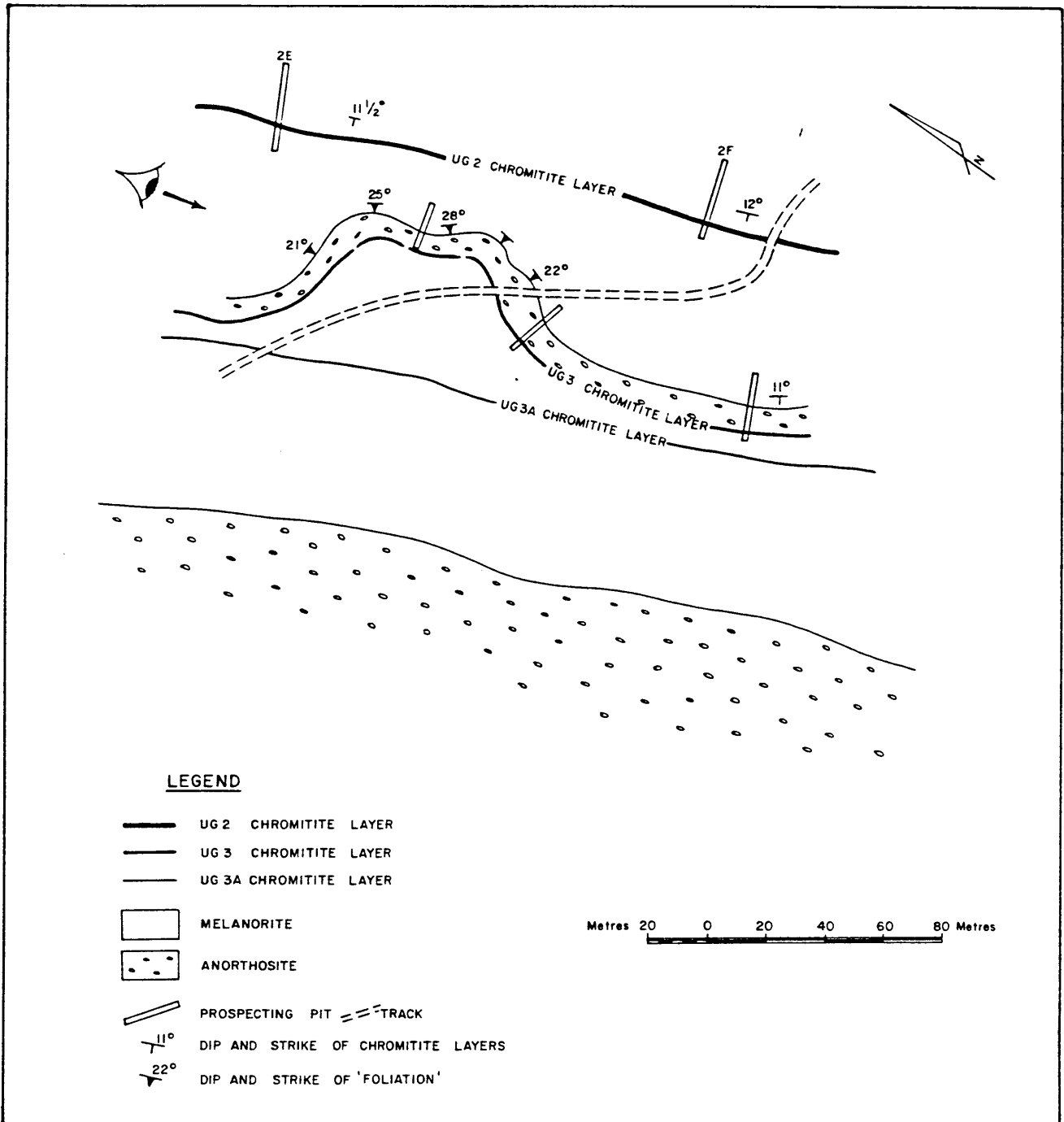


Figure 40 : A pothole mapped on the surface between Trenches 2E and 2F (for locality see Folder A). Note the direction of view of Figure 39.

anorthosite, the steeper centripetal dip of these layers and the distinct foliation imprinted upon the melanorites underlying the UG3 chromitite layer.

In summary, it is apparent that density contrast of individual layers coupled with internal viscosity differences within the crystal mush are probably the two prime factors in controlling the class 1 structural features. Such features occur preferentially at the contacts of cyclic units e.g. at the base of the UG1 cyclic unit and within the norites below the anorthosite layer at the top of the UG2 cyclic unit.

#### 6.1.2 Class II structural features

The class II structural features are defined as features associated with tectonic movement which post-date consolidation of the layering and may be recognised by bending or folding of the layering or brittle failure within the layering. Features can be grouped into three categories; those related to the intrusion of mafic pipes, dolerite dykes and faulting.

##### 6.1.2.1 Transgressive pegmatoids/pipes

Geological mapping defined three major pipes and many minor pipes. Magnetometer surveys during the borehole programme demonstrated that the distribution of the mafic pipes parallels the  $045^{\circ}$  joint direction. Many post-Bushveld dolerite dykes were also emplaced along this direction (Fig. 3 and Folder A). The structural effects imprinted on the surrounding layered rocks by the intrusion of pipes have been noted from various borehole intersections from which the UG2 chromitite layer contours and profiles were constructed (Figs. 41 and 42).

The vertical borehole MDH 5 was drilled close to Pipe C and intersected the UG2 chromitite layer 115 metres below its predicted position. This implied an increase in the dip from 11 to 18,5 degrees whereas actual measurements of the dip on the borehole core gave values of 22 degrees. Two other boreholes, MDH 19 and MDH 18 were drilled subsequently



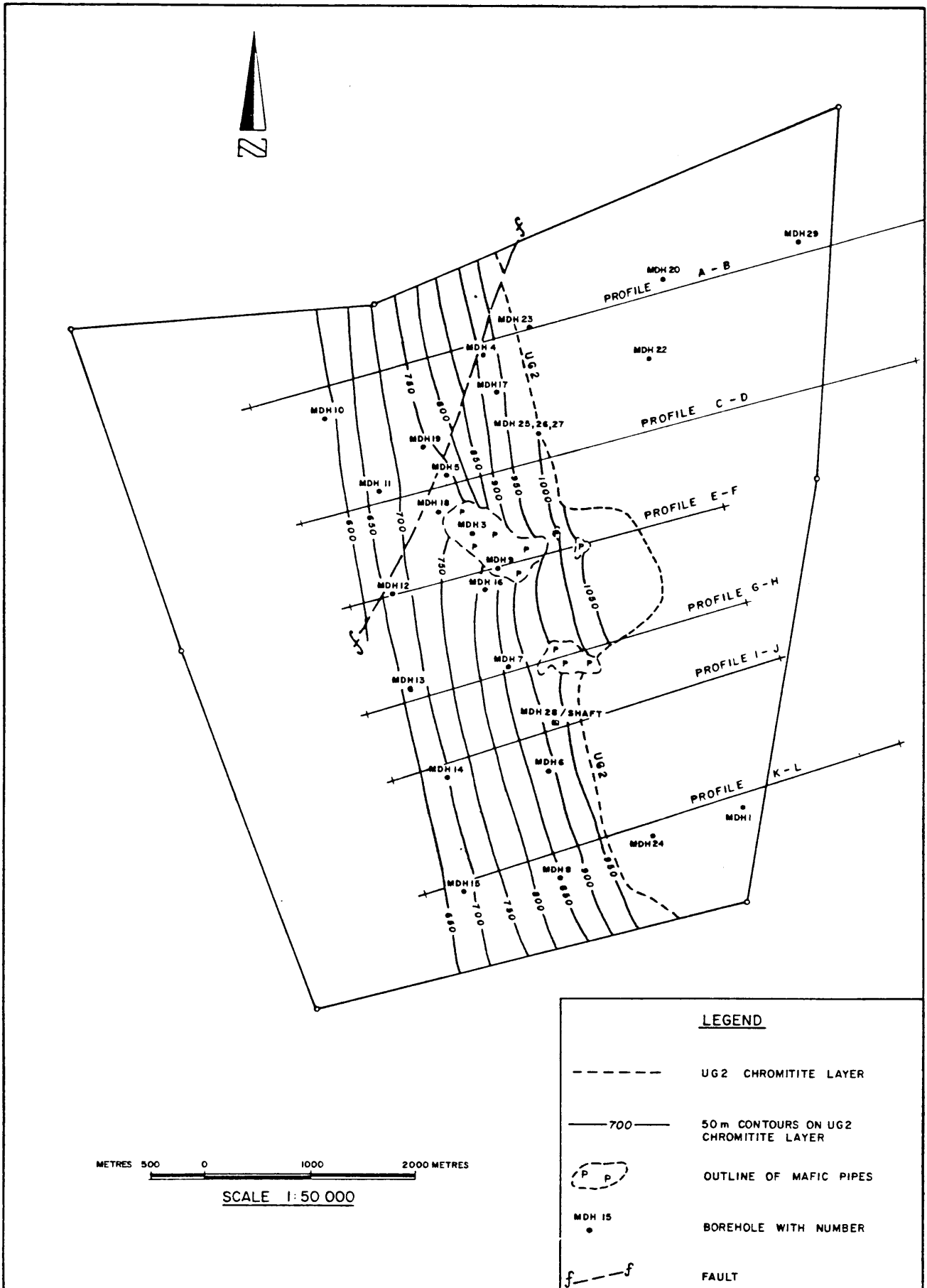


Figure 41 : The UG2 layer contours as determined by diamond drilling on Maandagshoek 254 KT.

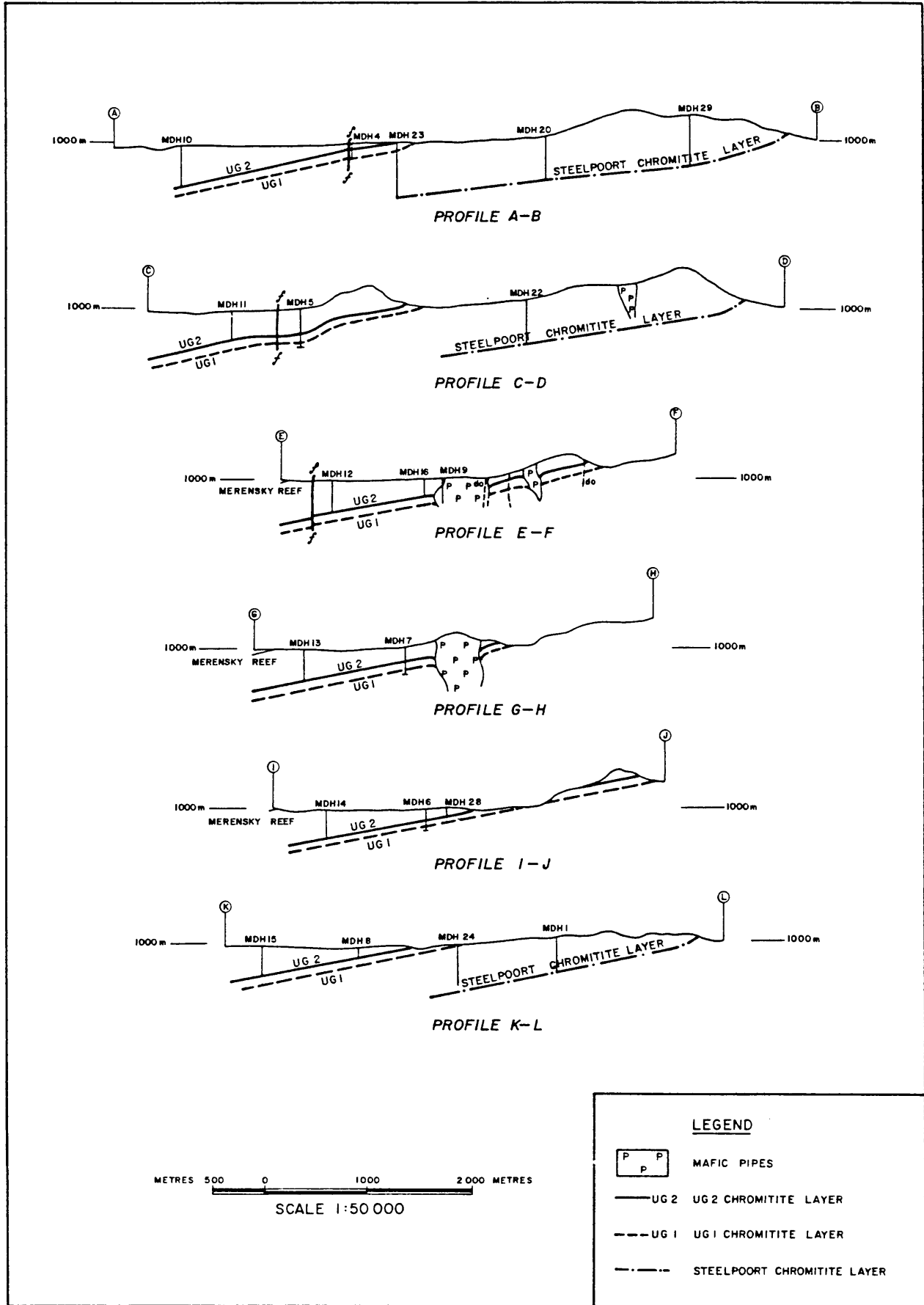


Figure 42 : UG1 and UG2 chromitite layer profiles on Maandagshoek 254 KT. For locality of profiles see Figure 41.

from which it became evident that considerable downwarping of the UG2 chromitite layer and associated layers have taken place in the proximity of the pipe (Fig. 43). Borehole MDH 3 drilled into pipe C intersected coarse-grained pyroxenite that contained minor amounts of clinopyroxene and olivine. The borehole was continued to a depth of over 300 metres, well past the intersection depths of the UG3A, UG3 and UG2 chromitite layers, but no chromitite or any layered rocks were intersected. Borehole MDH 9 intersected an apophysis of pipe C (Fig. 43), consisting of orthopyroxenite. The borehole was eventually stopped in poor ground within pipe C. Contacts between the pipe and the layered rocks are sharp. MDH 25, 26 and 27 were drilled to intersect the UG2 chromitite layer and pegmatoidal material largely consisting of pyroxenite was intersected in the boreholes. The UG2 chromitite layer was intersected in MDH 26, but its position was not predictable in relation to its expected down dip extension from surface. Downwarping and attenuation of the layering was indicated in the latter three boreholes.

Pipe B, located close to the eastern boundary of Maandagshoek, contains irregular blocks of chromitite which are tentatively identified as pieces of the UG1 chromitite layer. This chromitite is approximately 100 metres above its mapped position in the sequence.

The following is a summary of field observations of Pipes A, B and C.

- . The pipes do not all outcrop.
- . Magnetometer traverses clearly show the pipes to be aligned along a  $045^{\circ}$  joint direction which is commonly punctuated by dolerite dykes.
- . The pipes have highly magnetic cores of serpentinite with exsolved magnetite and coarse-grained to pegmatitic pyroxenite rims.
- . The contacts between the pipes and the enclosing layered rocks are sharp.

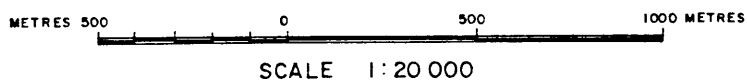
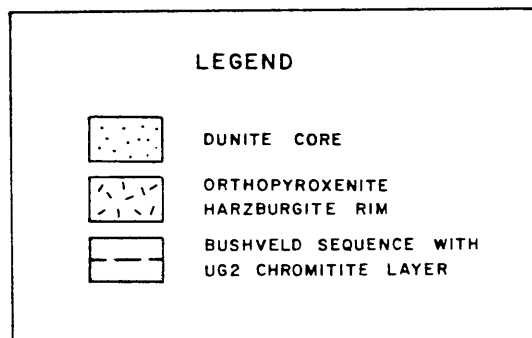
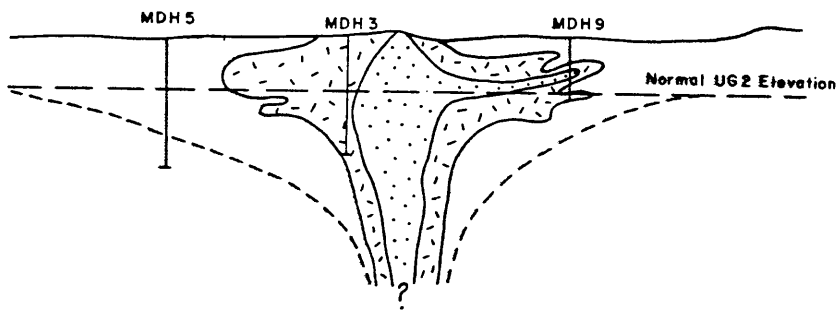


Figure 43 : An interpretation of the shape of Pipe C from magnetic, geological and borehole information.

- . Chromitite is not always found in the pipes and when observed cannot be related stratigraphically to the expected positions of observed layers.
- . Borehole information and the reef contour plans indicate a downwarping and attenuation of the layering towards the pipes.

#### 6.1.2.2 Origin of the pegmatoids/pipes

Mafic and ultramafic pipes have been described from many localities in the Bushveld Complex and several theories on their origin have been advanced. Liebenberg (1970, p.192) considers that the pipes of the critical zone of the eastern Bushveld Complex are a product of differentiation of an intercumulus liquid which has coalesced to form discrete pipe-like bodies. He notes that these pipes are more Na-rich than the surrounding norites and pyroxenites and also contain a sulphide suite which is usually more Fe- and Cu-rich than associated sulphides in the layered rocks. He does not postulate a mechanism whereby these bodies were formed or emplaced.

Cameron and Desborough (1964) carefully mapped irregularly shaped dunite and pyroxenite pegmatoids on the farms Grootboom and Annex Grootboom and suggest that replacement by metasomatism is indicated mainly because the chromitite layers are not disturbed. They further suggest that fluids, at high temperature and pressure, would be capable of converting the critical zone pyroxenite to pegmatoidal material. Such changes could essentially involve the additions of Fe, Ti, V and Mg and the concomitant loss of Si, Al, Na and Ca from the pipe environment. Such replacement processes are seen to be clearly possible and explain the preservation of chromitite layers in situ within the pegmatoids mapped by Cameron and Desborough (1964). A shortcoming of such a process is the lack of Si, Al and Na-rich products, derived from such metasomatic replacement, within the surrounding mafic rocks. Cameron and Desborough (1964, p. 221)

indicate that the Onverwacht pipe may also have been derived by replacement of bronzite by olivine and substantiate their argument by referring to observations by Wagner (1929) that large blocks of chromitite are found in this pipe at roughly the same position as the Steelpoort chromitite layer.

Ferguson and McCarthy (1970) have described a brecciated pipe-like body on Twêefontein. The sharp contacts of the pipe, rounded xenoliths, fractured and bent plagioclase laths within the xenoliths and xenoliths of chromitite, removed up to 60 metres above their stratigraphic position, are used as evidence to indicate that the pipe was forcefully injected. The authors considered the driving force to be due to a build-up of volatiles in a late ultramafic differentiate which overcame the lithostatic pressure and forcefully drove up into the layered rocks.

The structural features, especially the downward bending of the layers around the pipes observed in borehole core and mapping on Maandagshoek, are of great pertinence in deducing an origin of the pipes. The following attempts to define a model in which the pipes on Maandagshoek may be formed.

Ramberg (1967, p.101 - 105) studied salt domes in nature and their formation under experimental conditions, and found that the salt is derived principally from a source close to the root of the domes. The upward flow of the salt from the base of the dome causes a thinning in the source area and a collapse of the superincumbent sediments. Such a collapse around the salt domes is called a marginal or peripheral sink. He relates this phenomena to the deep syncline surrounding the Vredefort Dome.

Bridgewater et al. (1974, p. 57 - 58) observed such marginal synclines in the Ketilidian metamorphic rocks of southern Greenland, which are downfolded around intruding post-orogenic, mushroom-shaped intrusions of Rapakivi granite and have equated a pressure distribution model presented by

Ramberg (1967, p.104) to features seen in southern Greenland. In their model a viscous mass is forced up through an aperture in a rigid plate and lateral and outward spreading of the viscous material above the rigid plate and away from the aperture occurs. The premise of lateral spreading is dictated, and can only be attained, if the load pressure of the overlying rock is overcome by the hydrostatic pressure in the intruding material. The pressure regime existing in such a model will be such that the support in the rigid layer closest to the centre of the intrusion will be the least and it will be downfolded. The above concept is demonstrated by Ramberg (1967) and his diagrams are reproduced here as Figures 44a and 44b. The diagrams represent a flow pattern within a viscous layer in a cylinder overlain by a plunger which represents a rigid plate. The flow of the viscous mass is directed radially toward the hole while the horizontal pressure gradient points radially away from the hole as the plunger is pushed downwards into the cylinder. The volume of viscous material that flows through the aperture, with a radius  $r$ , is related to vertical compression and is given by :-

$$V = \pi(R - r^2) \frac{\sigma^h}{\sigma^t} \text{-----} (1)$$

where  $R$  is the outer radius of the layer and  $\frac{\sigma^h}{\sigma^t}$  is the rate of change of thickness of the viscous layer.

By using a constant  $c$  in Eq.2 which is related to the viscosity of the intruding material, the pressure distribution within the viscous layer may be given as

$$Pr = c(R^2 \ln r - \frac{1}{2}r^2 - R^2 \ln r_0 + \frac{1}{2}r_0^2) \frac{\sigma^h}{\sigma^t} + P_0 \text{----} (2)$$

where  $Pr$  = pressure in viscous layer at radius  $r$  from centre of hole,  $R$  = outer radius of layer,  $r_0$  = radius of hole and  $P_0$  = pressure at edge of central hole.

The above relationship (2) may be schematically portrayed by a pressure profile along a radius of  $r$  and also seen in Figure 45 (Curve A).

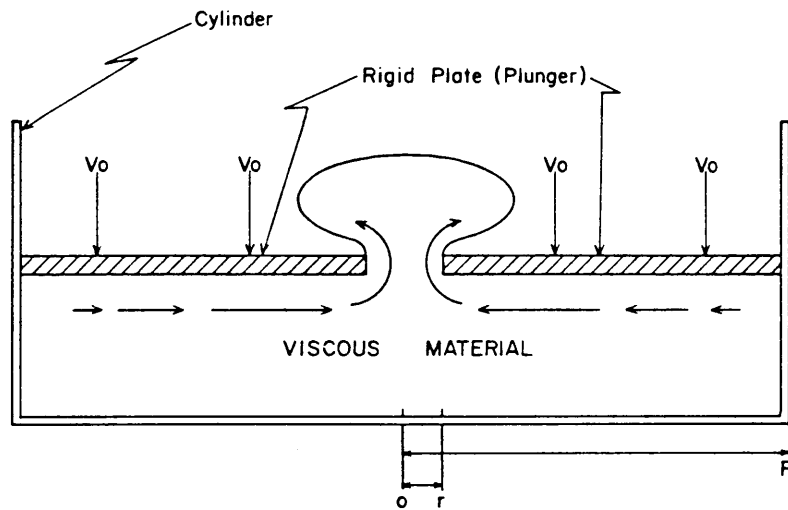


Figure 44a : Cross-section of a rigid plate, with a central aperture (radius= $r$ ), which is being pressed downwards onto a viscous mass.  $V_0$  is the rate of vertical motion of the plate. Flow direction of the viscous material is indicated by the arrows.

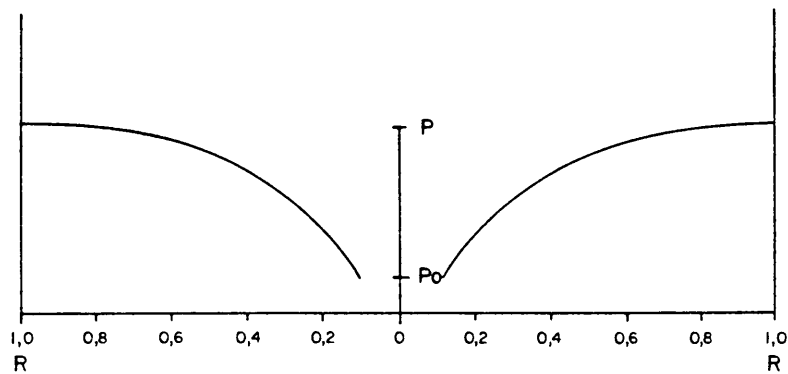


Figure 44b : Pressure distribution in the viscous mass in Figure 44a.



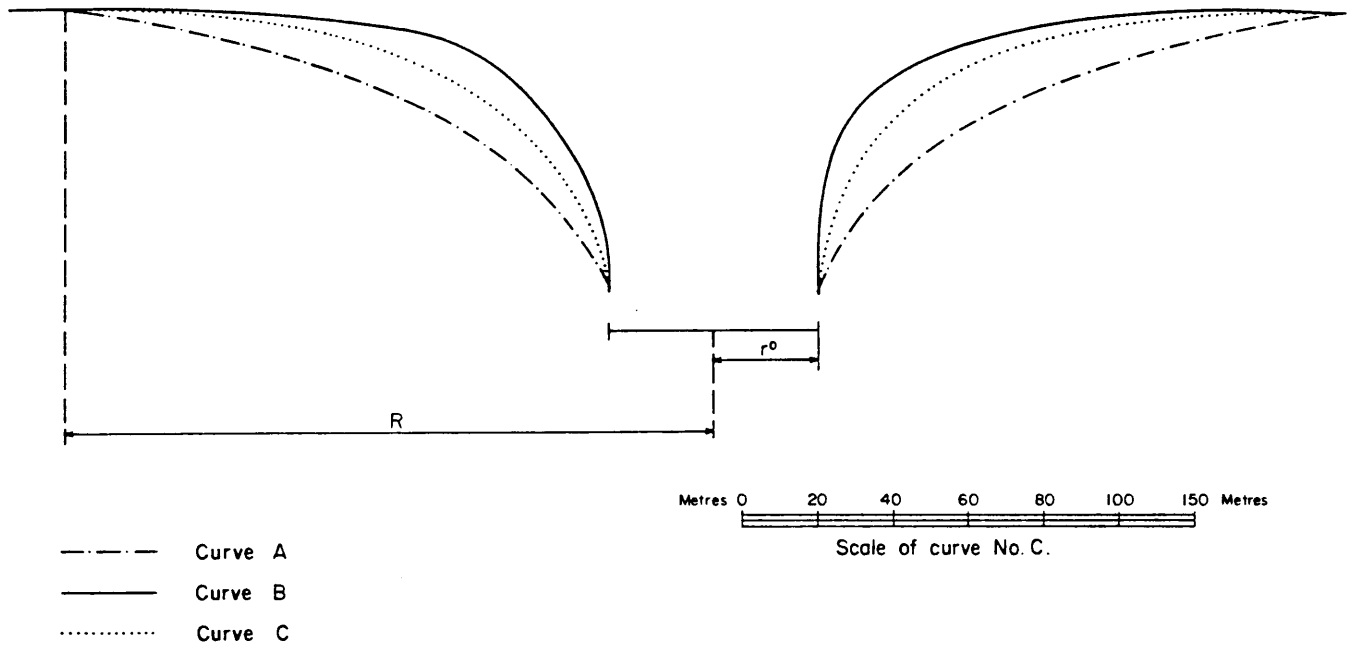


Figure 45 : Conceptual profiles at the interface of an intruding viscous mass of mafic magma of an incipient pipe and the layered rocks of the Bushveld Complex.

Curve A: Idealized profile from Ramberg (1967) calculated from Eq. 2 which assumes extrusion through a circular conduit with a strain rate directly proportional to the differential stress.

Curve B: Idealized profile, as in curve A, but altered by applying the Eyring model of steady-state flow in which the strain rate is directly proportional to differential stress.

Curve C: Profile at the level of the UG2 chromitite layer showing the interpreted dip of the layering into Pipe C as determined by boreholes MDH 5 and MDH 9.

The above relationship depends on the model in which the viscous material should have a large aerial extent relative to its thickness, and does not fit the features seen on Maandagshoek. Indications furthermore are that the pipes could have formed along planar joints or at the intersection of a joint pair and not at a round aperture. The pressure distribution given by the mathematical relationship in equation 2 in addition, is only valid at the inception of intrusion and from thence changes in a logarithmic manner.

Profiles closer to those observed in Greenland and on Maandagshoek may be mathematically derived by adopting the Eyring model for steady-state flow in which the rate of strain in the overburden is not the same as the pressure gradient but increases logarithmically with an increase in differential stress and is given as curve B (Fig. 45).

Curve C in Figure 45 is an idealised profile at the level of the UG2 chromitite layer showing the possible dip of the layering toward pipe C as determined by boreholes MDH5 and MDH9.

By applying the above concept the model envisaged for the intrusion of the pipes on Maandagshoek 254 KT is as follows :

- . The intercumulus material or late liquids rich in volatiles coalesce along inherent structural weaknesses along a fracture direction of  $045^{\circ}$ . A second joint direction of  $080^{\circ}$  could also be a control in some areas (Folder A).
- . For some reason, perhaps due to the downward compaction of the overlying crystal mush, the intercumulus liquid is forced to intrude upwards along structural weaknesses.
- . The incipient pipe intrudes upwards into the compact layering of the Complex and at a certain stage is impeded from moving upwards by a situation when lateral and outward intrusion occurs. The intruded layers in

- such a situation are suitably ductile to be bent downwards under the outward flowing pipe material.
- The apophyses of pipe material drilled represent such outward migrating pegmatoidal material and the downfolding of the layers in the upper group is thus explained.
- The dislocation of chromitite blocks, many metres above their normal stratigraphic position, may be explained by the upward movement of such pipe material.

#### 6.1.2.3 Dolerite dykes

The strike of the dolerite dykes lies between  $30^{\circ}$  and  $45^{\circ}$ . The dolerite dykes vary in size from a few centimetres to over 100 metres in thickness. The apparent influence of the dolerite dykes on the layering is negligible but underground observations in the adjoining chrome mine at Dilokong have shown that the dolerite dykes cause variations in the dip of the layering of up to  $15^{\circ}$  indicating that they were probably emplaced along pre-existing fractures or fault planes. Surface mapping has indicated no evidence for the presence of major faulting along the dykes.

#### 6.1.2.4 Faults

Lack of exposure has militated against any surface structural interpretations. The geological plan, (Folder A), shows that a fault, with a displacement of 60 metres and a bearing of 40 degrees, has been interpreted from borehole drilling. This direction parallels the major structural fabric of Maandagshoek.

## 7 ORIGIN OF THE CYCLIC UNITS

### 7.1 Development of the concept of cyclic units in the Bushveld Complex

Features of layering have frequently been reported from the Bushveld Complex but most earlier workers have dealt rather with large scale layering, its attendant cryptic layering and the persistent lateral extent of internal markers.

Lombaard (1934, p. 27 - 33), in explaining large scale layering, felt that the Complex was formed by intermittent supplies of a magma that was continuously changing in composition. In his model, differentiation within each individual heave of magma is responsible for the cryptic layering, while the magnetite layers are formed by gravity accumulation. Kuschke (1939) and Nel (1940) also described the cryptic layering in the Rustenburg Layered Suite but did not describe individual cyclic units.

Cyclic units in the Bushveld were first recognised by Wager (1957) when he described "rhythmic units" which he explained to be caused by the ability of chromite, orthopyroxene and plagioclase to nucleate. He reasoned that chromite, with its simple crystal structure, formed first, while feldspars with their more complex structures, crystallised last.

Ferguson and Botha (1963, p. 272 - 276) are of the opinion that differentiation took place in a closed chamber within which magmatic differentiation occurred after various minor additions of a magma. They also saw a combination of undercooling and convective overturn as a method of causing layering in the mafic sequence with separate differentiation of each overturned batch accounting for cryptic layering. Cousins and Feringa (1964) felt that the chromitite layers were formed by a gravitational settling of chromite but also warned that minor structural features, such as those associated with the UG1 chromitite layer, should not be

excluded in any theories of the genesis of the chromitite layers. McDonald (1967, p.182 - 185) recognised several cyclic units which consist of a chromitite layer overlain by a thick sequence of orthopyroxenite in the lower part of the critical zone in the western Bushveld. He proposed a model of bottom crystallisation, phase changes and gravity concentration in a very narrow zone above the floor of the magma chamber to account for these cyclic units.

Jackson (1970) drew attention to the similarity between the cyclic units in the Stillwater Complex and rock sequences in the Bushveld Complex. He considered the cyclic units to have formed by periodic convective overturn within the magma chamber as a result of which successive batches of magma were isolated near the floor of the intrusion, the crystallisation of each one of which followed a similar path on the liquidus in the  $MgO - CaO - Al_2O_3 - SiO_2$  system in which an indicated crystallization order is olivine, orthopyroxene, plagioclase. Cameron, in commenting on Jackson's (1970, p.423) paper, felt that the cyclic units of the Bushveld Complex are far more complex and varied than those of the Stillwater and Muskox complexes and that no one mechanism can fully explain all the various permutations observed. Cameron (1970) explained the composition variations of co-existing silicates and chromites in the transition and critical zones to be consistent with the concept of fractional crystallisation and gravitational accumulation of crystals. He called upon a mechanism of periodic changes in the oxygen fugacity to account for the chromititic intervals.

More recently Vermaak (1976, p.1284) has suggested that the rock components that make up the Merensky Suite could be called a cyclic unit while Von Gruenewaldt (1979, p.244 - 245) has suggested that the Merensky Reef be defined as "the basal pyroxenite portion of the Merensky cyclic unit which includes the porphyritic pyroxenite, the pegmatitic pyroxenite and any chromitite stringers that may be developed".

## 7.2 Setting and features of the cyclic units

The four cyclic units in the upper critical zone are enclosed within thick piles of isomodal cumulates above and below. The features associated with the cyclic units have been described while the following is a summary of those considered to be important in developing a hypothesis on the origin of these units.

### 7.2.1 Attitude of layering

The dip of the layering in the cyclic units on Maandagshoek, apart from in the vicinity of pipes, is regular and is between 11 to 12 degrees to the west. Gravity modelling, geological mapping and drilling in the eastern Bushveld Complex have shown it to have the shape of an elongated lobe with a  $010^{\circ}$  *strike* and a synclinal cross-section. The centripetal dip of the compartment as a whole is not regular and shows steeper dips closer to the margins with a gradual flattening towards the centre.

### 7.2.2 Geology of cyclic units

Cyclic units consist of chromitite, with or without olivine at the base, melanorite, norite, leuconorite and anorthosite above. Contacts may be sharp or gradational. Sharp phase contacts are usually found closer to the boundaries of individual cyclic units and are usually associated with monomineralic cumulates. The cyclic units and the individual internal layers are remarkably persistent along strike and dip.

### 7.2.3 Grain size variation

Sharp changes in the grain size, as reflected by the IC numbers at the top and the bottom of the cyclic units and an increase in the grain size of the rocks below the UG2 chromitite layer are noted. The IC numbers also reflect changes in the lithology in a sensitive manner.

### 7.2.4 Mineral composition variations

The En content of the orthopyroxene and the An content

of the plagioclase decrease and increase respectively upwards through the cyclic units. This simple trend is reversed when chromitite layers are approached where the En content of the bronzite increases. The upward basification in the anorthosite layers below overlying chromitite layers is especially accentuated in the layer below the UG3 chromitite layer.

#### 7.2.5 Trace element analyses

The platinoids, Cu and Ni are enriched in the chromitite layers, especially in the UG2 chromitite layer. In the plagioclase separates there is an increase of Rb at the top of the UG1 and UG2 cyclic units together with a reasonable inverse relationship between Rb and Sr. Zr within the plagioclase also shows an upward enrichment in the above two cyclic units. In the orthopyroxene there is a slight increase of V upwards in the cyclic units, an increase of Cr and Ni close to the chromitite layers and a decrease in Ni where sulphides are found.

#### 7.2.6 Structural features

Class 1 structural features, such as the lack of continuity of layers, folding features, rafting of chromitite blocks, minor faults and potholes, should be considered in any hypothesis on the origin of cyclic units.

### 7.3 The origin of the cyclic units in the upper part of the critical zone

#### 7.3.1 Review of proposed hypothesis

Jackson (1961) (1970) has explained that the convective overturn of separate batches of magma could be responsible for the individual cyclic units. Irvine (1970) has better quantified this concept in a study of heat transfer during the solidification of layered bodies. He shows that for convection to occur, there is a greater heat loss at the top of the magma pile and that the cooler denser magma found in this position descends to the floor and crystallises at the base.

If convective overturn is responsible for cyclic units of the critical zone it must be noted that this phenomena is an infrequent event, because of the thick sequences of isomodal rocks that separate the cyclic units. The different physico-chemical conditions that cause these two diverse types of layering are seen to be tied to the height of the intersection of the adiabatic and melting point gradients above the floor, whether convection occurs, the density and size of the crystallising minerals, the rate of crystallisation and whether the crystals in the liquid are able to sink (or rise) to form layers. With regard to the latter point, Campbell (1978, p.319 - 321) has questioned the ability of "magmatic sediments" to always act in a manner according to Stokes' Law. Centrifuge experiments by the above author indicate that size of crystals is a more important factor than density and that the production of monomineralic cumulates by crystal settling will be unlikely. In addition Campbell et al. (1978, p.376 - 377) have shown that certain plagioclases from the Skaergaard Intrusion have had a lower density than the iron-rich liquids from which they are postulated to have crystallised. Campbell (1978) and Campbell et al. (1978) postulate that cumulates form close to the magma chamber floor and that changes in the type of cumulate mineral present in the layers may not be caused by gravity settling and density sorting of crystals in the magma but be due to rhythmic changes of crystallizing phases in a zone of supercooling just above the floor of the magma chamber.

Hawkes (1967) attributes undercooling as the mechanism of formation of the cyclic layering observed in <sup>the</sup> Freetown Complex of Sierra Leone. The absence of cryptic layering is seen as evidence that crystal settling was not a dominant factor in the formation of the layers and that under equilibrium conditions the cumulus minerals crystallise and produce an isomodal cumulate, the olivine gabbros. When undercooling conditions prevailed the minerals crystallised in an order which is determined by their ease of nucleation, which in the case of the Freetown Complex was magnetite - olivine -



pyroxene - plagioclase and thus produced cyclic layers.

Sharkov (1972) and Yaroshevsky (1970) proposed a process which the former termed recurrent crystallisation to explain cyclic features in layered intrusions. The process, envisaged by these authors using the rock types in this study, is as follows :-

- . In a cooling magma chamber, liquidus and solidus isotherms are developed. Between these lies the crystallisation front isotherm.
- . As cooling progresses the most refractory minerals, first chromite and then orthopyroxene are removed from the liquid and deposited on the magma chamber floor. A diffusion front is formed ahead of the crystallisation front in which the component of plagioclase is concentrated.
- . The crystallisation process is gradually slowed down because of the increase in the concentration of least refractory components (plagioclase) and a zone of constitutional supercooling develops (Sharkov, 1972 p.596).
- . The slowing down of the crystallisation process causes a decrease in the thickness of the zone of crystallisation because of the gradual advance of the solidus isotherm which in turn leads to a decrease in the size of the diffusion zone.
- . The diffusion zone eventually becomes so thin that the crystallisation front moves into the overlying liquid and the process repeats itself.

Maaløe (1978, p.342 - 345) has also recognised that undercooling of the magma could be an important factor in producing the rhythmic layering observed in the Skaergaard Intrusion. He points out that, during crystallisation, temperature variations will affect the growth rate and nucleation rate of crystals. In addition to the above he has also emphasized the fact that during nucleation and crystal growth of one or more minerals from a magma the remaining melt would have

its composition changed to such an extent that its ability, or potential to nucleate other minerals would also change. By studying the size of the crystals through the rhythmic layers of the Skaergaard Intrusion he found that the most crystals per  $\text{cm}^3$  (crystal index) were associated with mono-mineralic rocks in the cyclic layer. From these observations Maaløe (1978) concluded that undercooling, with its associated high nucleation rate, is the driving force that causes cyclicity.

Goode (1976, p.389 - 396) uses the concept of nucleation to account for layering but introduces other variables. Essential to his hypothesis is whether crystallisation is uninterrupted (continuous) or whether it occurs in pulses (discontinuous), the distance between the floor and the nucleating crystals in the magma chamber and the ability of crystals to settle according to Stokes' Law. He considers that during pulses of discontinuous crystallisation, separation according to Stokes' Law will occur to produce density graded layers provided that the distance from the floor is great enough. During continuous crystallisation no separation occurs and isomodal rocks result. His theory omits to explain how pulses of crystallisation occur in a discontinuous or continuous manner.

### 7.3.2 Origin of the chromitite layers

The cyclic units of the upper critical zone have chromitite layers at their base and a study of the first layers that separated during cyclic crystallization may be useful in reconstructing the physico-chemical conditions that initiated cyclicity. Four main lines of investigation have been followed by various authors in the search for an adequate mechanism that initiated the crystallisation of chromitite layers.

- . Contamination of the basic parental magma by salic material, Irvine (1975).
- . Blending of a primitive magma with the more differentiated earlier liquid (Irvine 1977).

- . An increase in the oxygen fugacity: Cameron and Desborough (1969), Snethlage and Von Gruenewaldt (1977) and Snethlage and Klemm (1978).
- . Tectonically induced variations in the total pressure. Cameron (1977, 1980).

Irvine (1975, p.1003 - 1008) postulated that the formation of chromitite layers seen in the Muskox Intrusion and other large stratiform complexes was initiated by the contamination of a basic magma with a large quantity of salic melt. This mechanism was seen to lower the temperature and to change the composition of the resulting hybrid melt to cause chromite crystallisation. The presence of tiny spherical inclusions rich in silica and alkalis within the chromite, roof-rock melting, and contamination are used to substantiate this hypothesis. Irvine (1975, p.1014 - 1018) also suggested that the sulphides associated with chromitite layers of the Muskox Intrusion separated from the melt because of the decrease in sulphur solubility with an increase in the silica content.

Irvine (1977) realised the following problems in his (1975) hypothesis :-

- . The Fe-enrichment trend of the Bushveld magma can only be produced if the liquid is progressively depleted in the alkali component.
- . The experimental model proposed was too restrictive in many situations in that prohibitively large amounts of salic rock were needed to bring chromite onto the liquidus.

It is also felt that the repetitive nature of the chromitite layers, their extensive areal extent and their similar chemical characteristics would need a remarkably thorough mixing of the contaminants to effect the features seen in the Bushveld Complex. In addition the Bushveld Complex is at present considered as consisting of several compartments and the similar features seen in these various compartments are certainly not consistent with the hypothesis

of an extraneous source of salic contaminant to account for the chromitite layers.

Irvine (1977) therefore suggested that the addition and blending of a primitive liquid with the earlier differentiated liquid could produce chromitite layers to account for the main features seen in cyclic units in most stratiform complexes. Irvine (1977, p.276) illustrates and explains the essential features of the formation of chromitite, harzburgite, orthopyroxene in the system olivine - chromite - quartz (Fig. 46).

The possibility that changes in the oxygen fugacity is responsible for the formation of the chromitite layers in the Bushveld Complex has been mooted by several authors. Ulmer (1969, p.125 - 129) initially demonstrated by experiment in the system MgO - iron oxide -  $\text{Cr}_3\text{O}_3$  -  $\text{Al}_2\text{O}_3$  at a temperature of  $1300^\circ\text{C}$ , that the size of the stability field of chromite is dependent on oxygen fugacity, and that the size of this field reaches a maximum between  $10^{-5}$  to  $10^{-7}$  atmospheres. The influence of oxygen fugacity on the stability of chromite in the systems MgO - FeO -  $\text{Fe}_2\text{O}_3$  -  $\text{SiO}_2$ , Muan and Osborn (1956), and MgO - FeO -  $\text{Fe}_2\text{O}_3$  -  $\text{CaAl}_2\text{O}_8$  -  $\text{SiO}_2$ , Roeder and Osborn (1966) has been studied and the salient features and results are essentially that the size of the spinel field increases with increasing oxygen fugacity, and that in the latter system spinel and pyroxene become incompatible between oxygen fugacity values of  $10^{-9}$  -  $10^{-11}$ . Hill and Roeder (1974) substantiated the above two points while experimentally determining the liquidus phase relations of two tholeiitic basalts. They also established an order of crystallisation and the composition of the various phases in relation to the temperature and oxygen fugacity. It was found that the amount of chrome spinel formed was controlled by the oxygen fugacity, which in turn was reflected by the ferric content of the liquid. Sneath and Klemm (1978) have determined the oxygen fugacity and temperatures of formation of three comparable chromitite layers in the lower critical zone in the Zwartkop Chrome Mine and from borehole core in the lower

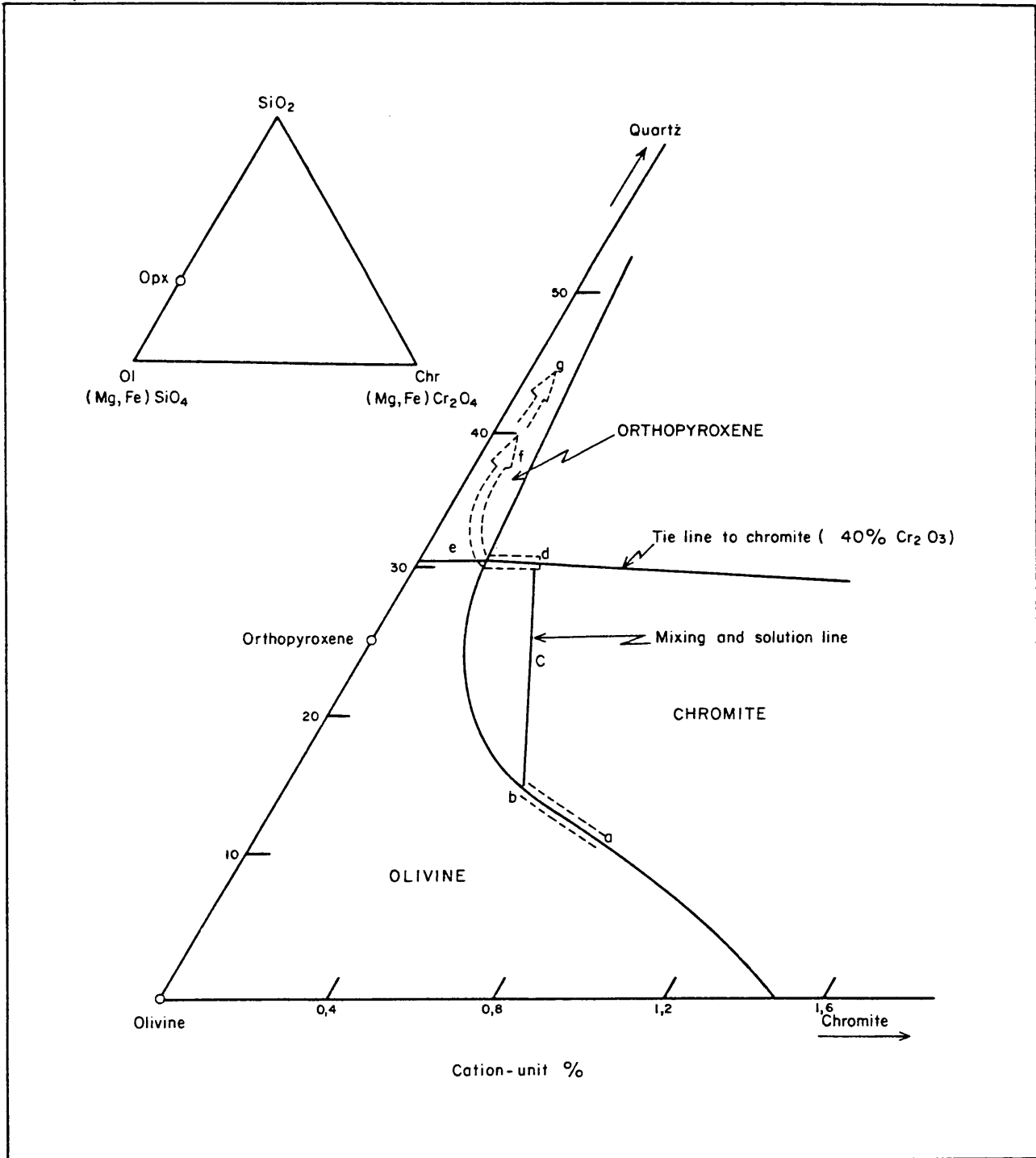


Figure 46 : Cation norm projection on the join olivine-chromite-quartz after Irvine (1977) illustrating the possible formation of chromitite layers by liquid mixing. Position 'g' represents the point to which the primary liquid has differentiated and at which orthopyroxene is on the liquidus. The addition of a primitive liquid of composition 'a' causes differentiation along the olivine-chromite cotectic to point 'b'. (Harzburgite at base of UG3A unit). Mixing and blending along a schematic line 'b' - 'c' causes only chromite to be precipitated (the various chromitite layers). Continued precipitation drives the liquid to the reaction point 'd', through point 'e' until eventually only orthopyroxene is precipitated at point 'f' (orthopyroxenite).

chromitite group on Maandagshoek. They have related these to Hill and Roeder's (1974) experimental results and showed that the oxygen fugacity of the chromitite layers are higher than those in the associated disseminated chromites. From this they conclude that isothermic oxygen fugacity changes could have been the trigger in mechanism for the formation of chromitite layers. Snethlage and Von Gruenewaldt (1977), in discussing the above work, consider the periodic increase in the oxygen fugacity to be related to assimilation of CO<sub>2</sub> and H<sub>2</sub>O from sediments in the floor of the Bushveld Complex and changes in the total pressure due to tectonic adjustments or intermittent release of pressure through a vent.

Cameron (1977, p.1093 - 1095 and 1980, p.869) has questioned the viability of oxygen fugacity as a trigger in the production of chromitite layers in the Bushveld Complex for the following reasons :-

- . A mechanism in which rapid and uniform propagation of changes in oxygen fugacity throughout individual magma chambers is yet to be found.
- . Chromite analyses from the massive layers shows an increase in the Al<sub>2</sub>O<sub>3</sub> content and the ratio Cr/Fe, when compared with associated disseminated chromites.

Hill and Roeder (1974, p. 721 - 723) found that the Al<sub>2</sub>O<sub>3</sub> content and the Cr/Fe ratio increase with decreasing oxygen fugacity which is diametrically opposite to the postulate that an increase in oxygen fugacity causes the formation of chromitite layers.

Cameron (1977), in discussing the controls of chromite formation in the eastern Bushveld Complex, explains the formation of the chromite layers to the influence of total pressure. He points out that total pressure produces the most uniform and pervasive effect of all the processes proposed, which is in keeping with the observed continuity of individual layers. Tectonic effects are called upon to account for the changes in total pressure.

### 7.3.3 Cyclic units - Towards a model

Some of a large variety of systems that operate during the cooling of a large mafic intrusion have been reviewed and must have been at least partially responsible for the formation of a cyclic unit. In most of the models described above a cyclic unit would be triggered by an event such as :-

- . A new influx of a primitive magma.
- . Convection or overturn of the magma bringing a less differentiated fraction from the roof to the floor.
- . Digestion of the surrounding rocks (usually roof rocks).
- . Tectonic adjustments of the magma chamber.

Most authors, although, emphasizing the perfect lateral continuity of the layering, resort to inconstant mechanisms such as described above to derive the chromitite layers and subsequently the cyclic units. The above listed triggers could initiate a cyclic unit, or perhaps, a series of cyclic units, but it is felt that a more universal system is needed to explain the extremely consistent features seen, not only in the upper chromitite group, but in many mafic complexes described in literature. The sentiment of Maaløe (1978, p.341 - 342) that "It is not likely that each intrusion has its own mechanism as similar rhythmic layering is observed in different intrusions" is endorsed.

Both major and trace element chemistry of mineral separates in the upper chromitite group show no dramatic compositional changes that would be indicative of the mixing of a primitive or undifferentiated magma with a differentiated melt to initiate the cyclic units. It should, however, be noted that this study was confined to the layers of the upper chromitite group and that sampling was only conducted to a few metres below the UG1 chromitite layer. Without a more complete picture there is no absolute evidence that mixing did not occur just below the level of the UG1 chromitite

or possibly at the contact of the lower sub-zone and the upper sub-zone of the upper critical zone (Fig. 4, p. 13). This option is left open in the following discussion.

The following hypothesis is suggested as a modification of the various models proposed for the origin of the cyclic units in the Bushveld Complex and is called the closed-cell cyclic unit. It is essentially a synthesis of ideas and models proposed by Hawkes (1967), Irvine (1970), Yaroshevsky (1970), Sharkov (1972), Maaløe (1978), Campbell (1978) and Campbell et al. (1978).

The model assumes a centroclinally-dipping floor of a magma chamber in which both the floor and the overlying isotherms are horizontal close to the middle and bend upwards at the outer limits of the intrusion. The cyclic units are rare features that are sandwiched between thick piles of isomodal cumulates.

Cyclicity could be initiated by any of the aforementioned mechanisms but the characteristically persistent, uniform and undisturbed nature of the layers adds credence to the ideas of Cameron (1977 and 1980) that pressure changes could trigger cyclicity.

Figure 47(a) shows the start of cyclicity in which the incipient chromitite layer lies above the solidus isotherm with the front of crystallisation and the liquidus isotherm above.

Chromite crystallises behind the crystallisation front and a diffusion zone is established ahead of this front where the chromite component is depleted.

Compositional supercooling (Sharkov, 1972) occurs in this diffusion zone by the increase in proportion of the less refractory constituents. Such supercooling essentially causes both the solidus and liquidus of the remaining magma to be lowered and eventually a phase change from chromite to pyroxene takes place (Fig. 47b). Diffusion continues until plagioclase appears on the liquidus.



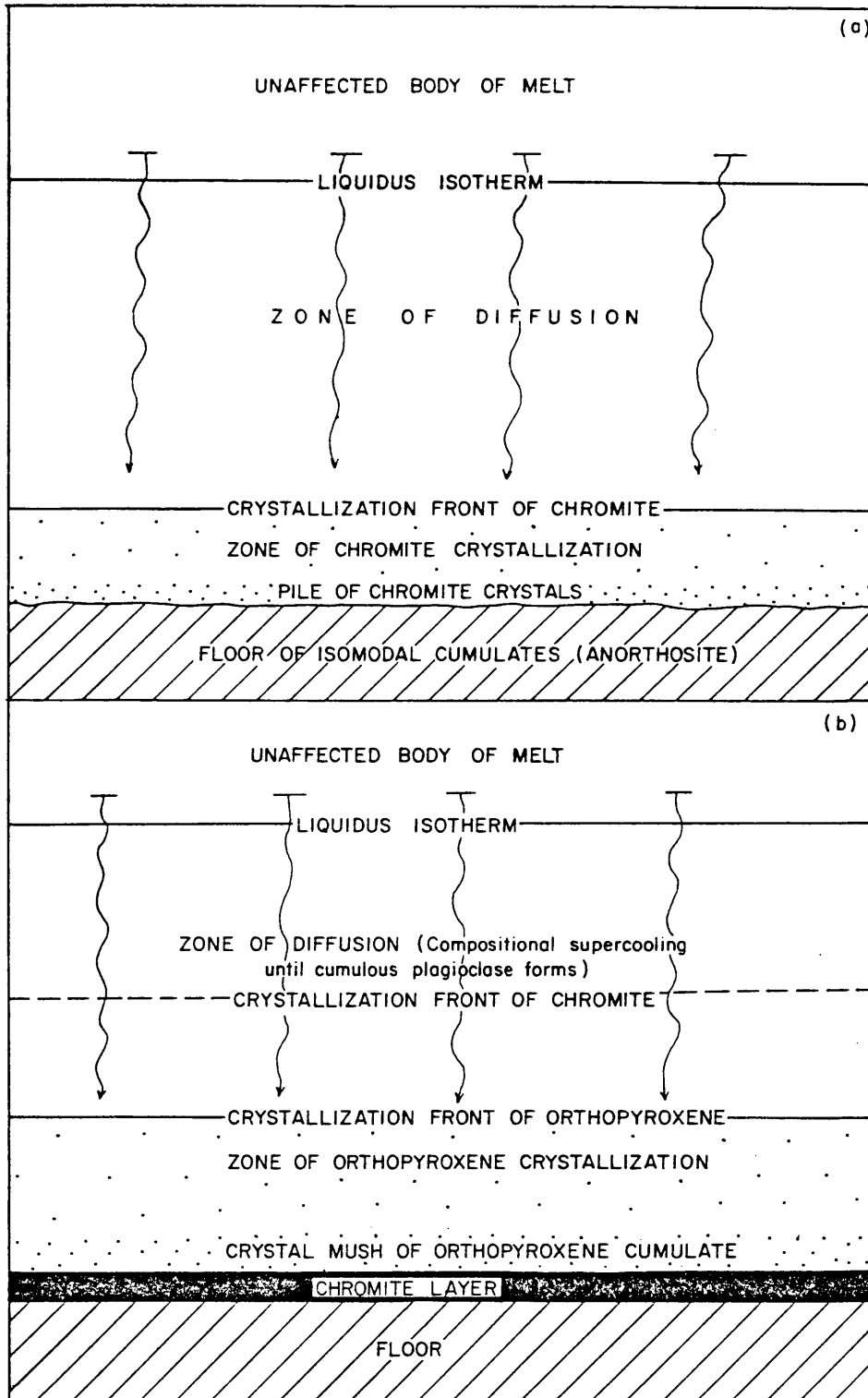


Figure 47 : Synoptic diagram showing the initial stage in the development of a cyclic unit.

(a) Cumulus chromite is the only mineral crystallizing.

(b) A phase change has taken place and orthopyroxene is crystallizing.

The zone of diffusion is smaller. Intercumulus plagioclase is crystallizing below the crystallization front of orthopyroxene and plagioclase is becoming enriched in the diffusion zone where compositional undercooling is taking place. The crystallization front of chromite is rising toward the unaffected body of melt.

Essential to the above concept is that the cell in which the cyclic unit forms is closed to the overlying magma. This sealing of the "closed cell cyclic unit" could possibly be caused by a matte of plagioclase crystals in the constitutionally supercooled region of the cell, which acts as a barrier to isolate the cell and on which the chromite of the next cycle can accumulate prior to the complete crystallisation of the lower cycle (Fig. 48). Such a matte of crystals could be formed by utilising their ability to float in magmas (Campbell, (1978) and Campbell et al. (1978)). Also essential to the formation of such a "closed cell cyclic unit" are that changes in the rock types are not primarily caused by gravity separation of the rock-forming minerals but by changes in the phases separating from the isolated batch of magma.

The above model may be used to illustrate several of the enigmatic problems associated with the study. As is illustrated in Figures 49(a) and (b) chromite can become a stable phase and form a layer above a rigid matte of plagioclase crystals which is in turn underlain by an unconsolidated mush of leuconorite. The weight of the high density chromitite layer can cause instability and disruption of the relatively rigid anorthosite matte resulting in slump features in the unconsolidated leuconorites as well as open basin and dome-like folds along the more rigid upper anorthosite-chromitite contact. Rupturing of the matte could also produce a pothole in which the underlying mush of leuconorites are stretched and attenuated (Figs. 39 and 40). Because of the rigid nature of the anorthosite layer such adjustments could also cause the minor faulting (Fig. 38).

In such a model, the knife-edge contacts seen at the bottom of cyclic units are in keeping with the theory that phase changes, rather than gravity separation, are the cause for the changes in rock types. Undercooling, which is generally reflected in an increase in nucleation sites, should be illustrated by an increase in the IC-numbers of

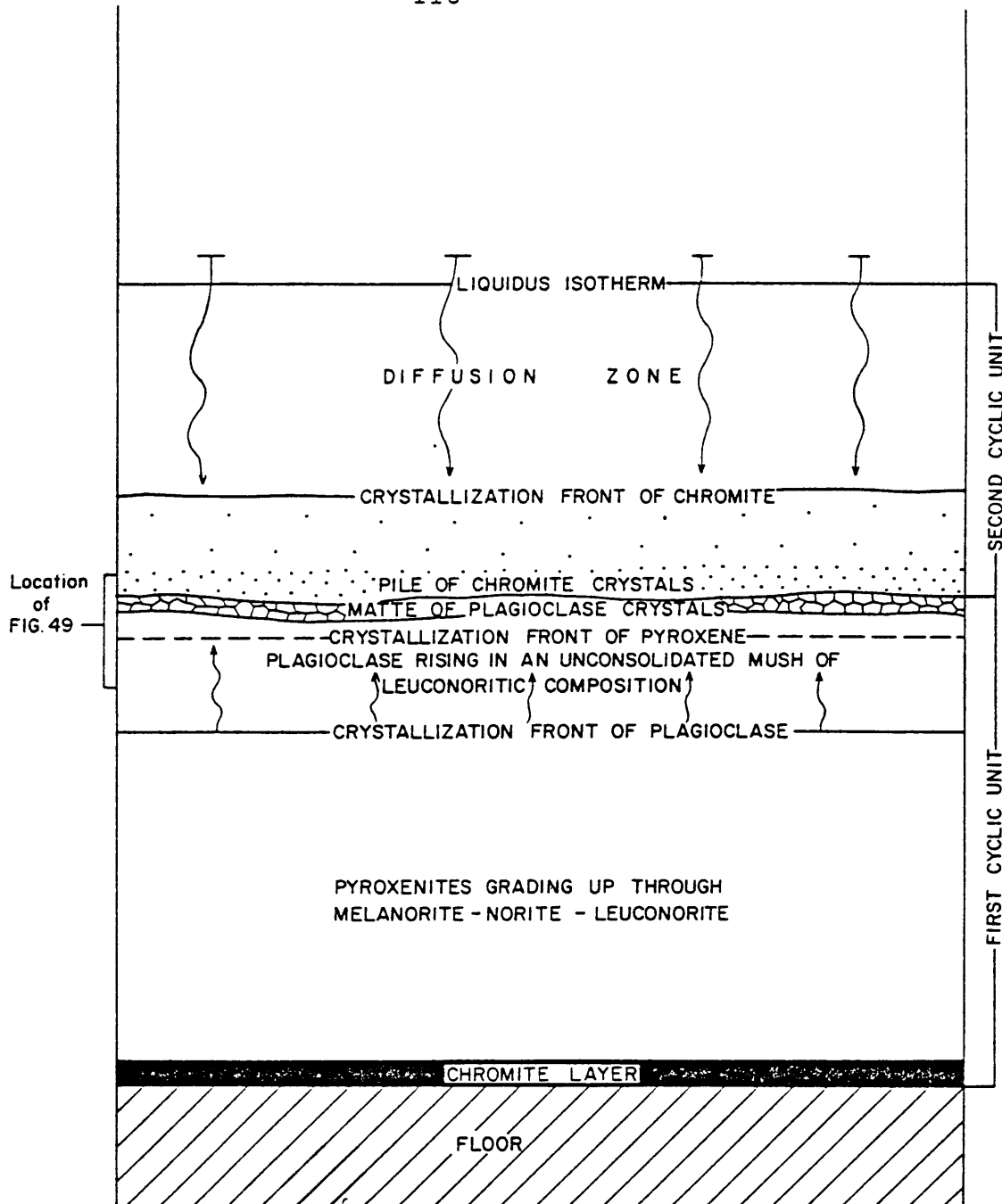


Figure 48 : Synoptic diagram illustrating the closing stages of crystallization of a cyclic unit. Plagioclase is on the liquidus in the first cyclic unit and clusters of plagioclase rise to form a rigid matte which effectively seals off the first cyclic unit. The crystallization front of chromite rises into the unaffected body of melt and chromite forms a layer above the plagioclase matte and begins the second cyclic unit.

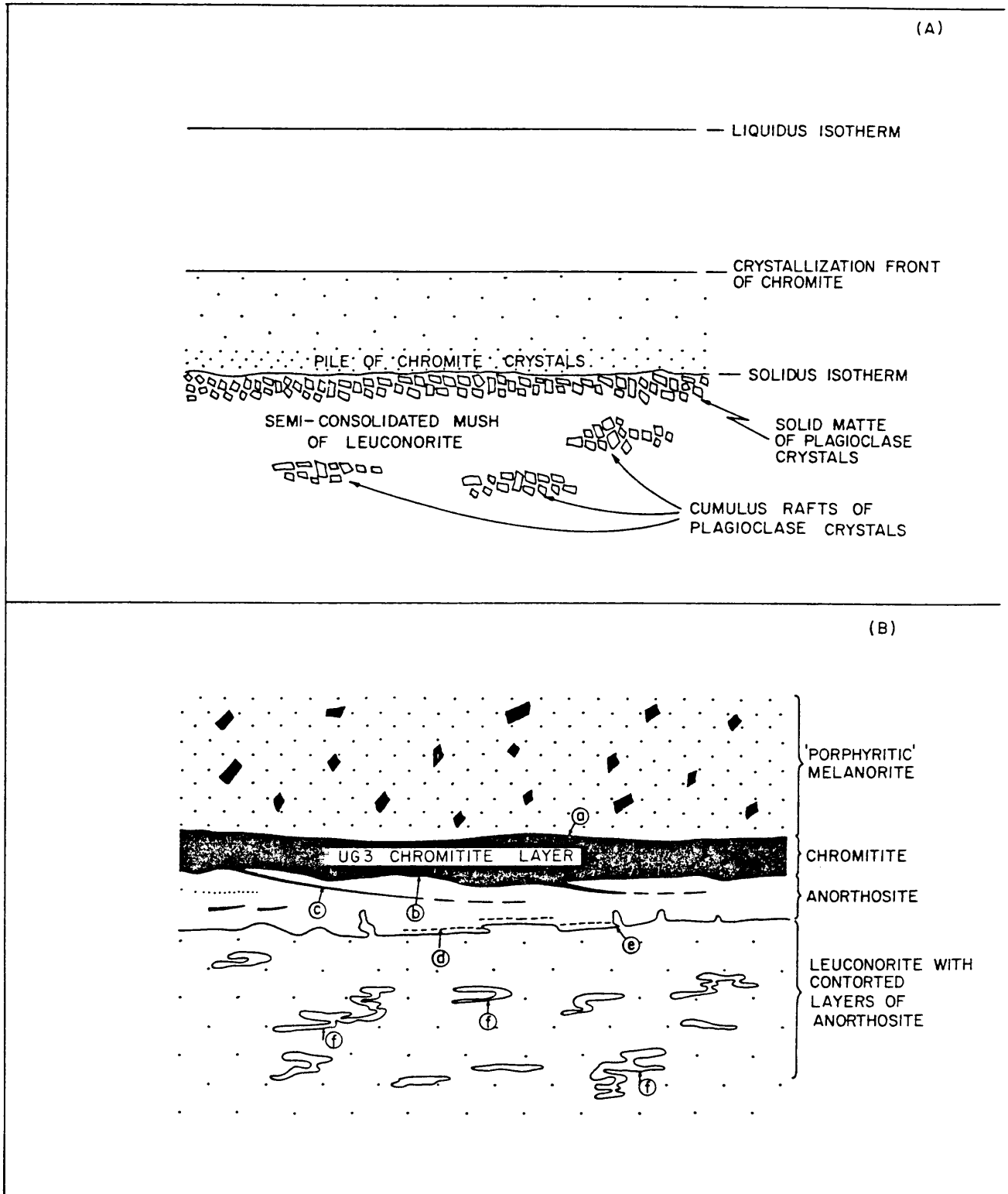


Figure 49 : Diagrammatic representation of the formation of a plagioclase matte (A) and the slump features observed below certain of the chromitite layers (For explanation see adjoining page).

the rock. Both the anorthosite at the top and the chromitite at the base of the cyclic units have high IC-numbers which fit into the model especially if it is assumed that the initial crystallisation of plagioclase results in floating of crystals to form a matte. It should, however, be borne in mind that the high IC numbers of the chromitite layers is also related to the low entropy of melting of chromite or its ease of nucleation which should result in rapid nucleation and thus a finer grained rock.

Each cyclic unit shows systematic changes in the major and minor element chemistry of the major component minerals in which the An-content of plagioclase and the En-content of orthopyroxene displays an irregular upward increase and decrease respectively. Reversals of this overall trend in the anorthosite layers could be caused by the first formed, anorthite-rich plagioclase floating to the top of the layer and being underplated by successively less anorthite-rich plagioclase as proposed by Vermaak (1976 , p.1290) for the anorthosite layers of the Merensky cyclic unit. The upward increase in the En-content of the orthopyroxenes towards the chromitite layers may be explained by the fact that the chromite removes Fe from the magma and increases the Mg component of the pyroxenes. The upward increase of Zr and the Rb/Sr ratio of the plagioclase separates of the cyclic units are consistent with the major element data that each cyclic unit represents a small isolated cell within which differentiation took place. It should, however, be noted that at the beginning of the next cyclic unit the compositions of the rocks are roughly the same composition as the preceding cyclic units.

The only major change in this relatively consistent pattern is the anomalously high value of the platinoid group elements Cu and Ni in the UG2 chromitite layer (Fig. 32). The gradual drop in Ni, in the orthopyroxenes, from the UG2 chromitite layer through the base of the anorthosite layer at the top of the UG3A cyclic unit (Fig. 32, p. 70), could illustrate

an effective sealing of these pyroxene-rich rocks from the overlying magma by the plagioclase matte. It has been suggested in Chapter 6 that an additional magma batch, slightly more enriched in platinoids relative to earlier magmas, could have intruded at a level between the middle and the upper chromitite groups. Borehole drilling on Maandagshoek 254 KT has shown the contact between the pyroxenite and anorthosite sub-zones of the critical zone to be punctuated by irregular layering and other disturbance features over a thickness of up to 200 metres. Differentiation of this primitive magma could have caused the build-up in platinoid minerals which eventuated in the precipitation of the platiniferous sulphides during the crystallisation of the UG2 and UG3 chromitite layers. These sulphides were enriched in PGE and Au by late highly fractionated inter-cumulus fluids which percolated upwards toward the UG2 chromitite layer. Because of the less permeable nature of the UG2 chromitite layer compared with the silicate-rich cumulates these late volatile-charged liquids could have accumulated below this layer to form the footwall pegmatoid.

## 8 CONCLUSIONS

This investigation of the upper chromitite group of the critical zone of the Bushveld Complex has shown that four cyclic units are present, namely the UG1, UG2, UG3 and UG3A cyclic units. These cyclic units can be defined as consisting of chromitite, with or without olivine at the base, and overlain upwards by melanorite, norite, leuconorite and anorthosite. The detailed mineralogical and major-trace element study of the cyclic units has shown that when a cyclic unit is well developed, as in the case of the UG1 and UG2 cyclic units, features of differentiation are also developed

The various layers and cyclic units have a relatively uniform dip. The influence of the pipes and to a lesser degree the faults have altered the dip of the layering and caused minor displacement which has resulted in the removal of about 10 per cent of the probable UG2 ore from the reserves. The discovery, however, of several ultramafic pipes, hitherto undetected by surface mapping, has opened up the possibility that new platinoid mineralization within such pipes may still be discovered. A hypothesis on the origin of the pipes, and concomitant structural disruption of the associated layers, is suggested as an alternative to a proposal that the pipes are formed by metasomatic alteration.

The origin of the cyclic units, chromitite layers, and associated platinoid mineralization remains an enigmatic problem but features seen in the UG1 chromitite layer and in the top of the UG2 cyclic unit point to the possibility that a closed cell cyclic unit hypothesis could prove to be a viable mechanism in the formation of cyclic units.

Indications during the study point to a strong correlation between PGE and Au with chromitite layers and base metal sulphide mineralization. The sulphide phase of the UG2 chromitite layer is enriched by a factor of 578 for Pt and 359 for Pd compared with calculated Pt and Pd levels in

sulphide liquids separating from a basaltic magma. Either the partition coefficients of 1000 for Pt and 1500 for Pd are too low or some other concentrator such as Fe-rich chromite must be called upon to collect the platinoids. The concept of a fresh pulse of magma with anomalous concentrations of platinoids emplaced at the onset of crystallisation of the Winterveld Norite-Anorthosite, may account for the higher concentrations of platinoids in the upper chromite group. Detailed studies of the distribution of platinoids on a ppb level throughout the Complex, but especially in the critical zone, could shed light on the above problem.

The UG2 chromitite layer was found to contain PGE and Au with an average content of 8,3 g/t over a width of 0,64 metres in 22 intersections in which, depending on the market situation, could become an economically viable mineral deposit.



## 9 ACKNOWLEDGEMENTS

The author wishes to thank Dr. H.J. Hanekom of the Mining Corporation Limited for his support and the generous allowance of three months paid study leave at Pretoria University to complete the laboratory studies of this investigation. I am especially indebted to Professor G von Gruenewaldt for guiding my studies, the care with which he criticised the manuscripts and his unwavering ability to make time for discussions during my study period.

Dr. Martin Sharpe, Senior Research Officer at the Bushveld Research Institute, sacrificed many hours both on and off duty to guide me through the preparation, analyses and computer processing of the mineral separates. I am deeply indebted to both he and Larry Hulbert for stimulating discussions and criticism of the initial draft of my manuscript. The list of persons which provided valuable comment during my study period is long but also among these are, included Professor A. Naldrett of Toronto University, Dr. Chris Lee of Johannesburg Consolidated Investment Company, Dr. Chris McLaren of the Council for Mineral Technology and members of the Friends of the Bushveld.

I would also like to thank my late father and my mother who provided me with the opportunity to start a geological career, my wife who accepted, with stoic resolution the destabilising effect that my studies had on our home life and who patiently typed the various manuscripts and to Miss M. Booysen of Mining Corporation who drafted the diagrams.

10 REFERENCES

- Ahrens, L.H. (1965). Distribution of the Elements in our Planet, McGraw Hill, 110 p.
- Bridgewater, D., Sutton, J., and Watterson, J. (1974). Crustal downfolding associated with igneous activity. Tectonophysics, 21, 57 - 77.
- Brynard, H.J., de Villiers, J.P.R. and Viljoen, E.A. (1976). A mineralogical investigation of the Merensky Reef at the Western Platinum Mines, near Marikana, South Africa. Econ. Geol., 71, 1299 - 1307.
- Burri, C., Parker, R.L. and Wenk, E. (1967). Die optische Orientierung der Plagioclase. Birkhäuser Verlag, Basel und Stuttgart, 334 p.
- Cameron, E.N. (1963). Structure and rock sequences of the Critical Zone of the Eastern Bushveld Complex. Miner. Soc. Am., Spec. Pap. 1, 93 - 107.
- Cameron, E.N. (1964). Chromite deposits of the eastern part of the Bushveld Complex, 131 - 168. In : Haughton, S.H., Editor. The geology of some ore deposits in Southern Africa, II. Geol. Soc. S. Afr., Johannesburg.
- Cameron, E.N. (1969). Postcumulus changes in the Eastern Bushveld Complex. Am. Miner., 54, 754 - 779.
- Cameron, E.N. (1970). Compositions of certain co-existing phases in the eastern part of the Bushveld Complex. Geol. Soc. S. Afr. Spec. Publ., 1, 46 - 58.
- Cameron, E.N. (1971). Problems of the Eastern Bushveld Complex. Fortschr. Miner., 48, 86 - 108.
- Cameron, E.N. (1977). Chromite in the central sector of the eastern Bushveld Complex, South Africa. Am. Miner., 62, 1082 - 1096.
- Cameron, E.N. (1978). The lower zone of the eastern Bushveld Complex in the Olifants River trough. J. Petrol., 19, 437 - 462.

- Cameron, E.N. (1980). Evolution of the lower critical zone, central sector, eastern Bushveld Complex, and its chromite deposits. Econ. Geol., 75, 845 - 871.
- Cameron, E.N. and Emerson, M.E. (1959). The origin of certain chromite deposits of the eastern part of the Bushveld Complex. Econ. Geol. Monogr., 4, 23 - 40.
- Cameron, E.N. and Desborough, G.A. (1964). Origin of certain magnetite-bearing pegmatites in the eastern part of the Bushveld Complex, South Africa. Econ. Geol., 59, 197 - 225.
- Cameron, E.N. and Desborough, G.A. (1969). Occurrence and characteristics of chromite deposits - Eastern Bushveld Complex. Econ. Geol., Monogr. 4, 23 - 40.
- Campbell, I.H. (1978). Some problems with the cumulus theory. Lithos, 11, 311 - 323.
- Campbell, I.H., Roeder, P.L. and Dixon, J.M. (1978). Plagioclase buoyancy in basaltic liquids as determined with a centrifuge furnace. Contrib. Mineral. Petrol., 67, 369 - 377.
- Chayes, F. (1956). Petrographic Modal Analyses. An Elementary Appraisal. J. Wiley & Sons, Inc., New York, 113 p.
- Cousins, C.A. (1973). Notes on the geochemistry of the platinum group elements. Trans. geol. Soc. S. Afr., 76, 77 - 81.
- Cousins, C.A. and Feringa, G. (1964). The chromite deposits in the western belt of the Bushveld Complex, 183 - 292. In. The Geology of Some Ore Deposits in Southern Africa, II. Geol. Soc. S. Afr., Johannesburg.
- Cousins, C.A. and Vermaak, C.F. (1976). The contribution of Southern African ore deposits to the geochemistry of the platinum group metals. Econ. Geol., 71, 1308 - 1323.
- Crocket, J.H., Teruta, Y. and Garth, J. (1976). The relative importance of sulfides, spinels and platinoid minerals

- as carriers of Pt, Pd, Ir and Au in the Merensky Reef at Western Platinum Limited near Marikana, South Africa. Econ. Geol., 71, 1308 - 1323.
- Davis, B.T.C. and Boyd, F.R. (1966). The join  $Mg_2SiO_6$  -  $CaMgSi_2O_6$  at 30 kilobars pressure and its application to pyroxenes from kimberlites. J. Geophys. Res., 71, 3567 - 3576.
- Deer, W.A., Howie, R.A. and Zussman, J. (1963). Rock forming minerals, vol. 4. Longman Group Ltd., London.
- De Waal, S.A. (1975). The mineralogy, chemistry, and certain aspects of reactivity of chromitite from the Bushveld Igneous Complex. Nat. Inst. f. Metall., Johannesburg, Rep. 03769, 79 p.
- De Waal, S.A. and Oosthuizen, G.A. (1974). Bosch 1 - a computer program to calculate the unit cell formula and certain cation ratios. Unpublished report, Nat. Inst. f. Metall., Johannesburg.
- Duke, V.W.A. (1972). An analysis of the mineral potential of the Steelpoort area, eastern Transvaal. Nat. Inst. f. Metall., Johannesburg, Rep. 1419, 12p.
- Ferguson, J. and Botha, E. (1963). Some aspects of the igneous layering in the basic zones of the Bushveld Complex. Trans. Geol. Soc. S. Afr., 66, 259 - 278.
- Ferguson, J. (1969). Compositional variations in minerals from mafic rocks of the Bushveld Complex. Trans. geol. Soc. S Afr., 72, 61 - 78.
- Ferguson, J. and McCarthy, T.S. (1970). Origin of an ultramafic pegmatoid in the eastern part of the Bushveld Complex. Geol. Soc. S. Afr. Spec. Publ., 1, 74 - 79.
- Ferguson, J. and Wright, I.H. (1970). Compositional variation of plagioclases in the critical series, Bushveld Complex. Geol. Soc. S. Afr. Spec. Publ., 1, 74 - 79.

- Flanagan, F.J. (1969). U.S. Geological Survey standards 11. First compilation of data for the U.S.G.S. rocks, Geochem. Cosmochim. Acta., 33, 81 - 120.
- Frey, F.A., Haskin, M.A., Poetz, J.A. and Haskin, L.A. (1968). Rare earth abundances in some basic rocks. J. Geophys. Res., 73, 6085 - 6098.
- Fuchs, W.A. and Rose, W.A. (1974). The geochemical behaviour of platinum and palladium in the weathering cycle in the Stillwater Complex, Montana. Econ. Geol., 69, 332 - 346.
- Gijbels, R.H., Millard, H.T., Desborough, G.A. and Bartel, A.J. (1974). Osmium, ruthenium, iridium and uranium in silicates and chromites from eastern Bushveld Complex. Geochim. Cosmochim. Acta, 38, 319 - 337.
- Goode, A.D.T. (1976). Small scale primary cumulus layering in the Kalka Layered Intrusion, Giles Complex, Central Australia. J. Petrol., 17, 379 - 397.
- Grimaldi, F.S. and Schnepfe, M.M. (1969). Mode of occurrence of platinum, palladium, and rhodium in chromite. U.S. Geol. Surv., Res. Paper 650-C, C149 - C151.
- Hamlyn, P.R. and Keays, R.P. (1979). Origin of chromite compositional variation in the Panton Sill, Western Australia, Contrib. Mineral. Petrol., 69, 75 - 82.
- Hawkes, D.D. (1967). Order of abundant crystal nucleation in a natural magma. Geol. Mag., 104, 473 - 486.
- Heier, K.S. (1962). Trace elements in feldspars - a review. Norsk. geol. tidsskrift, 42, 415 - 454.
- Hess, H.H. and Phillips, A.H. (1940). Optical properties and chemical composition of magnesian orthopyroxenes. Amer. Min., 25, 271 - 285.
- Hiemstra, S.A. (1979). The role of collectors in the formation of the Platinum deposits in the Bushveld Complex. Can. Mineral., 17, 469 - 482.

- Hill, R. and Roeder, P. (1974). The crystallisation of spinel from basaltic liquid as a function of oxygen fugacity. Journ. of Geol., 82, 709 - 729.
- Hulbert, L.J. and Von Gruenewaldt, G. (1980). Structure and petrology of the upper and lower chromitite layers on the farms Grasvally and Zoetveld, South of Potgietersrus. Inst. Geol. Res. Bushveld Complex. Res. Rep., 21, 43.
- Irvine, T.N. (1965). Chromium spinel as a petrogenetic indicator. Part 1. Theory. Can. J. Earth Sci., 2, 648 - 672.
- Irvine, T.N. (1967). Chromium spinel as a petrogenetic indicator. Part 2. Petrologic applications. Can. J. Earth. Sci., 4, 71 - 103.
- Irvine, T.N. (1970). Heat transfer during solidification of layered intrusions, I. Sheets and sills. Can. J. Earth Sci., 7, 1031 - 1061.
- Irvine, T.N. (1975). Crystallisation sequences in the Muskox Intrusion and other layered intrusions - 11. Origin of chromitite layers and similar deposits of other magmatic ores. Geochim. Cosmochim. Acta., 39, 991 - 1020.
- Irvine, T.N. (1977). Origin of chromitite layers in the Muskox Intrusion and other stratiform intrusions : A new interpretation. Geology, 5, 273 - 277.
- Irvine, T.N. and Smith, C.H. (1967). The ultramafic rocks in the Muskox Intrusion, Northwest Territories, Canada, 38 - 49. In: Wyllie, P.J. ed., Ultramafic and Related Rocks. John Wiley and Sons, Inc., New York, 464 p.
- Irvine, T.N. and Baragar, W.R.A. (1971). A guide to the classification of the common volcanic rocks. Can. J. Earth. Sci., 8, 523 - 548.
- Jackson, E.D. (1961). Primary textures and mineral associations in the ultramafic zone of the Stillwater Complex, Montana. U.S. geol. Surv. Prof. Paper, 358, 106 p.

- Jackson, E.D. (1969). Chemical variation in coexisting chromite and olivine in chromitite zones of the Stillwater Complex. Econ. Geol. Monogr., 4, 41 - 71.
- Jackson, E.D. (1970). The cyclic unit in layered intrusions - A comparison of repetitive stratigraphy in the ultramafic parts of the Stillwater, Muskox, Great Dyke, and Bushveld Complexes. Geol. Soc. S. Afr. Spec. Publ., 1, 391 - 424.
- Kuschke, G.S.J. (1939). The Critical Zone of the Bushveld Igneous Complex, Lydenburg District. Trans. geol. Soc. S. Afr., 42, 57 - 81.
- Lee, C.A. (1981). Post depositional structures in the Bushveld Complex mafic sequence. J. geol. Soc., 138, 327 - 342.
- Liebenberg, L. (1970). The sulphides in the layered sequence of the Bushveld Igneous Complex. Geol. Soc. S. Afr. Spec. Publ., 1, 108 - 207.
- Lombaard, B.V. (1934). On the differentiation and relationships of the rocks of the Bushveld Complex. Trans. geol. Soc. S. Afr., 37, 5 - 52.
- Lombaard, B.V. (1945). Die ontdekkers van platina in Transvaal. Historiese Studies. Univ. van Pretoria. Jaargang 6, 40 p.
- Maaløe, S. (1978). The origin of rhythmic layering. Miner. Mag., 42, 337 - 342.
- McDonald, J.A. (1967). Evolution of part of the Lower Critical Zone, farm Ruighoek, Western Bushveld. J. Petrol., 8, 165 - 209.
- McLaren, C.H. (1978). A mineralogical investigation of the platinum-group metals in the UG2 layer of the Bushveld Complex with special reference to the recovery of minerals from the ores. Metals Minerals Processing, 1, 19 - 27.
- McLaren, C.H. (1981). 'n Mineralogiese ondersoek van die platinum-groepminerale in die boonste chromitiet laag (UG2) van die Bosveldkompleks. Ph.D., Randse Afrikaanse Universiteit.

- Mertie, J.B. (1969). Economic geology of the platinum metals. U.S. Geol. Surv. Prof. Paper, 630, 120 p.
- Muan, A. and Osborn, E.F. (1956). Phase equilibrium at liquidus temperatures in the system MgO - FeO - Fe<sub>2</sub>O<sub>3</sub> - SiO<sub>2</sub>. J. Amer. Ceramic Soc., 39, 121 - 140.
- Naldrett, A.J. and Cabri, L.J. (1976). Ultramafic and related mafic rocks : their classification and genesis with special reference to the concentration of nickel sulphides and platinum-group elements. Econ. Geol., 71, 1131 - 1158.
- Naldrett, A.J. and Duke, J.M. (1980). Platinum metals magmatic sulphide ores. Science, 208, 1417 - 1424.
- Nel, H.J. (1940). The basal rocks of the Bushveld Igneous Complex, north of Pretoria. Trans. geol. Soc. S. Afr., 43, 37 - 68.
- Norrish, K. and Hutton, J.J. (1969). An accurate X-ray spectrographic method for analysis of a wide range of geological samples. Geochim. Cosmochim. Acta, 33, 431 - 453.
- Peyerl, W. (1982). The influence of the Driekop dunite on the platinoid mineralogy of the UG2 chromitite in its vicinity. Econ. Geol. (in press).
- Poldervaart, A. and Hess, H.H. (1951). Pyroxene in the crystallisation of basaltic magma. J. Geol., 59, 472 - 489.
- Ramberg, H. (1967). Gravity, deformation and the earths crust. Academic Press, New York, N.Y., 214 p.
- Razin, L.V. (1976). Geologic and genetic features of forsterite dunites and their platinum-group mineralisation. Econ. Geol., 71, 1371 - 1376.
- Razin, L.V. and Khomenko, G.A. (1969). Accumulation of osmium, ruthenium, and the other platinum-group metals in chrome spinel in platinum-bearing dunites. Trans. from Geokhimiya, 6, 659 - 672.



- Razin, L.V., Khvostov, U.P. and Novikov, V.A. (1965). Platinum metals in the essential and accessory minerals of ultra-mafic rocks. Geochemistry Internat., 2, 118 - 131.
- Roeder, P.L. and Osborn, E.F. (1966). Experimental data for the system MgO - FeO - Fe<sub>2</sub>O<sub>3</sub> - CaAl<sub>2</sub>Si<sub>2</sub>O<sub>8</sub> - SiO<sub>2</sub> and their petrologic implications. Amer. J. Sci., 264, 428 - 480.
- Roeder, P.L., Campbell, I.H. and Jamieson, H.E. (1979). A re-evaluation of the olivine-spinel geothermometer. Contrib. Mineral. Petrol., 68, 325 - 334.
- Sharkov, Y.E.V. (1972). Rhythmic stratification in layered intrusions and its origin. Internat. Geology Rev., 14, 592 - 598.
- Smith, J.V. (1972). Feldspar Minerals. Springer - Verlag Berlin.
- South African Committee for Stratigraphy (SACS), (1980). Stratigraphy of South Africa. Part 1 (Comp. L.E. Kent) Handb. geol. Surv. S. Afr. 8, 690 p.
- Snethlage, R. and von Gruenewaldt, G. (1977). Oxygen fugacity and its bearing on the origin of chromitite layers in the Bushveld Complex. 352 - 370. In D.D. Klemm and H.J. Schneider Eds. Time and Strata-Bound ore deposits. Springer Verslag, Berlin.
- Snethlage, R. and Klemm, D.D. (1978). Intrinsic oxygen fugacity measurements in chromites from the Bushveld Complex and their petrogenetic significance. Contrib. Mineral. Petrol., 67, 127 - 138.
- Streckeisen, A. (1976). To each plutonic rock its proper name. Earth Sc. Rev., 12, 1 - 33.
- Tarkian, M. and Stumpfl, E.F. (1975). Platinum mineralogy of the Driekop Mine, South Africa. Mineral Deposita 10, 71 - 85.
- Ulmer, G.C. (1969). Experimental investigations in chromite spinels. Econ. Geol., Monogr., 4, 114 - 131.

- Van der Plas, L. and Tobi, A.C. (1965). A chart for judging the reliability of point counting results. Am. J. Sc., 263, 37 - 90.
- Van der Walt, C.F.J. (1941). Chrome ores of the Western Bushveld Complex. Trans. geol. Soc. S. Afr., 44, 79 - 112.
- Vermaak, C.F. (1976). The Merensky Reef - thoughts on its environment and genesis. Econ. Geol., 71, 1270 - 1298.
- Von Gruenewaldt, G. (1979). A review of some recent concepts of the Bushveld Complex with particular reference to sulfide mineralization. Can. Mineral., 17, 233 - 276.
- Wager, L.R. (1957). Differing powers of crystal nucleation as a factor producing diversity in layered igneous intrusions. Geol. Mag., 96, 75 - 80.
- Wager, L.R., Brown, G.M. and Wadsworth, W.J. (1960). Types of igneous cumulates. J. Petrol., 1, 73 - 85.
- Wagner, P.A. (1929). The platinum deposits and mines of South Africa. Oliver and Boyd, Edinburgh.
- Wedepohl, K.H. (1972). Handbook of Geochemistry. Springer - Verlag. Berlin 1972.
- Wells, A.K. (1952). Textural features of some Bushveld norites. Miner. Mag., 29, 913 - 924.
- Wells, P.R.A. (1977). Pyroxene thermometry in simple and complex systems. Contr. Miner. Petrol., 62, 129 - 140.
- Willemse, J. and Frick, C. (1970). Stroomroef en die invloed van verskuiwings op die geomorfologie in die opvanggebied van die Steelpoortrivier. Trans. geol. Soc. S. S. Afr., 73, 159 - 171.
- Wood, B.J. and Banno, S. (1973). Garnet-orthopyroxene and orthopyroxene - clinopyroxene relationships in simple and complex systems. Contr. Mineral. Petrol., 42, 109 - 123.

Wright, T.L. and Fleischer, M. (1965). Geochemistry of the platinum metals. U.S. Geol. Survey Bull., 1214-A, A1 - A24.

Yaroshevsky, A.A. (1970). On the origin of rhythmic structures in igneous rocks. Geochem. Internat. 5, 562 - 574.

- 133 -  
APPENDIX I

Chemical analyses and structural formulae of plagioclase separates of borehole MDH 7. (For sample positions see Folder B).

Sample No.	A2	A4	A6	A8	A10	A12	A14	A16
SiO <sub>2</sub>	49,39	49,80	49,63	49,55	50,16	49,51	49,82	49,44
TiO <sub>2</sub>	0,03	0,03	0,04	0,03	0,03	0,03	0,03	0,03
Al <sub>2</sub> O <sub>3</sub>	32,46	32,39	32,68	32,71	32,80	32,97	33,15	33,00
FeO	0,40	0,35	0,46	0,36	0,36	0,39	0,48	0,38
MnO	0,01	0,01	0,01	0,01	0,01	0,01	0,01	0,01
MgO	0,20	0,20	0,48	0,23	0,20	0,18	0,19	0,16
CaO	15,52	15,40	14,30	15,52	15,46	15,66	15,71	15,74
Na <sub>2</sub> O	2,22	2,19	2,08	2,04	2,15	2,16	2,02	2,10
K <sub>2</sub> O	0,19	0,22	0,19	0,19	0,21	0,16	0,16	0,16
P <sub>2</sub> O <sub>5</sub>	0,02	0,03	0,04	0,03	0,03	0,02	0,02	0,02
Cr <sub>2</sub> O <sub>3</sub>	0,01	0,01	0,01	0,01	0,01	0,01	0,01	0,01
NiO	0,01	0,01	0,01	0,01	0,01	0,01	0,01	0,01
TOTAL	100,46	100,64	100,93	100,69	101,43	101,11	101,61	101,06
NUMBER OF IONS ON THE BASIS OF 32(O)								
Si	8,990	9,036	8,982	8,988	9,028	8,953	8,961	8,945
Ti	0,004	0,004	0,005	0,004	0,004	0,004	0,004	0,003
Al	6,962	6,926	6,969	6,990	6,955	7,025	7,025	7,035
Fe <sup>2+</sup>	0,060	0,053	0,070	0,054	0,054	0,059	0,073	0,058
Mn	0,001	0,001	0,002	0,002	0,001	0,001	0,001	0,001
Mg	0,054	0,055	0,129	0,062	0,054	0,047	0,050	0,043
Ca	3,026	2,993	2,967	3,016	2,981	3,034	3,029	3,051
Na	0,782	0,770	0,730	0,719	0,749	0,757	0,704	0,735
K	0,044	0,050	0,045	0,044	0,049	0,037	0,038	0,036
P	0,004	0,005	0,006	0,005	0,005	0,002	0,004	0,004
Cr	0,001	0,002	0,002	0,001	0,001	0,001	0,001	0,001
Ni	0,001	0,002	0,002	0,002	0,001	0,001	0,002	0,002
Z	15,952	15,962	15,951	15,978	15,983	15,978	15,986	15,980
X	3,975	3,935	3,958	3,909	3,899	3,943	3,906	3,934
<u>Ca</u> Ca+Na+K	78,5	78,5	79,3	79,8	78,9	79,2	80,3	79,8

Sample No.	A18	A20	A22	A24	A26	A28	A30	B1
SiO <sub>2</sub>	49,14	49,76	49,98	48,44	49,75	49,23	49,20	49,45
TiO <sub>2</sub>	0,03	0,04	0,03	0,03	0,03	0,03	0,03	0,03
Al <sub>2</sub> O <sub>3</sub>	32,83	32,80	33,07	31,63	32,64	32,56	32,84	32,70
FeO	0,40	0,39	0,44	0,46	0,44	0,47	0,43	0,41
MnO	0,01	0,01	0,01	0,02	0,01	0,01	0,01	0,01
MgO	0,19	0,21	0,12	0,27	0,21	0,20	0,16	0,20
CaO	15,59	15,68	15,83	15,25	15,62	15,78	15,65	15,57
Na <sub>2</sub> O	1,91	2,15	2,04	2,05	2,01	1,95	2,12	2,17
K <sub>2</sub> O	0,17	0,17	0,17	1,01	0,19	0,14	0,29	0,27
P <sub>2</sub> O <sub>5</sub>	0,02	0,03	0,02	0,03	0,03	0,03	0,05	0,03
Cr <sub>2</sub> O <sub>3</sub>	0,01	0,01	0,01	0,01	0,01	0,01	0,01	0,01
NiO	0,01	0,01	0,01	0,01	0,01	0,01	0,01	0,01
TOTAL	100,31	101,26	101,73	99,22	100,95	100,42	100,80	100,85
NUMBER OF IONS ON THE BASIS OF 32(0)								
Si	8,951	8,983	8,979	8,976	9,004	8,965	8,934	8,970
Ti	0,004	0,006	0,004	0,004	0,004	0,004	0,004	0,004
Al	7,047	6,977	7,000	6,907	6,960	6,986	7,027	6,988
Fe <sup>2+</sup>	0,061	0,059	0,065	0,071	0,066	0,071	0,065	0,063
Mn	0,001	0,001	0,001	0,002	0,001	0,002	0,001	0,002
Mg	0,051	0,056	0,033	0,073	0,056	0,055	0,045	0,054
Ca	3,042	3,032	3,047	3,028	3,028	3,078	3,045	3,025
Na	0,673	0,752	0,711	0,739	0,708	0,690	0,746	0,762
K	0,038	0,040	0,040	0,238	0,045	0,033	0,067	0,062
P	0,004	0,004	0,004	0,005	0,005	0,005	0,008	0,004
Cr	0,001	0,001	0,002	0,001	0,001	0,001	0,001	0,001
Ni	0,001	0,001	0,001	0,002	0,002	0,001	0,001	0,001
Z	15,998	15,960	15,979	15,883	15,964	15,951	15,961	15,958
X	3,876	3,952	3,908	4,163	3,916	3,940	3,983	3,978
<u>Ca</u> Ca+Na+K	81,0	79,3	80,2	75,6	80,1	81,0	78,9	78,6

Sample No.	C7	UG3B	UG3C	D1	D6	D9	D10
SiO <sub>2</sub>	49,05	49,35	49,25	49,47	50,74	51,98	50,35
TiO <sub>2</sub>	0,02	0,03	0,02	0,02	0,02	0,02	0,02
Al <sub>2</sub> O <sub>3</sub>	32,77	32,43	32,98	30,61	31,70	30,42	31,90
FeO	0,40	0,48	0,41	0,30	0,29	0,45	0,49
MnO	0,01	0,01	0,01	0,01	0,01	0,01	0,02
MgO	0,20	0,24	0,08	0,07	0,77	0,59	0,50
CaO	15,73	15,31	15,40	15,75	15,01	14,10	14,93
Na <sub>2</sub> O	1,90	1,60	2,25	2,21	2,45	2,23	2,23
K <sub>2</sub> O	0,81	1,02	0,32	0,18	0,25	0,31	0,21
P <sub>2</sub> O <sub>5</sub>	0,03	0,03	0,02	0,04	0,04	0,03	0,04
Cr <sub>2</sub> O <sub>3</sub>	0,01	0,01	0,01	0,01	0,01	0,01	0,01
NiO	0,01	0,01	0,01	0,01	0,01	0,01	0,01
TOTAL	100,94	100,52	100,76	98,76	101,30	100,16	100,73

	NUMBER OF IONS ON THE BASIS OF 32(0)						
Si	8,919	8,997	8,942	9,164	9,139	9,418	9,119
Ti	0,003	0,004	0,003	0,003	0,003	0,003	0,003
Al	7,022	6,967	7,056	6,682	6,729	6,495	6,807
Fe <sup>2+</sup>	0,060	0,073	0,063	0,059	0,043	0,068	0,074
Mn	0,001	0,002	0,001	0,001	0,001	0,002	0,002
Mg	0,054	0,065	0,021	0,019	0,207	0,160	0,135
Ca	3,063	2,990	2,995	3,125	2,897	2,737	2,897
Na	0,670	0,563	0,791	0,793	0,856	0,785	0,784
K	0,187	0,238	0,074	0,044	0,057	0,072	0,050
P	0,005	0,005	0,004	0,007	0,006	0,005	0,006
Cr	0,001	0,001	0,001	0,001	0,002	0,002	0,001
Ni	0,001	0,001	0,001	0,001	0,001	0,002	0,003
Z	15,941	15,964	15,998	15,846	15,868	15,913	15,926
X	4,045	3,942	3,956	4,053	4,073	3,836	3,955
Ca	78,1	78,9	77,6	78,9	76,0	76,2	77,7
Ca+Na+K							

Sample No.	D11	D14	D18	E1	E2	E4	E6	E8
SiO <sub>2</sub>	49,59	49,00	51,70	48,80	50,60	50,67	50,61	49,69
TiO <sub>2</sub>	0,03	0,01	0,08	0,03	0,04	0,04	0,04	0,04
Al <sub>2</sub> O <sub>3</sub>	32,56	32,13	30,32	32,69	32,35	31,77	32,12	31,76
FeO	0,43	0,38	0,64	0,45	0,46	0,45	0,34	0,32
MnO	0,01	0,01	0,02	0,01	0,01	0,01	0,01	0,01
MgO	0,16	0,41	0,82	0,19	0,31	0,32	0,18	0,13
CaO	15,49	15,12	14,40	15,40	15,40	15,42	15,20	15,09
Na <sub>2</sub> O	2,16	2,23	2,24	2,01	2,12	2,09	2,16	2,19
K <sub>2</sub> O	0,59	0,19	0,40	0,29	0,37	0,33	0,28	0,26
P <sub>2</sub> O <sub>5</sub>	0,03	0,03	0,08	0,03	0,04	0,04	0,05	0,05
Cr <sub>2</sub> O <sub>3</sub>	0,01	0,01	0,01	0,01	0,02	0,01	0,01	0,01
NiO	0,01	0,01	0,01	0,01	0,01	0,01	0,01	0,01
<b>TOTAL</b>	<b>101,07</b>	<b>99,53</b>	<b>100,72</b>	<b>99,92</b>	<b>101,73</b>	<b>101,16</b>	<b>101,01</b>	<b>99,56</b>
NUMBER OF IONS ON THE BASIS OF 32(O)								
Si	8,990	8,994	9,350	8,934	9,085	9,146	9,135	9,106
Ti	0,004	0,002	0,011	0,004	0,006	0,006	0,006	0,006
Al	6,954	6,950	6,462	7,053	6,845	6,757	6,831	6,858
Fe <sup>2+</sup>	0,066	0,058	0,096	0,068	0,069	0,068	0,051	0,050
Mn	0,002	0,002	0,002	0,001	0,002	0,001	0,001	0,001
Mg	0,042	0,113	0,220	0,051	0,084	0,087	0,047	0,036
Ca	3,008	2,973	2,790	3,020	2,963	2,983	2,940	2,962
Na	0,760	0,793	0,784	0,713	0,740	0,731	0,754	0,778
K	0,138	0,045	0,092	0,069	0,084	0,075	0,064	0,062
P	0,005	0,005	0,013	0,004	0,006	0,006	0,001	0,007
Cr	0,001	0,002	0,002	0,002	0,003	0,002	0,001	0,001
Ni	0,001	0,001	0,001	0,001	0,002	0,002	0,002	0,002
Z	15,944	15,944	15,812	15,987	15,930	15,903	15,966	15,964
X	4,027	3,994	4,001	3,933	3,959	3,961	3,867	3,905
<u>Ca</u> Ca+Na+K	77,6	78,0	76,1	79,4	78,3	78,7	78,2	77,9

Sample No.	E10	E12	E14	E16	E18	E20	E22	E24
SiO <sub>2</sub>	50,62	50,89	50,66	50,60	50,91	50,88	50,48	50,28
TiO <sub>2</sub>	0,05	0,04	0,04	0,04	0,04	0,04	0,04	0,04
Al <sub>2</sub> O <sub>3</sub>	31,98	32,08	31,73	31,87	31,87	32,00	31,75	32,13
FeO	0,40	0,32	0,31	0,32	0,30	0,29	0,33	0,31
MnO	0,01	0,01	0,01	0,01	0,01	0,01	0,01	0,01
MgO	0,15	0,17	0,24	0,26	0,15	0,10	0,22	0,13
CaO	14,96	15,11	15,04	15,14	14,97	14,99	14,98	15,10
Na <sub>2</sub> O	2,23	2,25	2,10	2,06	2,19	2,29	2,24	2,30
K <sub>2</sub> O	0,31	0,30	0,31	0,30	0,31	0,29	0,29	0,29
P <sub>2</sub> O <sub>5</sub>	0,04	0,04	0,04	0,03	0,03	0,04	0,04	0,04
Cr <sub>2</sub> O <sub>3</sub>	0,01	0,01	0,01	0,01	0,01	0,01	0,01	0,01
NiO	0,01	0,01	0,01	0,01	0,01	0,01	0,01	0,01
<b>TOTAL</b>	<b>100,77</b>	<b>101,23</b>	<b>100,50</b>	<b>100,65</b>	<b>100,80</b>	<b>100,94</b>	<b>100,40</b>	<b>100,65</b>
NUMBER OF IONS ON THE BASIS OF 32(O)								
Si	9,158	9,163	9,183	9,161	9,197	9,181	9,165	9,114
Ti	0,007	0,006	0,005	0,006	0,005	0,005	0,006	0,005
Al	6,818	6,806	6,778	6,800	6,783	6,804	6,792	6,861
Fe <sup>2+</sup>	0,061	0,048	0,048	0,049	0,046	0,043	0,050	0,047
Mn	0,002	0,001	0,001	0,001	0,001	0,001	0,001	0,001
Mg	0,039	0,046	0,064	0,070	0,040	0,027	0,058	0,036
Ca	2,900	2,915	2,920	2,937	2,898	2,898	2,914	2,931
Na	0,781	0,786	0,739	0,722	0,767	0,801	0,787	0,808
K	0,071	0,069	0,071	0,069	0,072	0,067	0,068	0,066
P	0,006	0,006	0,006	0,005	0,005	0,006	0,006	0,006
Cr	0,002	0,001	0,001	0,001	0,001	0,001	0,001	0,001
Ni	0,001	0,001	0,001	0,001	0,001	0,001	0,002	0,001
Z	15,976	15,969	15,961	15,961	15,980	15,985	15,957	15,975
X	3,870	3,879	3,856	3,861	3,836	3,850	3,893	3,902
<u>Ca</u> Ca+Na+K	77,3	77,3	78,3	78,8	77,5	76,9	77,3	77,0



Sample No.	E26	E28	E30	E32	E34	E36	E38	E40
SiO <sub>2</sub>	49,38	50,30	49,43	49,33	50,11	50,00	50,24	50,50
TiO <sub>2</sub>	0,04	0,04	0,04	0,04	0,04	0,03	0,03	0,03
Al <sub>2</sub> O <sub>3</sub>	31,96	32,37	31,83	32,25	32,22	31,64	32,23	31,33
FeO	0,33	0,34	0,45	0,38	0,39	0,64	0,48	0,62
MnO	0,01	0,01	0,01	0,01	0,01	0,01	0,01	0,01
MgO	0,17	0,19	0,38	0,20	0,29	0,71	0,48	0,67
CaO	14,98	15,35	15,30	15,48	15,24	15,00	15,16	15,18
Na <sub>2</sub> O	2,28	2,27	2,20	2,20	2,24	2,09	2,19	2,12
K <sub>2</sub> O	0,26	0,21	0,26	0,24	0,26	0,23	0,25	0,25
P <sub>2</sub> O <sub>5</sub>	0,03	0,04	0,03	0,03	0,04	0,03	0,03	0,04
Cr <sub>2</sub> O <sub>3</sub>	0,01	0,01	0,02	0,01	0,01	0,01	0,01	0,01
NiO	0,01	0,01	0,01	0,01	0,01	0,01	0,01	0,01
TOTAL	99,46	101,14	99,98	100,18	100,86	100,40	101,72	100,77

## NUMBER OF IONS ON THE BASIS OF 32(0)

Si	9,063	9,077	9,045	9,005	9,072	9,096	9,071	9,154
Ti	0,005	0,005	0,005	0,005	0,005	0,004	0,004	0,005
Al	6,910	6,882	6,861	6,937	6,873	6,783	6,856	6,691
Fe <sup>2+</sup>	0,050	0,052	0,069	0,059	0,058	0,097	0,072	0,093
Mn	0,001	0,001	0,002	0,001	0,001	0,002	0,002	0,003
Mg	0,048	0,052	0,103	0,055	0,077	0,191	0,131	0,182
Ca	2,945	2,967	2,997	3,027	2,956	2,923	2,933	2,948
Na	0,812	0,793	0,779	0,779	0,788	0,738	0,767	0,747
K	0,062	0,048	0,060	0,055	0,061	0,054	0,058	0,059
P	0,005	0,006	0,005	0,005	0,006	0,004	0,005	0,006
Cr	0,002	0,002	0,002	0,002	0,002	0,002	0,002	0,002
Ni	0,001	0,001	0,001	0,002	0,001	0,001	0,001	0,001
Z	15,973	15,959	15,906	15,942	15,945	15,879	15,927	14,845
X	3,931	3,927	4,023	3,990	3,955	4,016	3,964	4,046
<u>Ca</u> Ca+Na+K	77,1	77,9	78,1	78,4	77,7	78,7	78,0	78,5

Sample No.	E42	E44	E46	E48	E52	E54	E56	E60
SiO <sub>2</sub>	49,86	49,75	50,49	50,44	52,31	51,14	52,56	51,34
TiO <sub>2</sub>	0,03	0,03	0,03	0,02	0,05	0,03	0,04	0,03
Al <sub>2</sub> O <sub>3</sub>	31,00	31,68	32,12	32,38	30,00	31,71	29,95	31,23
FeO	0,60	0,52	0,43	0,38	0,44	0,43	0,59	0,48
MnO	0,01	0,01	0,01	0,01	0,02	0,01	0,01	0,01
MgO	0,58	0,53	0,45	0,31	0,50	0,43	0,77	0,41
CaO	14,90	15,01	14,99	15,05	14,52	14,43	13,39	14,51
Na <sub>2</sub> O	2,28	2,11	2,16	2,31	2,42	2,50	2,17	2,47
K <sub>2</sub> O	0,24	0,24	0,20	0,33	0,26	0,28	0,45	0,25
P <sub>2</sub> O <sub>5</sub>	0,04	0,03	0,03	0,03	0,07	0,03	0,08	0,03
Cr <sub>2</sub> O <sub>3</sub>	0,01	0,01	0,01	0,01	0,03	0,01	0,01	0,01
NiO	0,01	0,01	0,01	0,01	0,01	0,01	0,01	0,01
TOTAL	99,56	99,93	100,93	101,28	100,63	101,01	100,03	100,78
NUMBER OF IONS ON THE BASIS OF 32(0)								
Si	9,151	9,089	9,117	9,089	9,452	9,218	9,517	9,274
Ti	0,005	0,004	0,004	0,003	0,006	0,005	0,006	0,004
Al	6,703	6,821	6,835	6,875	6,388	6,735	6,391	6,648
Fe <sup>2+</sup>	0,092	0,080	0,066	0,057	0,066	0,064	0,090	0,073
Mn	0,002	0,002	0,002	0,001	0,003	0,002	0,002	0,002
Mg	0,159	0,144	0,122	0,084	0,134	0,116	0,209	0,110
Ca	2,929	2,939	2,900	2,905	2,811	2,785	2,600	2,807
Na	0,811	0,748	0,756	0,806	0,846	0,873	0,763	0,866
K	0,057	0,055	0,046	0,075	0,061	0,066	0,104	0,058
P	0,006	0,004	0,005	0,005	0,010	0,005	0,012	0,005
Cr	0,002	0,002	0,002	0,001	0,004	0,002	0,002	0,001
Ni	0,002	0,002	0,002	0,001	0,002	0,002	0,001	0,002
Z	15,854	15,910	15,952	15,964	15,840	15,953	15,908	15,922
X	4,065	3,980	3,905	3,938	3,941	3,920	3,789	3,928
$\frac{Ca}{Ca+Na+K}$	77,1	78,5	78,3	76,7	75,6	74,8	75,0	75,2

Sample No.	E64	E66	E68	E78	E80	E82	E86	E87
SiO <sub>2</sub>	49,81	50,34	49,95	50,58	53,85	49,97	50,29	49,67
TiO <sub>2</sub>	0,02	0,04	0,07	0,03	0,04	0,02	0,02	0,03
Al <sub>2</sub> O <sub>3</sub>	31,79	32,10	32,08	30,70	29,05	32,24	32,43	31,81
FeO	0,56	0,50	0,41	0,52	0,47	0,47	0,32	0,42
MnO	0,01	0,01	0,02	0,03	0,01	0,01	0,01	0,02
MgO	0,48	0,35	0,25	0,42	0,35	0,49	0,27	0,45
CaO	15,09	15,15	15,03	14,98	12,66	15,14	14,86	15,08
Na <sub>2</sub> O	2,12	2,25	1,57	1,57	2,28	1,18	1,57	2,34
K <sub>2</sub> O	0,41	0,38	0,47	0,40	0,35	0,21	0,24	0,47
P <sub>2</sub> O <sub>5</sub>	0,03	0,03	0,03	0,05	0,05	0,02	0,02	0,03
Cr <sub>2</sub> O <sub>3</sub>	0,01	0,01	0,01	0,01	0,01	0,02	0,01	0,02
NiO	0,01	0,01	0,01	0,01	0,01	0,01	0,01	0,01
TOTAL	100,34	101,17	99,90	99,30	99,12	99,77	100,05	100,37

	NUMBER OF IONS ON THE BASIS OF 32(0)							
Si	9,076	9,094	9,110	9,275	9,782	9,102	9,130	9,058
Ti	0,004	0,005	0,010	0,004	0,006	0,003	0,003	0,004
Al	6,825	6,833	6,894	6,633	6,219	6,921	6,937	6,835
Fe <sup>2+</sup>	0,085	0,075	0,063	0,080	0,071	0,072	0,049	0,064
Mn	0,002	0,002	0,002	0,004	0,002	0,002	0,001	0,003
Mg	0,131	0,093	0,068	0,116	0,095	0,134	0,072	0,124
Ca	2,945	2,931	2,938	2,943	2,464	2,954	2,890	2,946
Na	0,750	0,788	0,557	0,559	0,803	0,416	0,552	0,826
K	0,096	0,087	0,109	0,094	0,081	0,050	0,055	0,111
P	0,005	0,004	0,005	0,007	0,008	0,003	0,004	0,004
Cr	0,002	0,002	0,001	0,001	0,001	0,002	0,002	0,001
Ni	0,001	0,002	0,002	0,001	0,002	0,002	0,002	0,001
Z	15,901	15,927	16,004	15,908	16,001	16,023	16,067	15,893
X	4,021	3,989	3,755	3,809	3,533	3,638	3,630	4,086
$\frac{Ca}{Ca+Na+K}$	77,7	77,0	81,5	81,9	73,6	86,4	82,7	75,9

Sample No.	E88	E91	F1	F2	F5
SiO <sub>2</sub>	49,50	49,84	49,79	50,79	51,98
TiO <sub>2</sub>	0,03	0,03	0,02	0,02	0,01
Al <sub>2</sub> O <sub>3</sub>	32,33	32,38	32,40	32,41	32,54
FeO	0,41	0,34	0,41	0,36	0,32
MnO	0,01	0,01	0,01	0,01	0,01
MgO	0,22	0,29	0,33	0,31	0,28
CaO	14,77	14,90	15,06	15,18	15,08
Na <sub>2</sub> O	2,38	2,29	2,30	2,32	2,31
K <sub>2</sub> O	0,42	0,47	0,15	0,17	0,12
P <sub>2</sub> O <sub>5</sub>	0,03	0,03	0,02	0,03	0,02
Cr <sub>2</sub> O <sub>3</sub>	0,01	0,02	0,01	0,01	0,01
NiO	0,01	0,01	0,01	0,01	0,01
TOTAL	100,12	100,61	100,51	101,62	102,69

## NUMBER OF IONS ON THE BASIS OF 32(0)

Si	9,033	9,048	9,041	9,112	9,203
Ti	0,004	0,004	0,002	0,002	0,002
Al	6,952	6,928	6,932	6,852	6,789
Fe <sup>2+</sup>	0,063	0,052	0,062	0,054	0,048
Mn	0,002	0,001	0,001	0,002	0,002
Mg	0,059	0,080	0,089	0,084	0,073
Ca	2,887	2,897	2,928	2,917	2,861
Na	0,841	0,807	0,808	0,805	0,794
K	0,098	0,109	0,035	0,039	0,027
P	0,005	0,004	0,004	0,004	0,004
Cr	0,002	0,003	0,002	0,002	0,002
Ni	0,002	0,001	0,002	0,001	0,001
Z	15,985	15,976	15,973	15,964	15,992
X	3,963	3,958	3,933	3,910	3,814
<u>Ca</u> Ca+Na+K	75,5	76,0	77,7	77,6	77,7

APPENDIX II

Anorthite content of plagioclase of the upper critical zone.

UG1 CYCLIC UNIT

Sample No.	Depth Metres	Eulerian Angles	2V	RI of Glass	XRF	Average
F5	254,60	78,0	76,0	-	-	77,0 (2)
F4	253,60	79,0	76,0	-	78,2	77,1 (3)
F2	251,60	78,2	77,0	-	78,4	77,9 (2)
F1	250,60	-	-	-	78,4	78,4 (1)

Analysis of F Series

No. of Samples	3	3	-	3	9
Range	78,0-79,0	76,0-77,0	-	78,2-78,4	77,00-78,4
Mean	78,4	76,4	-	78,3	77,65
S.D. of Samples	0,52	0,57	-	0,11	0,43
S.D. of Population	0,42	0,47	-	0,09	0,40

E92	249,56	77,0	-	-	-	77,0 (1)
E91	248,70	77,0	77,5	-	78,3	77,6 (3)
E88	246,00	77,5	-	-	77,6	77,4 (3)
E87	245,47	-	-	-	78,1	78,1 (1)
E86	245,27	-	-	-	83,9	83,9 (1)
E78	238,10	77,5	77,0	-	84,1	79,5 (3)
E68	227,80	77,0	79,0	-	84,0	80,0 (3)
E67	226,80	75,5	77,0	-	-	76,2 (2)
E66	225,80	77,5	78,0	-	78,8	78,1 (3)
E65	224,80	-	79,0	-	-	79,0 (1)
E64	223,80	78,0	80,0	-	79,7	79,2 (3)
E60	219,50	77,0	77,0	-	78,8	77,6 (3)
E56	215,50	78,0	77,0	-	77,3	77,4 (3)
E54	213,00	-	-	-	76,2	76,2 (1)
E52	211,70	78,5	78,0	-	76,8	77,8 (3)
E51	211,00	79,0	-	-	-	79,0 (1)
E49	210,00	79,0	-	-	-	79,0 (1)
E48	209,50	78,5	77,0	-	78,3	77,9 (3)
E47	206,80	79,5	-	-	-	79,5 (1)
E46	206,00	75,0	77,0	-	79,3	76,5 (3)
E45	204,80	76,5	-	-	-	76,5 (1)
E44	202,50	78,5	77,0	-	79,7	78,4 (3)
E43	201,00	77,0	-	-	-	77,0 (1)
E42	200,40	79,0	78,0	-	78,3	78,4 (3)
E41	198,60	78,0	-	-	-	78,0 (1)
E40	197,00	77,2	78,0	-	79,8	78,35 (3)
E39	195,95	77,0	-	-	-	77,0 (1)
E38	195,00	76,0	77,0	-	79,2	77,4 (3)
E37	194,00	75,6	-	-	-	75,6 (1)
E36	191,50	76,0	77,9	-	79,8	77,9 (3)
E34	187,50	-	-	-	79,0	79,0 (1)
E33	186,00	77,5	-	-	-	77,5 (1)
E32	185,00	77,0	77,9	-	79,5	78,1 (3)
E31	184,00	76,5	-	-	-	76,5 (1)
E29	182,00	76,5	-	-	-	76,5 (1)
E28	181,00	-	-	-	79,4	79,4 (1)
E26	179,00	77,5	80,0	-	78,3	78,6 (3)
E24	177,00	75,5	79,0	-	78,3	77,6 (3)
E23	176,00	78,0	77,0	-	-	77,5 (2)
E22	175,00	77,0	78,0	-	78,7	77,9 (3)
E20	173,00	-	-	-	78,3	78,3 (1)
E19	172,00	78,0	78,0	-	-	78,0 (2)
E18	171,00	78,0	-	-	79,0	78,5 (2)
E17	170,00	79,0	80,0	-	-	79,5 (2)
E16	169,00	79,0	79,0	-	80,2	79,4 (3)
E14	167,00	77,0	78,0	-	79,8	78,3 (3)
E13	166,00	79,5	79,5	-	-	79,5 (2)
E12	164,80	-	-	-	78,8	78,8 (1)
E11	163,80	79,0	79,0	-	-	79,0 (2)
E10	162,70	78,0	77,0	-	78,8	77,9 (3)
E9	161,80	79,0	79,0	-	-	79,0 (2)
E8	161,00	-	-	-	79,2	79,2 (1)
E6	158,80	81,0	79,0	-	79,6	79,9 (3)
E5	157,70	79,5	80,0	-	-	79,7 (2)

Sample No.	Depth Metres	Eulerian Angles	2V	RI of Glass	XRF	Average
E4	157,00	79,0	79,0	-	80,5	79,4 (3)
E3	156,00	82,0	81,0	-	-	81,5 (2)
E2	155,30	77,5	78,0	-	80,1	78,5 (3)
E1	155,00	-	-	-	80,8	80,8 (1)

Analysis of E Series

No. of Samples	48	36	-	36	120
Range	73,0-82,0	77,0-81,0	-	76,2-84,1	75,6-83,9
Mean	77,7	78,2	-	79,35	78,37
S.D. of Samples	1,51	1,12	-	1,71	1,18
S.D. of Population	1,49	1,11	-	1,69	1,17

UG2 CYCLIC UNIT

D18	149,50	-	-	-	78,0	78,0 (1)
D15	147,22	76,5	80,0	-	-	77,75 (2)
D14	147,00	75,7	79,0	-	-	77,4 (2)
D13	146,00	78,5	78,5	-	78,9	78,6 (3)
D11	144,86	77,5	78,5	-	79,8	78,6 (3)
D10	144,46	76,0	78,0	-	78,7	77,6 (3)
D9	144,00	76,5	79,0	-	77,7	77,7 (3)
D6	141,00	76,7	79,0	-	77,1	77,6 (3)
D4	139,00	76,5	78,0	-	79,8	78,1 (3)
D3	138,00	76,7	77,5	-	78,3	77,5 (3)
D1	135,90	78,5	78,0	79,5	77,6	78,4 (4)

Analysis of the D Series

No. of Samples	10	10	1	9	30
Range	76,0-78,5	77,5-80,0	79,5	77,1-79,8	77,4-78,6
Mean	76,92	78,55	79,5	78,46	78,0
S.D. of Samples	0,95	0,72	-	0,95	0,43
S.D. of Population	0,90	0,68	-	0,89	0,42

UG3 CYCLIC UNIT

C1	131,00	77,0	77,5	-	82,0	78,8 (3)
----	--------	------	------	---	------	----------

UG3A CYCLIC UNIT

B1	124,48	78,0	78,5	-	79,9	78,8 (3)
A30	124,0	78,5	79	79,5	80,2	79,3 (4)
A29	123,0	79,5	-	-	-	79,5 (1)
A28	122,0	77,5	79,5	-	82,4	79,8 (3)
A26	121,0	78,0	-	-	81,1	79,5 (2)
A25	120,0	77,5	-	-	-	77,5 (1)
A24	117,90	79,2	80,0	-	80,3	79,8 (3)
A23	116,90	78,2	-	-	-	78,2 (1)
A22	116,00	80,0	79,0	-	81,0	80,0 (3)
A21	115,00	80,0	-	-	-	80,0 (1)
A20	114,00	-	77,0	-	80,1	78,6 (3)
A18	111,90	79,5	79,0	-	81,8	80,1 (3)
A17	111,00	81,5	-	-	-	81,5 (1)
A16	110,00	79,0	77,5	-	80,6	79,0 (3)
A15	109,00	80,5	-	-	-	80,5 (1)
A14	108,00	79,0	79,0	-	81,1	79,7 (3)
A13	107,00	77,0	-	-	-	77,0 (1)
A12	106,00	77,5	78,0	-	80,2	78,6 (3)
A11	105,00	77,0	-	-	-	77,0 (1)
A10	104,00	77,0	76,0	76,5	79,9	77,3 (4)
A9	103,00	75,5	76,0	-	-	75,7 (2)
A8	102,00	76,5	-	-	80,8	78,6 (2)
A7	101,00	77,5	80	-	-	78,7 (2)
A6	99,80	-	-	-	80,3	80,3 (1)
A5	99,00	78,7	-	-	-	78,75 (1)
A4	98,00	78,5	78,0	-	79,5	78,7 (3)
A3	97,0	80,0	-	-	-	80,0 (1)
A2	96,0	78,5	77,0	-	79,4	78,3 (3)
A1	95,0	79,0	76,0	-	-	77,5 (2)

Sample No.	Depth Metres	Eulerian Angles	2V	RI of Glass	XRF	Average
------------	--------------	-----------------	----	-------------	-----	---------

Analysis of the A Series

No. of Samples	26	15	2	15	58
Range	75,5-81,5	76,0-80,0	76,5-79,5	79,4-82,4	77,4-78,6
Mean	78,56	78,06	78,0	80,56	78,0
S.D. of Samples	1,40	1,42	2,12	0,79	0,43
S.D. of Population	1,37	1,37	1,5	0,76	0,42

Note: Average An content of plagioclase is calculated according to  

$$\text{XRF An} = \frac{\text{An}}{100-\text{Or}}$$

See Folder B for position of analysed samples in the sequence.

APPENDIX III

The distribution of Y, Zr, Sr and Rb of 64 plagioclase separates from borehole MDH 7. Sample positions may be seen on Folder B.

SAMPLE NO.	ZIRCONIUM	YTTRIUM	STRONTIUM	RUBIDIUM
A2	7	5	465	4
A4	6	4	472	4
A6	8	5	475	3
A8	5	4	462	4
A10	7	5	472	4
A12	7	5	473	3
A14	5	4	474	3
A16	6	4	468	Trace
A18	8	5	467	Trace
A20	7	4	459	Trace
A22	6	4	464	3
A24	100	5	468	3
A26	7	4	457	Trace
A28	5	5	464	Trace
A30	7	6	463	5
B1	5	6	477	3
C4	80	4	493	4
C7	5	4	410	25
UG3A	4	3	136	88
UG3B	4	5	337	70
UG3C	4	5	457	8
D1	5	4	470	3
D4	5	4	462	4
D6	3	3	473	Trace
D11	6	5	496	12
D13	5	4	502	Trace
E1	Trace	Trace	472	5
E2	15	5	464	9
E4	12	5	444	9
E6	10	5	470	5
E8	7	4	467	4
E10	12	6	456	5
E12	8	4	458	5
E14	8	6	460	3
E16	8	5	458	3
E18	8	5	456	4
E20	9	5	459	4
E22	6	Trace	466	3
E24	6	4	467	5
E26	7	4	473	4
E28	4	Trace	461	4
E30	6	4	471	3
E32	7	5	469	4
E34	8	5	462	4
E36	5	4	465	Trace
E38	5	4	474	3
E40	6	3	487	5
E44	6	4	475	4
E46	Trace	Trace	477	3
E48	5	4	493	6
E52	22	3	471	3
E54	6	5	481	4
E56	11	5	471	7
E60	5	5	506	Trace
E62	57	7	384	12
E64	3	3	503	8
E66	Trace	Trace	487	7
E76	Trace	Trace	493	5
E87	Trace	Trace	452	11
E88	5	4	478	13
E91	7	4	460	16
F1	3	4	460	Trace
F2	6	4	475	Trace
F5	Trace	4	479	Trace



APPENDIX IV

Chemical analyses and structural formulae of ortho-pyroxene separates from borehole MDH 7. (For sample positions see Folder B).

Sample No.	A2P	A6P	A8P	A10P	A12P	A14P	A18P	A20P
SiO <sub>2</sub>	55,92	55,80	55,25	54,37	54,45	54,89	53,54	52,15
TiO <sub>2</sub>	0,23	0,24	0,22	0,22	0,21	0,85	0,22	0,30
Al <sub>2</sub> O <sub>3</sub>	1,62	1,86	1,57	1,41	1,54	1,57	2,08	2,50
FeO	13,82	13,46	13,44	13,63	13,53	13,46	14,04	15,50
MnO	0,27	0,27	0,27	0,27	0,27	0,27	0,28	0,31
MgO	27,23	26,73	27,39	27,86	27,81	27,93	26,78	25,15
CaO	1,38	1,61	1,51	1,44	1,51	1,24	1,92	2,22
Na <sub>2</sub> O	0,09	0,19	0,13	0,11	0,11	0,12	0,12	0,11
K <sub>2</sub> O	-	0,01	-	-	-	0,10	-	-
P <sub>2</sub> O <sub>5</sub>	0,01	0,01	0,01	0,01	0,01	0,01	0,01	0,01
Cr <sub>2</sub> O <sub>3</sub>	0,40	0,40	0,40	0,40	0,41	0,40	0,35	0,27
NiO	0,10	0,10	0,10	0,10	0,10	0,10	0,10	0,10
TOTAL	101,07	100,68	100,29	99,82	99,95	100,94	99,44	98,62
NUMBER OF IONS ON THE BASIS OF 6(O)								
Si	1,978	1,980	1,971	1,954	1,953	1,948	1,939	1,922
Ti	0,006	0,006	0,006	0,006	0,006	0,023	0,006	0,008
Al	0,016	0,014	0,023	0,040	0,041	0,029	0,055	0,070
Al	0,052	0,064	0,043	0,020	0,024	0,037	0,034	0,039
Fe <sup>2+</sup>	0,409	0,399	0,401	0,410	0,406	0,400	0,425	0,477
Mn	0,008	0,008	0,008	0,008	0,008	0,008	0,009	0,010
Mg	1,436	1,414	1,456	1,493	1,487	1,478	1,446	1,382
Ca	0,052	0,061	0,058	0,055	0,058	0,047	0,075	0,088
Na	0,006	0,013	0,009	0,008	0,008	0,008	0,009	0,008
K	-	-	-	-	-	-	-	-
P	-	-	-	-	-	-	-	-
Cr	0,011	0,011	0,011	0,011	0,011	0,011	0,010	0,008
Ni	0,003	0,003	0,003	0,003	0,003	0,003	0,003	0,002
TOTAL	3,977	3,973	3,989	4,008	4,005	3,992	4,001	4,014
Mg	75,5	75,2	75,8	76,2	76,2	76,6	74,3	71,0
Fe	21,8	21,5	21,1	20,9	20,8	21,0	21,8	24,5
Ca	2,8	3,3	3,0	2,8	3,0	2,5	3,8	4,5
$\frac{Mg}{Mg+Fe^{2+}}$	0,7784	0,7798	0,7841	0,7945	0,7933	0,7871	0,7847	0,7609

Sample No.	A22P	A24P	A28P	B2P	B3P	B6P	B12P	C1P
SiO <sub>2</sub>	51,40	51,92	52,67	54,47	54,65	53,97	54,57	54,18
TiO <sub>2</sub>	0,37	0,37	0,21	0,17	0,18	0,18	0,21	0,23
Al <sub>2</sub> O <sub>3</sub>	3,63	3,87	2,28	1,56	1,58	1,36	3,06	1,16
FeO	16,24	15,86	13,94	13,30	13,57	13,71	8,77	14,08
MnO	0,33	0,31	0,28	0,27	0,27	0,27	0,20	0,28
MgO	22,31	22,03	26,49	27,93	27,62	27,46	29,04	27,41
CaO	4,07	4,60	2,64	1,45	1,60	1,54	2,65	1,57
Na <sub>2</sub> O	0,11	0,11	0,11	0,08	0,09	0,09	0,09	0,09
K <sub>2</sub> O	0,01	0,01	0,02	0,01	0,03	0,01	0,03	0,01
P <sub>2</sub> O <sub>5</sub>	0,01	0,01	0,01	0,01	0,01	0,01	0,01	0,01
Cr <sub>2</sub> O <sub>3</sub>	0,21	0,24	0,40	0,37	0,42	0,41	0,75	0,45
NiO	0,07	0,08	0,08	0,09	0,09	0,10	0,09	0,09
TOTAL	98,76	99,41	99,13	99,71	100,11	99,11	99,47	99,56

## NUMBER OF IONS ON THE BASIS OF 6(0)

Si	1,907	1,911	1,920	1,955	1,957	1,956	1,931	1,958
Ti	0,010	0,010	0,006	0,005	0,005	0,005	0,005	0,006
Al	0,083	0,079	0,074	0,040	0,038	0,039	0,064	0,036
Al	0,076	0,089	0,024	0,026	0,029	0,019	0,063	0,013
Fe <sup>2+</sup>	0,504	0,488	0,425	0,399	0,406	0,415	0,259	0,425
Mn	0,010	0,010	0,009	0,008	0,008	0,008	0,259	0,425
Mg	1,234	1,209	1,439	1,495	1,474	1,483	0,006	0,008
Ca	0,162	0,181	0,103	0,056	0,061	0,059	0,100	0,061
Na	0,008	0,008	0,008	0,006	0,007	0,006	0,100	0,061
K	0,001	0,001	-	0,001	0,001	-	0,002	0,001
P	-	-	-	-	-	-	-	-
Cr	0,006	0,007	0,011	0,011	0,012	0,011	0,021	0,013
Ni	0,002	0,002	0,002	0,002	0,002	0,003	0,002	0,003
TOTAL	4,003	3,995	4,021	4,004	4,000	4,004	3,992	4,008

Mg	65,0	64,2	73,2	76,7	75,9	75,7	80,8	75,2
Fe	26,5	26,2	21,6	20,5	20,9	21,2	13,9	21,7
Ca	8,5	9,6	5,3	2,9	3,2	3,0	5,3	3,1
$\frac{Mg}{Mg+Fe^{2+}}$	0,7145	0,7124	0,8012	0,7945	0,7863	0,7901	0,8551	0,7860

Sample No.	C23P	C4P	D2P	D6P	D9P	D10P	D4P	D12P
SiO <sub>2</sub>	54,47	54,25	53,99	54,16	53,88	54,43	52,94	55,15
TiO <sub>2</sub>	0,21	0,18	0,21	0,17	0,16	0,14	0,22	0,16
Al <sub>2</sub> O <sub>3</sub>	1,21	1,34	1,15	1,21	1,25	1,36	3,08	1,27
FeO	14,01	13,81	13,55	12,95	12,83	12,55	13,77	12,97
MnO	0,27	0,27	0,28	0,28	0,27	0,26	0,31	0,26
MgO	27,35	27,62	28,25	28,72	28,74	28,93	25,69	29,05
CaO	1,60	1,53	1,40	1,34	1,28	1,26	2,40	1,25
Na <sub>2</sub> O	0,09	0,09	0,09	0,09	0,08	0,07	0,09	0,10
K <sub>2</sub> O	0,01	0,01	-	-	-	-	0,01	-
P <sub>2</sub> O <sub>5</sub>	-	0,01	0,01	0,01	0,01	0,01	0,01	0,01
Cr <sub>2</sub> O <sub>3</sub>	0,45	0,45	0,31	0,33	0,38	0,41	0,37	0,40
NiO	0,10	0,10	0,11	0,11	0,11	0,14	0,19	0,11
TOTAL	99,77	99,65	99,36	99,37	98,99	99,56	99,08	100,73

NUMBER OF IONS ON THE BASIS OF 6(0)								
Si	1,962	1,955	1,950	1,950	1,947	1,951	1,925	1,956
Ti	0,006	0,005	0,006	0,005	0,004	0,004	0,006	0,004
Al	0,032	0,041	0,044	0,045	0,049	0,045	0,069	0,040
Al	0,020	0,016	0,005	0,006	0,004	0,012	0,063	0,013
Fe <sup>2+</sup>	0,422	0,416	0,409	0,390	0,388	0,376	0,419	0,385
Mn	0,008	0,008	0,009	0,008	0,008	0,008	0,009	0,008
Mg	1,468	1,484	1,521	1,542	1,548	1,546	1,392	1,536
Ca	0,061	0,059	0,054	0,052	0,050	0,048	0,093	0,047
Na	0,006	0,006	0,006	0,006	0,006	0,005	0,007	0,007
K	-	-	0,001	-	-	-	-	-
P	-	-	-	-	-	-	-	-
Cr	0,013	0,013	0,009	0,009	0,011	0,011	0,011	0,011
Ni	0,003	0,003	0,003	0,003	0,003	0,004	0,005	0,003
TOTAL	4,001	4,006	4,017	4,016	4,018	4,010	3,999	4,010

Mg	75,2	75,7	76,6	77,7	78,0	78,4	73,1	78,0
Fe	21,6	21,2	20,6	19,7	19,5	19,1	22,0	19,5
Ca	3,2	3,0	2,7	2,6	2,5	2,5	4,9	2,4
<u>Mg</u>								
Mg+Fe <sup>2+</sup>	7,800	0,7905	0,8103	0,8203	0,8239	0,8203	0,7695	0,8175

Sample No.	D14P	D16P	D18P	D24P	E4P	E6P	E8P	E10P
SiO <sub>2</sub>	54,74	54,52	53,39	54,06	54,30	53,66	53,29	54,34
TiO <sub>2</sub>	0,14	0,17	0,23	0,24	0,20	0,30	0,28	0,27
Al <sub>2</sub> O <sub>3</sub>	1,37	1,40	1,74	1,38	2,75	1,78	1,59	1,40
FeO	12,54	12,56	11,76	13,43	14,69	14,43	14,73	14,26
MnO	0,25	0,26	0,24	0,26	0,30	0,29	0,30	0,29
MgO	28,65	28,83	29,00	27,33	25,67	26,54	26,75	27,64
CaO	1,03	1,40	1,93	1,63	1,56	2,17	1,94	1,70
Na <sub>2</sub> O	0,10	0,07	0,09	0,09	0,09	0,09	0,10	0,10
K <sub>2</sub> O	-	0,01	0,01	0,01	0,01	0,03	-	0,01
P <sub>2</sub> O <sub>5</sub>	-	0,01	0,01	0,01	0,01	0,01	0,01	0,01
Cr <sub>2</sub> O <sub>3</sub>	0,49	0,60	0,60	0,48	0,44	0,45	0,45	0,44
NiO	0,10	0,12	0,14	0,10	0,09	0,10	0,10	0,10
TOTAL	99,41	99,95	99,04	99,02	100,11	99,85	99,54	100,56
NUMBER OF IONS ON THE BASIS OF 6(O)								
Si	1,962	1,948	1,926	1,958	1,952	1,941	1,937	1,947
Ti	0,004	0,004	0,006	0,006	0,005	0,008	0,007	0,007
Al	0,034	0,048	0,068	0,036	0,043	0,051	0,056	0,046
Al	0,024	0,011	0,008	0,023	0,073	0,025	0,012	0,013
Fe <sup>2+</sup>	0,376	0,375	0,355	0,407	0,441	0,436	0,448	0,427
Mn	0,008	0,008	0,007	0,008	0,009	0,009	0,009	0,009
Mg	1,531	1,536	1,559	1,476	1,375	1,431	1,449	1,476
Ca	0,039	0,054	0,074	0,063	0,060	0,084	0,076	0,065
Na	0,007	0,005	0,006	0,007	0,006	0,007	0,007	0,006
K	-	-	-	0,001	-	0,001	-	-
P	-	-	-	-	-	-	-	-
Cr	0,014	0,017	0,014	0,014	0,012	0,013	0,013	0,012
Ni	0,003	0,003	0,004	0,003	0,003	0,003	0,003	0,003
TOTAL	4,002	4,009	4,027	4,002	3,979	4,009	4,017	4,011
Mg	78,7	78,2	78,4	75,8	73,1	73,3	73,5	75,0
Fe	19,3	19,1	17,8	20,9	23,7	22,4	22,7	21,7
Ca	2,0	2,7	3,8	3,2	3,2	4,3	3,8	3,3
$\frac{Mg}{Mg+Fe^{2+}}$	0,8048	0,8179	0,8508	0,7868	0,7570	0,7784	0,7859	0,7917

Sample No.	E12P	E14P	E16P	E18P	E20P	E22P	E24P	E26P
SiO <sub>2</sub>	53,61	53,87	53,46	54,16	54,12	53,49	52,14	52,98
TiO <sub>2</sub>	0,26	0,27	0,28	0,25	0,27	0,26	0,26	0,24
Al <sub>2</sub> O <sub>3</sub>	1,50	1,48	1,62	1,13	1,44	1,44	1,33	1,39
FeO	14,02	14,02	14,39	14,52	13,98	13,71	14,36	14,17
MnO	0,28	0,28	0,29	0,28	0,28	0,27	0,28	0,28
MgO	27,56	27,39	26,76	27,00	27,54	26,48	26,67	26,58
CaO	1,53	1,58	1,99	1,66	1,65	1,68	1,55	1,50
Na <sub>2</sub> O	0,10	0,11	0,10	0,10	0,11	0,14	0,11	0,10
K <sub>2</sub> O	-	0,01	-	-	0,01	0,02	0,01	-
P <sub>2</sub> O <sub>5</sub>	0,01	0,01	0,01	0,01	0,01	0,01	-	-
Cr <sub>2</sub> O <sub>3</sub>	0,10	0,10	0,10	0,10	0,10	0,10	0,10	0,10
TOTAL	99,40	99,55	99,42	99,64	99,63	98,03	97,26	97,78
NUMBER OF IONS ON THE BASIS OF 6(O)								
Si	1,942	1,947	1,942	1,960	1,948	1,961	1,938	1,952
Ti	0,007	0,007	0,008	0,007	0,007	0,007	0,007	0,006
Al	0,051	0,046	0,050	0,033	0,045	0,032	0,055	0,042
Al	0,013	0,017	0,019	0,015	0,016	0,030	0,003	0,018
Fe <sup>2+</sup>	0,425	0,424	0,437	0,439	0,421	0,420	0,446	0,437
Mn	0,009	0,009	0,009	0,008	0,008	0,008	0,009	0,009
Mg	1,488	1,476	1,449	1,456	1,478	1,447	1,478	1,460
Ca	0,059	0,061	0,077	0,064	0,063	0,066	0,061	0,059
Na	0,007	0,008	0,007	0,007	0,008	0,010	0,008	0,007
K	-	-	-	-	-	0,001	-	-
P	-	-	-	-	-	-	-	-
Cr	0,012	0,012	0,012	0,012	0,012	0,012	0,013	0,013
Ni	0,003	0,003	0,003	0,003	0,003	0,003	0,003	0,003
TOTAL	4,016	4,010	4,013	4,004	4,009	3,997	4,021	4,006
Mg	75,5	75,3	73,8	74,3	75,3	74,7	74,4	74,6
Fe	21,5	2,6	22,3	22,4	21,4	21,9	22,5	22,3
Ca	3,0	3,1	3,9	3,3	3,2	3,4	3,1	3,0
$\frac{Mg}{Mg+Fe^{2+}}$	0,7979	0,7906	0,7842	0,7762	0,7929	0,7749	0,7964	0,7793

Sample No.	E28P	E30P	E32P	E34P	E36P	E38P	E40P	E42P
SiO <sub>2</sub>	54,74	53,93	53,95	53,95	53,43	54,76	54,31	54,40
TiO <sub>2</sub>	0,24	0,25	0,23	0,24	0,23	0,19	0,21	0,21
Al <sub>2</sub> O <sub>3</sub>	1,94	1,94	1,63	1,63	1,87	1,47	1,43	1,36
FeO	14,07	14,03	13,94	14,03	13,02	12,56	12,36	12,68
MnO	0,28	0,29	0,29	0,29	0,27	0,26	0,25	0,26
MgO	26,70	26,68	27,10	27,04	27,53	28,31	28,20	28,15
CaO	1,87	2,15	1,82	1,83	1,81	1,46	1,58	1,43
Na <sub>2</sub> O	0,10	0,18	0,10	0,10	0,13	0,12	0,13	0,10
K <sub>2</sub> O	0,01	0,01	0,01	-	-	-	-	-
P <sub>2</sub> O <sub>5</sub>	0,01	0,01	-	0,01	0,01	0,01	0,01	0,01
Cr <sub>2</sub> O <sub>3</sub>	0,47	0,47	0,42	0,43	0,37	0,35	0,37	0,40
NiO	0,10	0,10	0,10	0,10	0,10	0,10	0,10	0,10
TOTAL	99,53	100,08	99,59	99,66	98,77	99,59	98,95	99,10
NUMBER OF IONS ON THE BASIS OF 6(0)								
Si	1,944	1,943	1,949	1,949	1,940	1,961	1,958	1,960
Ti	0,007	0,007	0,006	0,007	0,006	0,005	0,005	0,006
Al	0,049	0,050	0,045	0,044	0,054	0,034	0,037	0,034
Al	0,034	0,032	0,025	0,025	0,026	0,028	0,024	0,024
Fe <sup>2+</sup>	0,425	0,423	0,421	0,424	0,395	0,376	0,373	0,382
Mn	0,009	0,009	0,009	0,009	0,008	0,008	0,008	0,008
Mg	1,440	1,432	1,459	1,456	1,489	1,511	1,516	1,512
Ca	0,072	0,083	0,070	0,071	0,070	0,056	0,061	0,055
Na	0,007	0,013	0,007	0,007	0,009	0,009	0,009	0,007
K	0,001	-	-	-	-	-	-	-
P	-	-	-	-	-	-	-	-
Cr	0,013	0,013	0,012	0,012	0,011	0,010	0,010	0,011
Ni	0,003	0,003	0,003	0,003	0,003	0,003	0,003	0,003
TOTAL	4,004	4,008	4,006	4,007	4,011	4,001	4,004	4,002
Mg	74,3	73,9	74,8	74,7	76,2	77,8	77,7	77,6
Fe	22,0	21,8	21,6	21,7	20,2	19,4	19,1	19,6
Ca	3,7	4,3	3,6	3,6	3,6	2,9	3,1	2,8
$\frac{Mg}{Mg+Fe^{2+}}$	0,7769	0,7831	0,7844	0,7826	0,8065	0,8027	0,8089	0,8011

Sample No.	E44P	E46P	E48P	E52P	E58P	E60P	E62P	E64P
SiO <sub>2</sub>	54,19	54,97	54,47	54,22	53,44	54,22	54,95	53,82
TiO <sub>2</sub>	0,21	0,20	0,17	0,18	0,21	0,18	0,23	0,18
Al <sub>2</sub> O <sub>3</sub>	1,83	1,39	1,33	1,53	1,70	1,57	1,14	2,04
FeO	12,49	12,45	12,64	12,41	13,48	13,54	14,14	13,40
MnO	0,26	0,26	0,26	0,26	0,27	0,27	0,28	0,28
MgO	27,87	28,76	28,54	28,35	27,08	27,67	27,43	27,45
CaO	1,60	1,34	1,31	1,58	1,68	1,80	1,70	1,85
Na <sub>2</sub> O	0,14	0,08	0,10	0,13	0,08	0,11	0,10	0,11
K <sub>2</sub> O	-	-	-	-	-	-	0,01	-
P <sub>2</sub> O <sub>5</sub>	0,01	0,01	0,01	0,01	0,01	0,01	-	0,01
Cr <sub>2</sub> O <sub>3</sub>	0,46	0,39	0,43	0,48	0,43	0,49	0,42	0,45
NiO	0,10	0,10	0,10	0,10	0,10	0,10	0,10	0,10
<b>TOTAL</b>	<b>99,16</b>	<b>99,97</b>	<b>99,36</b>	<b>99,25</b>	<b>98,48</b>	<b>99,96</b>	<b>100,50</b>	<b>99,69</b>
NUMBER OF IONS ON THE BASIS OF 6(O)								
Si	1,951	1,960	1,957	1,950	1,948	1,948	1,966	1,938
Ti	0,006	0,005	0,005	0,005	0,006	0,005	0,006	0,005
Al	0,043	0,035	0,038	0,045	0,046	0,047	0,028	0,057
Al	0,034	0,023	0,018	0,020	0,027	0,019	0,020	0,029
Fe <sup>2+</sup>	0,376	0,371	0,380	0,373	0,411	0,407	0,423	0,403
Mn	0,008	0,008	0,008	0,008	0,008	0,008	0,008	0,008
Mg	1,496	1,528	1,528	1,520	1,471	1,482	1,462	1,474
Ca	0,061	0,051	0,050	0,061	0,065	0,069	0,065	0,071
Na	0,010	0,006	0,006	0,009	0,005	0,007	0,007	0,008
K	-	-	-	-	-	-	-	-
P	-	-	-	-	-	-	-	-
Cr	0,012	0,011	0,012	0,013	0,012	0,014	0,012	0,013
Ni	0,003	0,003	0,003	0,003	0,003	0,003	0,003	0,003
<b>TOTAL</b>	<b>4,001</b>	<b>4,001</b>	<b>4,005</b>	<b>4,007</b>	<b>4,002</b>	<b>4,009</b>	<b>4,000</b>	<b>4,009</b>
Mg	77,4	78,3	78,0	77,3	75,5	75,7	75,0	75,6
Fe	19,5	19,0	19,4	19,1	21,2	20,8	21,7	20,7
Ca	3,2	2,6	2,6	3,1	3,4	3,5	3,3	3,7
$\frac{Mg}{Mg+Fe^{2+}}$	0,8015	0,8078	0,8097	0,8148	0,7883	0,7977	0,7777	0,7984

Sample No.	E66P	E68P	E70P	E72P	E74P	E76P	E78P	E80P
SiO <sub>2</sub>	54,41	53,19	54,26	54,32	54,35	53,68	54,24	54,55
TiO <sub>2</sub>	0,17	0,22	0,26	0,25	0,24	0,16	0,22	0,21
Al <sub>2</sub> O <sub>3</sub>	1,46	1,91	1,17	1,11	1,18	1,55	1,48	1,17
FeO	13,55	13,32	14,34	14,51	14,62	14,00	14,22	14,47
MnO	0,27	0,28	0,28	0,29	0,29	0,29	0,29	0,30
MgO	27,65	26,89	27,03	26,94	26,75	26,99	26,74	27,23
CaO	1,70	1,85	1,76	1,91	2,04	1,68	1,88	1,78
Na <sub>2</sub> O	0,10	0,11	0,10	0,12	0,11	0,12	0,11	0,13
K <sub>2</sub> O	-	0,02	0,04	0,01	0,01	-	0,01	-
P <sub>2</sub> O <sub>5</sub>	0,01	-	0,01	0,01	0,01	0,01	0,02	0,01
Cr <sub>2</sub> O <sub>3</sub>	0,46	0,43	0,43	0,43	0,45	0,48	0,45	0,44
NiO	0,10	0,09	0,10	0,10	0,10	0,10	0,10	0,10
TOTAL	99,94	98,38	100,07	99,77	99,99	99,17	99,70	100,15

NUMBER OF IONS ON THE BASIS OF O(6)								
Si	1,954	1,942	1,956	1,963	1,961	1,949	1,959	1,962
Ti	0,005	0,006	0,007	0,007	0,006	0,004	0,006	0,006
Al	0,041	0,052	0,037	0,030	0,033	0,047	0,035	0,032
Al	0,021	0,030	0,013	0,017	0,017	0,019	0,028	0,017
Fe <sup>2+</sup>	0,407	0,406	0,432	0,438	0,441	0,425	0,429	0,435
Mn	0,008	0,009	0,008	0,009	0,009	0,009	0,009	0,009
Mg	1,480	1,464	1,452	1,451	1,439	1,461	1,439	1,460
Ca	0,068	0,072	0,079	0,065	0,073	0,069	0,071	0,061
Na	0,007	0,008	0,008	0,008	0,008	0,009	0,007	0,006
K	-	0,001	0,002	-	-	-	-	-
P	-	-	-	-	-	-	-	-
Cr	0,013	0,012	0,012	0,013	0,014	0,014	0,013	0,012
Ni	0,003	0,003	0,003	0,003	0,003	0,003	0,003	0,003
TOTAL	4,007	4,005	4,009	4,004	4,005	4,009	4,000	4,003

Mg	75,7	75,3	74,0	74,2	73,7	74,7	74,0	74,6
Fe	20,8	20,9	22,0	22,4	22,6	21,7	22,3	22,2
Ca	3,5	3,8	4,0	3,3	3,7	3,5	3,6	3,1
$\frac{\text{Mg}}{\text{Mg}+\text{Fe}^{2+}}$	0,8015	0,8078	0,8097	0,8148	0,7883	0,7977	0,7702	0,7751



Sample No.	E82P	E86P	E90P	F1P	F5P
SiO <sub>2</sub>	54,75	54,29	54,52	54,10	53,53
TiO <sub>2</sub>	0,14	0,12	0,17	0,13	0,11
Al <sub>2</sub> O <sub>3</sub>	1,60	2,04	1,62	2,13	2,38
FeO	13,55	13,45	12,74	13,55	13,94
MnO	0,28	0,28	0,26	0,29	0,32
MgO	27,21	27,33	28,41	26,75	25,34
CaO	1,48	1,60	1,75	1,64	2,84
Na <sub>2</sub> O	0,14	0,12	0,12	0,14	0,22
K <sub>2</sub> O	-	0,04	-	0,04	-
P <sub>2</sub> O <sub>5</sub>	0,01	0,20	-	0,15	-
Cr <sub>2</sub> O <sub>3</sub>	0,43	0,49	0,49	0,36	0,28
NiO	0,10	0,11	0,11	0,09	0,09
TOTAL	99,69	100,07	100,19	99,37	99,93

NUMBER OF IONS ON THE BASIS OF O(6)

Si	1,957	1,944	1,946	1,951	1,949
Ti	0,004	0,003	0,004	0,003	0,003
Al	0,029	0,053	0,050	0,046	0,048
Al	0,038	0,033	0,018	0,044	0,054
Fe <sup>2+</sup>	0,407	0,403	0,380	0,409	0,424
Mn	0,009	0,008	0,008	0,009	0,010
Mg	1,457	1,459	1,512	1,438	1,375
Ca	0,057	0,061	0,067	0,063	0,111
Na	0,010	0,008	0,008	0,010	0,015
K	-	0,002	-	0,002	-
P	-	0,006	0,004	-	-
Cr	0,012	0,014	0,014	0,010	0,008
Ni	0,003	0,003	0,003	0,003	0,003
TOTAL	3,993	3,997	4,010	3,992	4,000

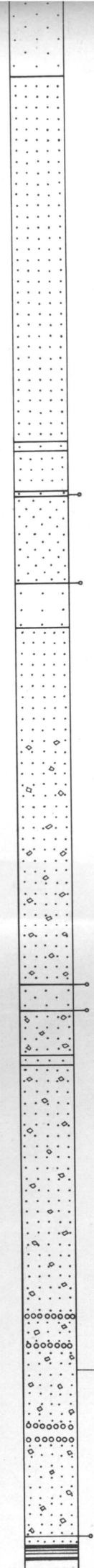
Mg	75,6	75,7	77,2	75,1	76,5
Fe	21,4	21,1	19,4	21,6	22,2
Ca	3,0	3,2	3,4	3,3	5,8
$\frac{\text{Mg}}{\text{Mg}+\text{Fe}^{2+}}$	0,7817	0,7857	0,8142	0,7788	0,7650

APPENDIX V

The distribution of Zn, Cu, Co, V, Ni and Cr in 55 orthopyroxene separates from borehole MDH 7. (Sample positions may be seen on Folder B).

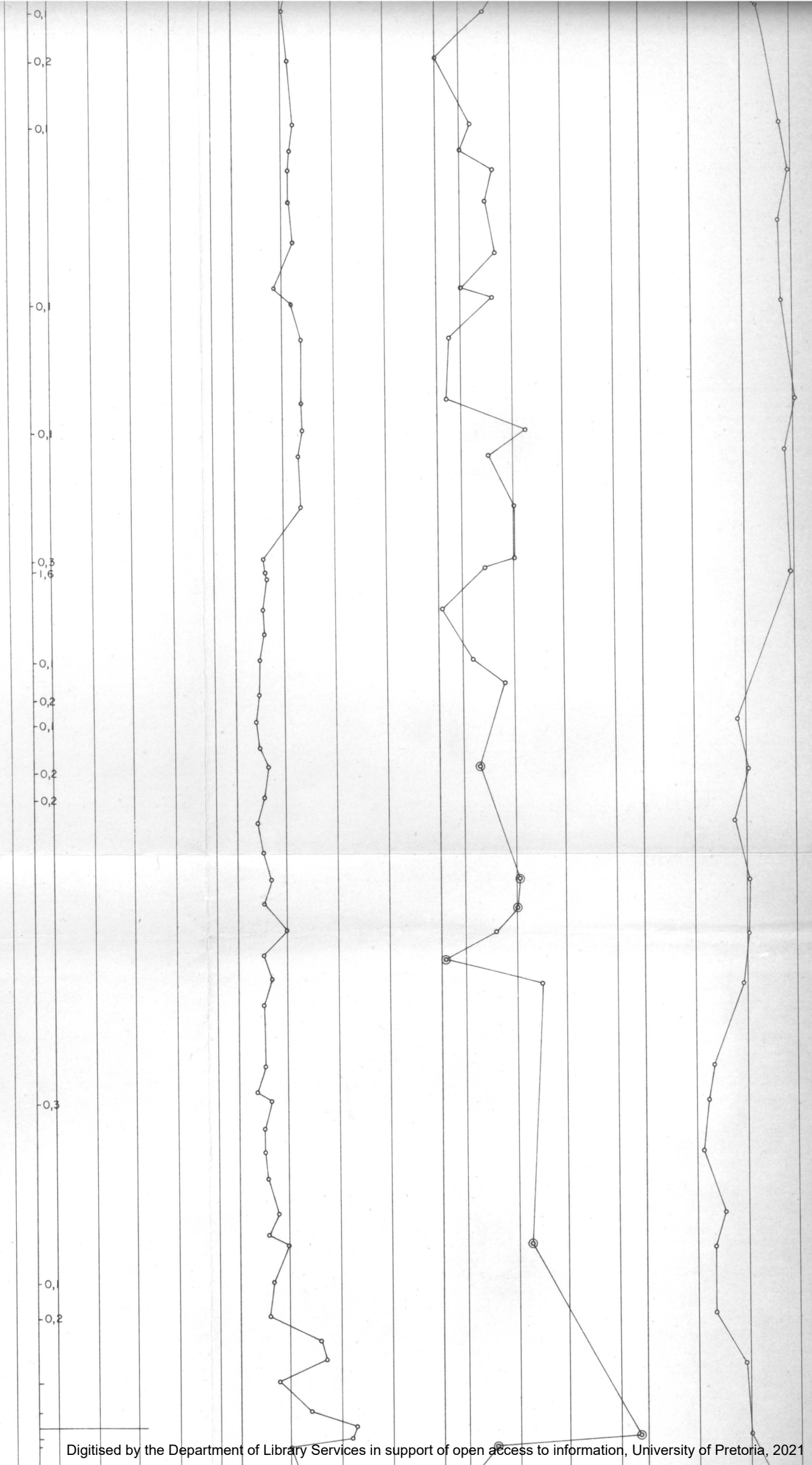
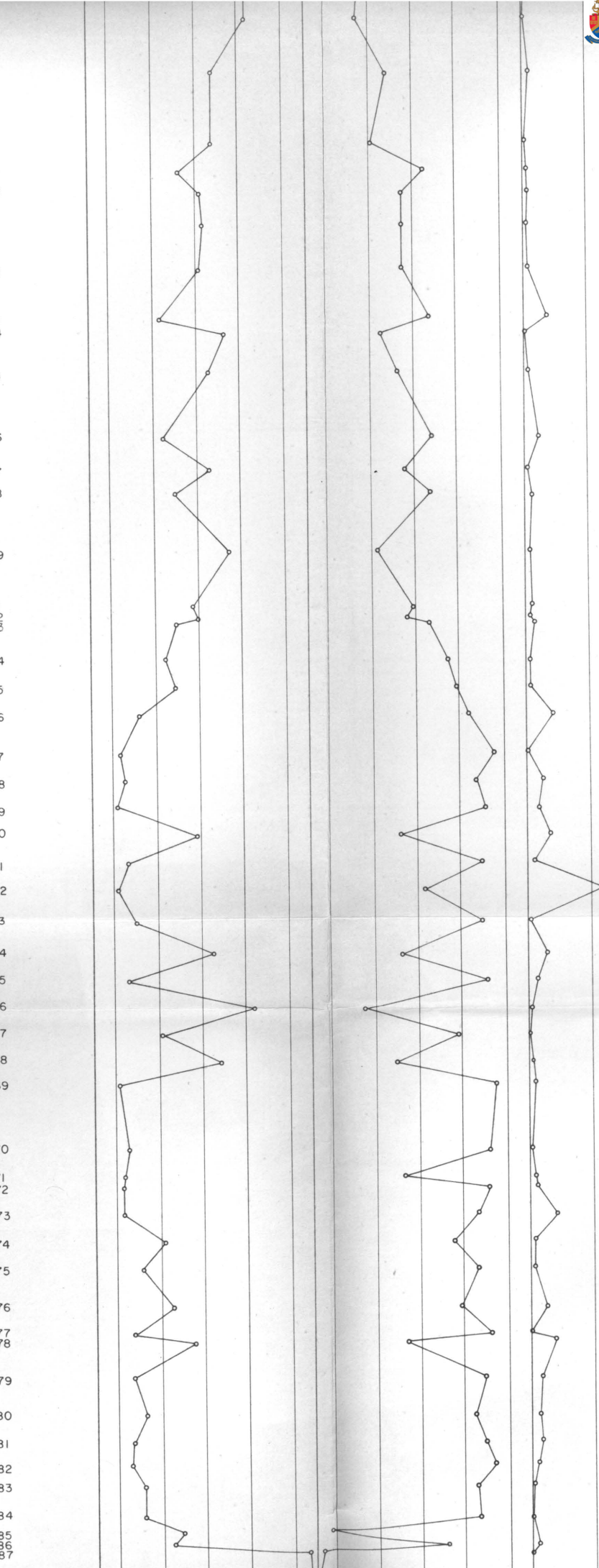
SAMPLE NO.	ZINC	COPPER	NICKEL	COBALT	CHROMIUM	VANADIUM
A2	107	16	612	106	2843	127
A4	109	14	624	108	2801	126
A6	100	29	609	107	2799	129
A8	103	13	620	105	2780	125
A10	109	10	624	107	2857	127
A14	105	11	608	108	2782	123
B2	96	23	567	106	2728	110
B4	89	17	507	109	2981	128
B6	103	14	609	107	2990	127
C1	96	18	611	108	3243	126
C23	1233	10	671	106	3183	109
C4	104	9	634	105	3194	104
D2	94	9	657	112	1978	154
D4	96	15	661	104	2042	145
D6	95	10	721	113	2670	156
D9	96	7	712	103	2890	152
D10	94	8	1004	109	2787	156
D12	98	10	703	109	3464	147
D14	94	7	679	109	3341	211
D16	85	10	738	118	3207	83
D19	74	11	1437	109	2335	146
D22	101	12	701	109	3057	125
D24	100	101	615	110	3609	130
E12	109	11	617	112	3072	147
E14	111	11	630	109	3043	146
E18	119	10	617	113	3072	145
E20	111	8	624	113	2987	139
E22	112	11	607	110	3095	141
E26	115	9	597	107	3152	134
E28	114	10	568	108	3217	133
E30	104	11	581	108	3241	138
E36	98	9	599	111	2584	122
E38	94	12	641	112	2477	110
E40	95	11	649	111	2586	111
E44	98	11	620	107	4488	129
E46	98	9	654	114	2744	113
E48	107	11	707	115	3060	113
E52	96	9	670	113	3364	113
E54	96	12	608	107	4043	124
E56	104	8	620	108	3209	122
E58	108	9	606	108	3072	122
E60	109	18	628	110	3446	130
E62	112	14	601	112	2990	135
E64	109	97	630	112	3261	136
E66	109	3	647	110	2831	136
E70	114	11	614	108	2897	146
E74	121	13	628	111	3215	150
E76	106	10	616	111	3439	140
E78	113	9	618	112	3247	145
E80	119	Trace	603	114	3255	148
E82	103	11	642	115	3123	121
E86	92	8	694	116	3514	103
E90	50	10	691	92	3658	109
F5	106	10	526	117	1970	140
F1/2	95	8	549	131	3145	171

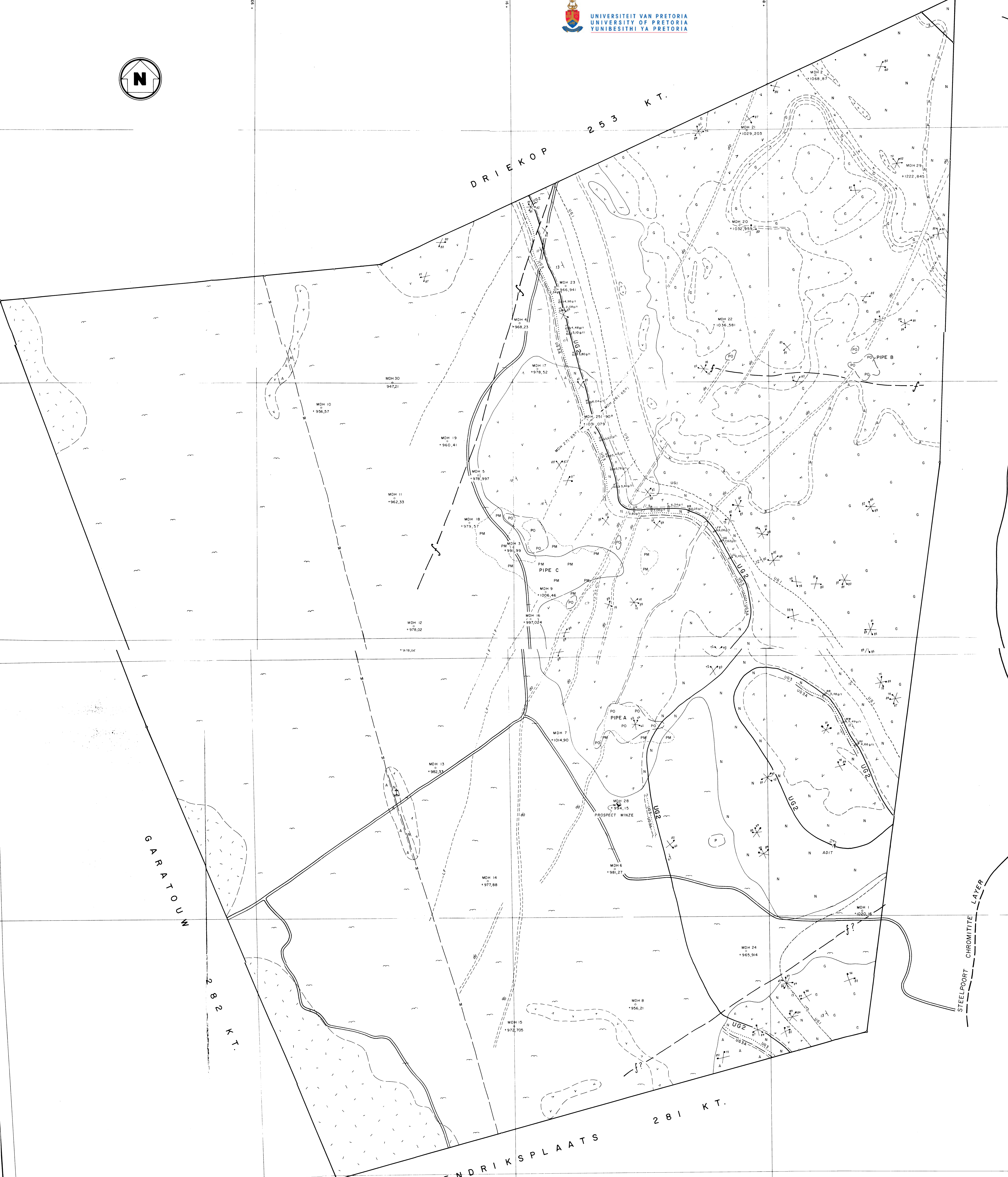
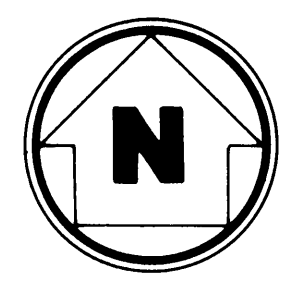
190  
200  
210  
220  
230  
240



UG 1 CYCLIC UNIT  
SECTION E/A

E36  
E37  
E38  
E39  
E40  
E41  
E42  
E43  
E44  
E45  
E46  
E47  
E48  
E49  
E51  
E52  
E53  
E54  
E55  
E56  
E57  
E58  
E59  
E60  
E61  
E62  
E63  
E64  
E65  
E66  
E67  
E68  
E69  
E70  
E71  
E72  
E73  
E74  
E75  
E76  
E77  
E78  
E79  
E80  
E81  
E82  
E83  
E84  
E85  
E86  
E87  
F88





STEELPOORT CHROMITITE LAYER

MOOIHOEK 255 KT.

**LEGEND**

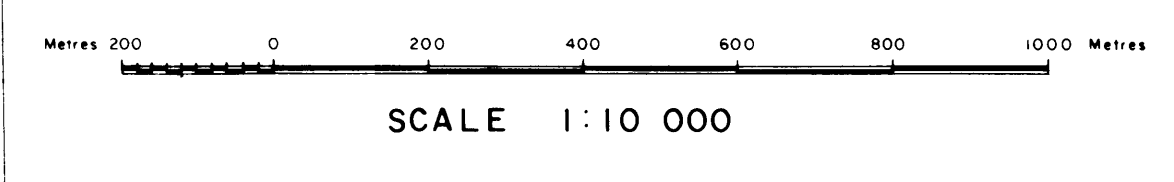
- ALLUVIUM
- LINEAR FEATURES (INFERRED FROM MAGNETIC SURVEY)
- DOLERITE DYKES (INFERRED FROM MAGNETIC SURVEY)
- DOLERITE DYKES (MAPPED ON SURFACE)
- MAFIC PIPES (IDENTIFIED BY MAGNETOMETER)
- MAFIC PIPES (OUTCROPPING)
- GABBRO, NORITE
- ANORTHOSITE
- GABBRO-NORITE
- NORITE
- MELANORITE
- MERENSKY REEF
- UG3 CHROMITITE LAYER
- UG2 CHROMITITE LAYER
- UG1 CHROMITITE LAYER
- INFERRED FAULTS
- DIP AND STRIKE
- JOINTS
- TRENCH NUMBER AND ASSAY (PI + PD)
- BOREHOLE NUMBER AND ELEVATION
- ROAD
- DISCOVERY SITE OF MERENSKY REEF

**MAIN ZONE**

- GABBRO, NORITE
- ANORTHOSITE
- GABBRO-NORITE
- NORITE
- MELANORITE

**CRITICAL ZONE**

- MERENSKY REEF
- UG3 CHROMITITE LAYER
- UG2 CHROMITITE LAYER
- UG1 CHROMITITE LAYER



MINING CORPORATION LTD.